THESIS FOR THE DEGREE OF LICENTIATE OF ENGINEERING

Chemical-Looping Combustion with Natural Gas Using NiO-Based Oxygen Carriers

CARL LINDERHOLM

Department of Energy and Environment
CHALMERS UNIVERSITY OF TECHNOLOGY
Göteborg, Sweden 2008

Chemical-Looping Combustion with Natural Gas
Using NiO-Based Oxygen Carriers

CARL LINDERHOLM

Department of Energy and Environment
Division of Energy Technology
Chalmers University of Technology
SE-41296 Göteborg
Sweden

Printed in Sweden
Chalmers Reproservice
Göteborg 2008

Chemical-Looping Combustion with Natural Gas
Using NiO-Based Oxygen Carriers

CARL LINDERHOLM

Department of Energy and Environment
Chalmers University of Technology

Abstract

CO_2 capture and storage has been proposed as an alternative to mitigate global warming. Chemical-looping combustion is an unmixed combustion concept where fuel and combustion air are kept separate by means of an oxygen carrier and the CO_2 capture is inherently achieved. The work presented in this thesis has been conducted in two chemical-looping combustors, and focuses on the experimental evaluation of NiO-based oxygen carriers prepared by commercially available production methods. Investigations in a 10-kW reactor system using natural gas as fuel evaluate the long-term performance of different oxygen carriers. The most important results in this thesis concern particles prepared by spray-drying, which were subjected to > 1000 h of operation with fuel. Fuel conversion was good, and increased with (a) decreased circulation, and (b) increased fuel-reactor temperature. Combustion efficiency close to 99% was accomplished using these spray-dried particles. At the end of the test series, the continuous loss of fine material was 0.003%/h, which corresponds to a particle life time of 33000 h. No decrease in reactivity was seen during these long-term tests. Experiments in a 300-W chemical-looping combustor investigate the possibility to optimize the methane conversion – while retaining the oxygen-transport capacity – by mixing different NiO-based oxygen carriers. The study confirmed that such optimization is indeed feasible.

Keywords: chemical-looping combustion, oxygen carrier, CO_2 capture, nickel oxide, fluidized bed

Publications

This licentiate thesis is based on the following papers:

I. Linderholm, C., Abad, A., Mattisson, T., Lyngfelt, A. 2008. 160 h of chemical-looping combustion in a 10 kW reactor system with a NiO-based oxygen carrier. *International Journal of Greenhouse Gas Control* 2:520-530.

II. Linderholm, C., Mattisson, T., Lyngfelt, A. 2008. Long-term integrity testing of spray-dried particles in a 10-kW chemical-looping combustor using natural gas as fuel. Submitted for publication.

III. Linderholm, C., Jerndal, E., Mattisson, T., Lyngfelt, A. 2008. Investigation of NiO-based mixed oxides in a 300-W chemical-looping combustor. Submitted for publication.

Contents

Acknowledgements

I want to express my sincere gratitude to my supervisor Anders Lyngfelt, who gave me the opportunity to work with things I care a great deal about. I also wish to thank him for his interest in my work, and his never-fading enthusiasm for the chemical-looping technologies.

Furthermore, I would like to thank my co-supervisor Associate Professor Tobias Mattisson for his availability and positive attitude, Nicolas Berguerand and Magnus Rydén for their help and their company in the lab, Erik Jerndal and Henrik Leion for help with particle imaging and being such good people, Ulrik Rosén and Lennart Darell for valuable technical assistance in the lab, and finally, everyone at the Division of Energy Technology for offering such a positive and relaxed working atmosphere.

1. Introduction

In spite of serious concerns about the potential effects of global warming, the fossil fuel related CO_2 emissions continue to increase, as is illustrated in figure 1. On a global scale, 80% of the primary energy supply is satisfied by fossil fuels [1].

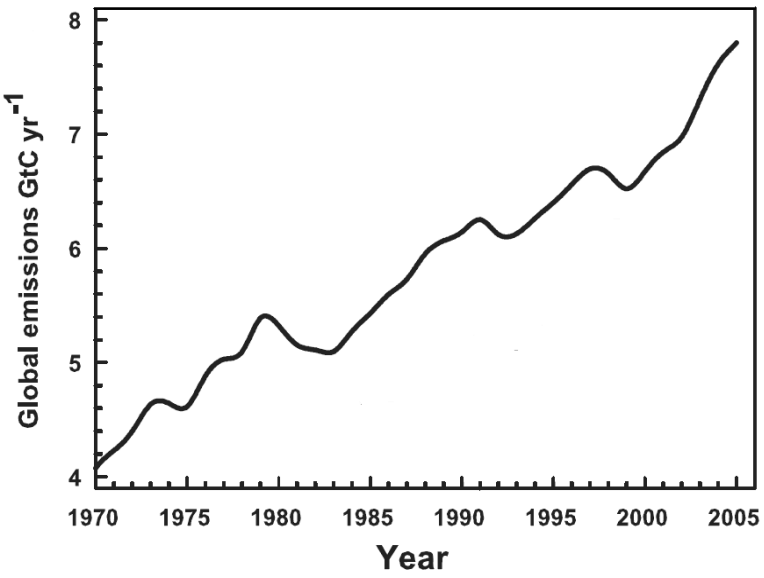

Figure 1. Annual global CO_2 emissions from fossil fuel burning and cement manufacture in GtC yr^{-1} 1970-2005. From AR4, IPCC [2].

1.1 Observations of global warming

The fourth Assessment Report from IPCC states that, "since 1750, it is extremely likely that humans have exerted a substantial warming influence on climate" [2]. This warming influence is due mainly to the burning of fossil fuels, a process in which the greenhouse gas CO_2 is produced and subsequently released into the atmosphere. The globally averaged CO_2 concentration (on dry air) is currently 385 ppm [3], a 37% increase from the pre-industrial (AD 1000-1750) levels of 275-285 ppm.

As shown in figure 2, there is evidence that the global average surface temperature is increasing and that the sea level is rising. Of the twelve years 1995-2006, eleven rank among the twelve warmest years since 1850, i.e. since the beginning of instrumentally recorded temperature [2].

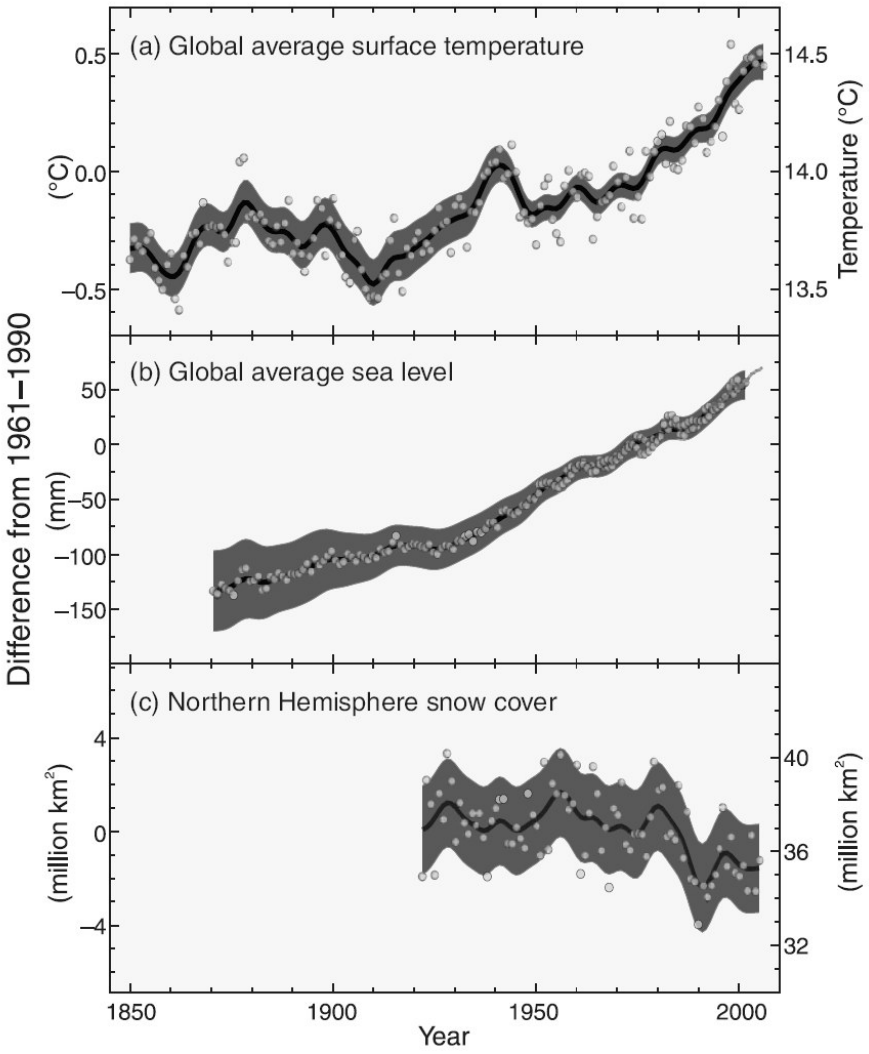

Figure 2. Observed changes in (a) global average surface temperature; (b) global average sea level from tide gauge and satellite data; and (c) Northern Hemisphere snow cover for March-April. All differences are relative to corresponding averages for the period 1961-1990. Smoothed curves represent decadal averaged values while circles show yearly values. The shaded areas are the uncertainty intervals estimated from a comprehensive analysis of known uncertainties (a and b) and from the time series (c). From AR4 Synthesis report, IPCC [2].

1.2 The greenhouse effect and radiative forcing

All objects at a temperature above absolute zero emit thermal radiation. The temperature of an object determines the frequency distribution of the radiation. In general, the hotter the object is, the higher the frequency and hence the shorter the wavelength. The climate on Earth is powered by the Sun's high-frequency thermal radiation, ranging from visible to ultraviolet. The surface temperature of the Earth is significantly lower than that of the Sun, which explains why Earth radiates at lower frequencies – longer wavelengths, primarily in the infrared part of the spectrum. A major portion of the radiation emitted from the surface is

absorbed by the atmosphere and then re-radiated back to Earth. Of course, this does not upset the overall radiation balance; incoming radiation still equals outgoing radiation, but the effect of the atmosphere is to increase the surface temperature, since the temperature must be sufficiently high to generate thermal radiation equivalent to the sum of incoming solar and infrared radiation. This phenomenon is commonly referred to as the greenhouse effect.

The greenhouse effect is caused by naturally occurring atmospheric gases, e.g. CO_2, called greenhouse gases (GHGs). Anthropogenic emissions of GHGs compromise the radiative balance of the Earth-atmosphere system, and the magnitude of the compromise is usually described in terms of radiative forcing. The radiative forcing relates the *change* in the radiative balance at the tropopause, i.e. at the top of the troposphere, for example between 1750 and 2005; a change that is brought about by an alteration in, for example,

- the concentration of a GHG,
- the occurrence of aerosols (particles),
- incident solar radiation,
- cloud cover, which affects the albedo of the planet, i.e. the fraction of reflected solar light.

Positive forcings lead to warming of climate and negative forcings lead to a cooling. It should be noted that radiative forcings do not need to have an anthropogenic origin.

It is conceivable to define radiative forcing at any height in the atmosphere. However, the primary concern of human beings is the response of the surface-troposphere system, because that is what will have a direct effect on the surface temperature. Hence, the radiative forcing is defined at the tropopause, because there is a strong coupling between the surface, the boundary layer and the free troposphere due to mixing. The mixing is the result of winds, condensation, precipitation et cetera. In contrast, the vertical mixing in the stratosphere, which is the atmospheric layer above the troposphere, is by far not as strong; it is more stratified, hence the name.

The most important greenhouse gases are, by order of impact, water vapour, carbon dioxide, ozone, methane and nitrous oxide, all of which are naturally occurring. The reason why the two most abundant atmospheric species, N_2 and O_2 – comprising 99% of the dry atmosphere – exert almost no greenhouse effect, ultimately comes down to quantum mechanics: atoms and

molecules can only accept or deliver photons in discrete energy levels, and diatomic molecules have a limited number of vibrational and rotational energies, which are the important ones for absorbing IR-radiation from Earth, i.e. of wavelengths 4-50 μm. Instead, it is the much rarer and more complex – primarily tri-atomic – atmospheric molecules that ensure an average surface temperature above the freezing point of water. The strength of the radiative forcing exercised by these molecules depends on three main factors [4]: (i) the ability of a given gas to absorb infrared radiation; (ii) to what extent other GHGs are already absorbing at the wavelengths where the given gas is able to absorb; and (iii) the magnitude of the radiation emitted from the Earth's surface at the wavelengths where the given gas is able to absorb. Some absorption bands may be almost saturated, which means that more or less all IR-radiation emanating from Earth at that frequency is already absorbed or scattered, and hence that an emission of a GHG that absorbs strongly at this frequency will have a relatively small impact on the radiative balance. In contrast, GHGs that absorb in the atmospheric window (8-12 μm), which is far from saturated, will have a more linear relationship between forcing and increase in concentration.

Figure 3 describes the change in the radiative balance at the tropopause from 1750 to 2005 expressed in terms of radiative forcing. It is clear that CO_2 is the largest single contributor to the change in the radiative balance. It is also evident that the cloud albedo effect constitutes the largest single uncertainty.

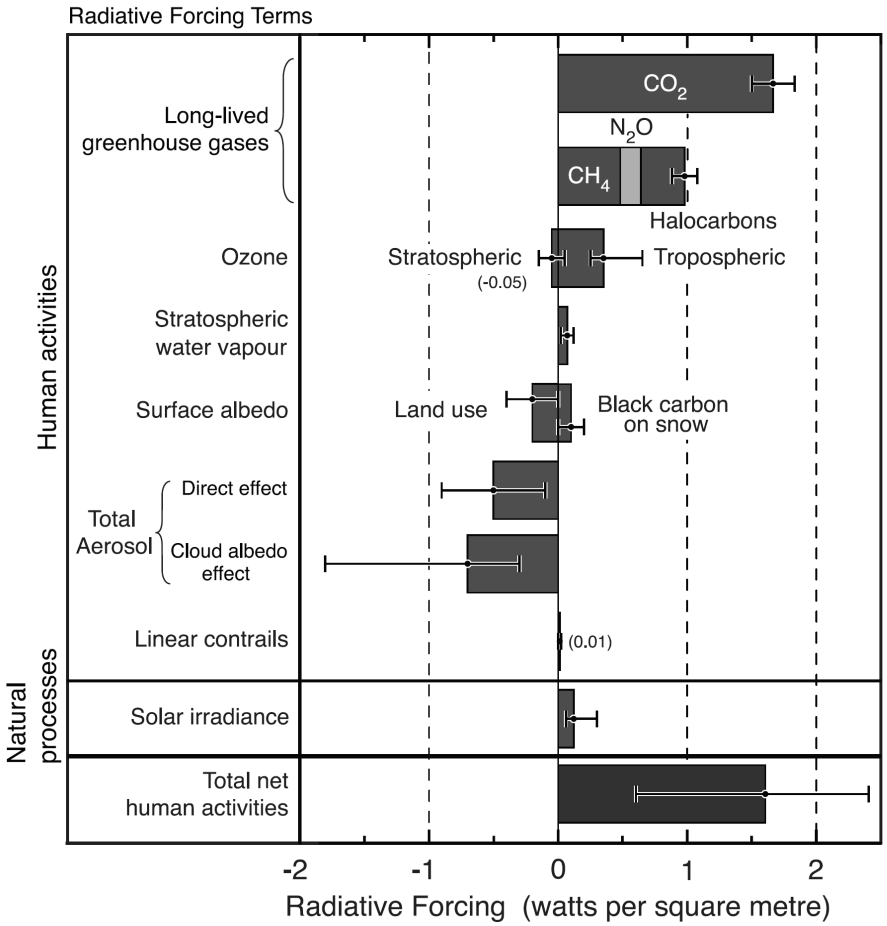

Figure 3. Radiative forcing of climate between 1750 and 2005. Summary of the principal components of the radiative forcing of climate change. The values represent the forcings in 2005 relative to the start of the industrial era (about 1750). Human activities cause significant changes in long-lived gases, ozone, water vapour, surface albedo, aerosols and contrails. The only increase in natural forcing of any significance between 1750 and 2005 occurred in solar irradiance. The thin black line attached to each bar represents the range of uncertainty for the respective value. From AR4, IPCC [2].

It is difficult to translate a radiative forcing into an actual temperature change at Earth's surface. One way to describe this climate response is by introducing the climate sensitivity, λ. Here, the surface temperature change is linearly related to the radiative forcing,

$$\Delta T_s = \lambda \Delta R, \tag{1}$$

which thus treats the initial and the final climate states as being at equilibrium. ΔT_s is the change in global and annual mean surface air temperature, and ΔR is the radiative forcing. It is standard practice to include the fast feedback processes, such as the water vapour feedback, in this definition of climate sensitivity.

The feedback is the response of the climate system to the initial change, i.e. the response to the radiative forcing. The feedback might amplify or dampen the initial change. The water vapour feedback is projected to be the single largest feedback, and since H_2O is a GHG, it is a positive feedback. How does the water vapour feedback work? A positive radiative forcing will lead to higher temperatures and thus more evaporation, i.e. more water vapour in the troposphere, which in turn increases the radiative forcing and consequently the surface temperature will increase as well. The reason why water vapour is considered a feedback and not a forcing has to do with its short residence time in the troposphere, which is approximately 10 days.

1.3 Carbon sequestration

There are several ways in which to reduce anthropogenic CO_2 emissions: increase the use of renewable sources of potential energy, such as hydro-, wind and solar power; promote CO_2 uptake in biomass; switch from fossil fuels to biomass; expand the nuclear power sector; and finally, reduce global energy intensity. However, it is likely that society will remain highly dependent on fossil fuels for some time to come. Hence an additional alternative to reduce the net emissions of CO_2 has been suggested: combining the use of fossil fuels with CO_2 capture and storage (CCS), also known as carbon sequestration, which, in an idealized case, would yield a "carbon neutral" source of heat and power. Because more or less undiluted CO_2 is needed for storage, the first step of CO_2 sequestration is the separation of CO_2 from any other gases present in the flue gas, i.e. primarily nitrogen. This is accomplished in the capture part of CCS, as will be discussed below. Implementation of CCS is actually feasible on any large stationary point source of CO_2, e.g. power plants using fossil fuels or biomass, steel and cement industries, refineries and natural gas processing facilities. CCS is a novel concept that can be based on old, or proven, technology.

1.3.1 CO_2 capture

The capture part of CCS can be achieved in a variety of ways [5], most of which are associated with a substantial energy penalty. Three major paths to achieve CO_2 separation can be distinguished: (a) post-combustion, where CO_2 is separated from a CO_2-rich gas stream, e.g. the flue gas from a conventional power plant, by for example chemical absorption, (b) pre-combustion, which involves the conversion of a carbon containing fuel to a mixture of CO_2 and H_2, from which CO_2 is separated prior to combustion, and finally (c) oxyfuel, where

the fuel is burnt in a mixture of oxygen and recycled CO_2 instead of air, which requires a primary air separation step. Chemical-looping combustion is a CO_2 capture technology that is often classified as an oxyfuel process, but could more adequately be placed in a separate category: unmixed combustion, together with fuel cells.

1.3.1.1 Chemical-looping technologies

Chemical-looping combustion (CLC), which is the topic of this thesis, has also been referred to as unmixed combustion, since the fuel, e.g. natural gas, and the oxidizing agent, e.g. air, are kept apart. The segregation of fuel and combustion air, which is achieved by means of an oxygen carrier, is the reason why the CO_2 separation can be inherently achieved in CLC.

Chemical-looping can also be used for the production of hydrogen from natural gas with capture of carbon dioxide. The technique, chemical-looping reforming (CLR) relies on the same principles as CLC. The difference between the two concepts lies in the desired output, which in CLC is heat, and in CLR primarily hydrogen. CLR was first proposed by Mattisson and Lyngfelt in 2001 [6] and has since been widely investigated [7,8,9,10,11], but it will not be further discussed in this thesis.

The overall advantage with chemical-looping technologies is the elimination of the energy intensive gas separation steps that are associated with other capture technologies.

1.3.2 CO_2 storage

Available options for the final handling of produced CO_2 include underground geological storage, ocean storage and mineral carbonation. Geological storage, which presently seems to be the most plausible alternative, basically means returning the carbon to whence it came. Potential geological storage sites include depleted oil and gas reservoirs, deep unmineable coal seams, deep unused saline water-saturated reservoir rocks (aquifers), and sites where enhanced oil recovery using CO_2 is practiced. The engineered injection of CO_2 into subsurface geological formations has been undertaken since the 1970s for the purpose of enhanced oil recovery. The first large-scale CO_2 storage project was started in 1996 by Statoil and its partners at the Sleipner gas field in the North Sea, where almost 1 Mt CO_2 has been injected annually in the Utsira aquifer [5].

1.3.3 CO_2 transportation

Transportation of CO_2 from production site to storage site should constitute no major obstacle. Large-scale transportation of CO_2 has already been practiced for decades for use in enhanced oil recovery. In USA, 2500 km of pipeline transports an annual amount of more than 40 Mt CO_2 [5].

2. Chemical-looping combustion

Chemical-looping combustion (CLC) is a combustion concept with inherent separation of CO_2. The process uses a solid oxygen carrier, which consists of metal oxide, to transfer the oxygen from air to fuel. The particulate oxygen carrier circulates in a reactor system composed of a fuel reactor, where oxygen-carrier particles are reduced by the fuel, and an air reactor, where the particles are regenerated to the oxidized state. A general representation of the CLC concept is shown in figure 4. In this thesis, MeO and Me are denotations used to describe a generic oxygen carrier in its oxidized and reduced forms. It should be pointed out that the reduced form of the oxygen carrier (Me) may very well be a metal oxide as well, albeit in a more reduced form than the oxidized form.

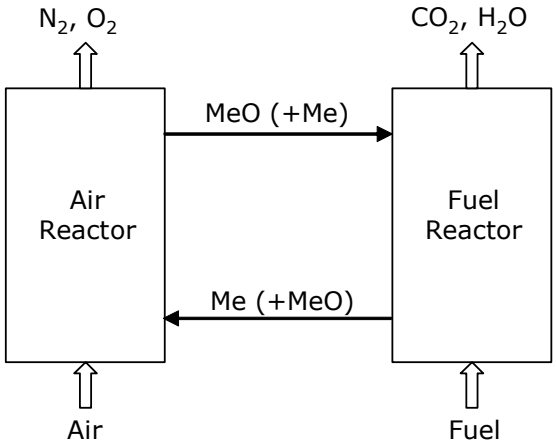

Figure 4. Schematic representation of chemical-looping combustion. After condensing the water produced in the fuel reactor, pure CO_2 is obtained. The gas stream exiting the air reactor contains nitrogen and unreacted oxygen.

In CLC, a hydrocarbon fuel, i.e. natural gas reacts with the metal oxide according to

$$C_nH_{2m} + (2n + m)\,MeO \rightarrow n\,CO_2 + m\,H_2O + (2n + m)\,Me \quad (2)$$

This reaction takes place in the fuel reactor and produces only CO_2 and H_2O. Thus, after condensing the steam, pure CO_2 is obtained. The reduced metal oxide in the oxygen-carrier particles is regenerated in the air reactor,

$$Me + \tfrac{1}{2}\,O_2 \rightarrow MeO. \quad (3)$$

The flue gas from the air reactor will contain nitrogen and some unreacted oxygen. Reaction (3) is invariably highly exothermic, whereas reaction (2) can be either endo- or exothermic, depending on fuel and on the metal oxide used as oxygen carrier. However, the total amount of heat evolved from the reactions (2) and (3) is the same as in conventional combustion. It should be mentioned that not all of the metal oxide/metal reacts in each cycle, i.e. that full conversion from MeO to Me and back to MeO, as indicated by reactions (2) and (3) is not obtained, nor necessarily desired, in a real system.

2.1 Fluidization

When a bed of particles is subjected to an upward fluid flow with a velocity greater than the minimum fluidization velocity (u_{mf}), the bed becomes fluid-like, with fluid-like properties. u_{mf} is reached when the drag force by upward moving gas equals the weight of particles in the bed. The required gas velocity depends on the properties of the gas and particles. The terminal velocity (u_t) is the gas velocity at which the drag force acting on a single particle is equal to the weight of the particle. When $u_{superficial} > u_t$, entrainment occurs, which means that particles are carried away from the fluidization vessel by the gas stream.

2.2 Origins of CLC

The CLC concept was first presented in 1954 by Lewis and Gilliland as a means of CO_2 production [12]. In the 1980s, it was suggested that CLC had potential to increase the thermal efficiency of a power process by using the fuel reactor as a heat sink [13,14]. However, this would place a high demand on the reactivity of the oxygen carrier as well as the design of the reactor system, and this option is not considered here. The use of CLC as a CO_2 capture technology was recognized in 1994 by Ishida et al. [15]. In 2001, Lyngfelt et al. [16] proposed a reactor design with two interconnected fluidized beds, between which the solid oxygen carrier is circulated. In this design (figure 5), the air reactor is a high velocity fluidized bed that provides the driving force for particle carryover to the fuel reactor, which is a bubbling fluidized bed.

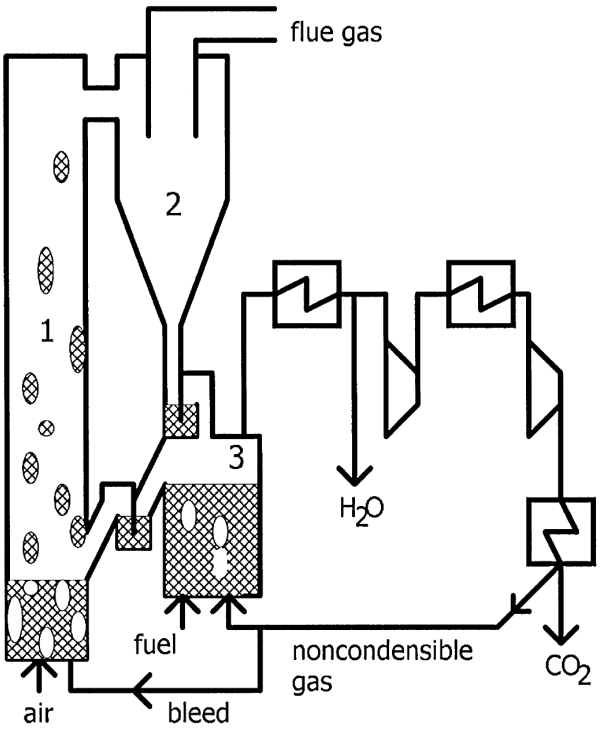

Figure 5. The CLC process as suggested by Lyngfelt et al [16]. The process is based on CFB-technology with a high velocity riser (1), a cyclone (2) for separation of the streams of solids and gas, and a bubbling bed (3) where particles are reduced in a reaction with fuel. The fuel reactor exit gas is successively cooled and compressed in order to condense the water and obtain storage-ready CO_2. A possible option could be to recycle non-condensable gases to the fuel reactor, and a fraction could be bled to the riser to avoid accumulation of non-combustible gases, such as N_2, in the recycling loop.

2.3 Oxygen carriers

Most of the work on chemical-looping technologies has been focused on the development and testing of oxygen carrier particles. Most reported work on CLC has been accomplished using oxygen-carrier particles where the active component is combined with an inert material [17], although a few authors have presented data from tests with pure metal oxides, e.g. iron ore [18] and ilmenite [19]. A thorough thermodynamic analysis of different metal oxides [20] showed that Fe_2O_3/Fe_3O_4, Cu_2O/Cu, Mn_3O_4/MnO and NiO/Ni were most suitable for CLC processes using natural gas as fuel. Options for oxygen-carrier preparation include freeze-granulation [21], spray-drying [22], impregnation [23], co-precipitation [24], spin-flash drying (paper I) and a few others.

Oxygen carriers can be characterized from a physical, chemical, economical or environmental viewpoint. The ideal oxygen carrier should have

- A porous structure with a large surface area, thus increasing the

accessibility of the reacting gases to the metal oxide.

- High rates of oxidation and reduction. This is necessary in order to minimize the size of the reaction chambers and the amount of needed material.
- High fluidizability and resistance to agglomeration.
- Sufficient mechanical strength and stability in fluidized beds and low tendency of attrition and fragmentation. It is desirable to minimize the production of fines and maximize particle lifetime.
- Sufficient oxygen ratio,

$$R_0 = \frac{m_{ox} - m_{red}}{m_{ox}}, \tag{4}$$

where m_{ox} and m_{red} are masses of a fully oxidized and a fully reduced sample. A high R_0 is usually considered an advantage since it means that excessive circulation rate of the solid material can be avoided.

- High melting temperature in oxidized as well as reduced form. Materials become soft when their melting temperature is approached. Operating a CLC system close to the melting temperature of the oxygen carrier may result in agglomeration.
- Capability to convert the fuel entirely to CO_2 and H_2O, i.e. no thermodynamical limitations.
- Low cost with respect to production and raw materials.
- Environmental compatibility and low toxicity.

An additional feature of the ideal oxygen carrier is that no or little solid carbon should form on particles. Coking may occur through pyrolysis,

$$C_nH_{2m} \rightarrow n\,C + m\,H_2, \tag{5}$$

or through the Boudouard reaction,

$$2\,CO \rightarrow C + CO_2, \tag{6}$$

and it is well established that both reactions can be catalyzed by metallic surfaces. However,

problems with coking are not usually encountered in the CLC-environment, as has been demonstrated, for example, in the 10-kW unit (papers I and II). This is likely due to the high concentration of H_2O and CO_2 in the fuel reactor which tend to counteract the formation of carbon.

The major part of the experimental research done on oxygen carriers has been performed in laboratory batch reactors, where particles are subjected alternately to oxidizing and reducing conditions, thus simulating the chemical-looping process. Investigations in continuous chemical-looping systems are necessary in order to obtain a more comprehensive understanding of the behaviour of the particles. A number of chemical-looping combustors for gaseous fuel ranging from 0.3-120 kW_{th} have been designed and operated for a combined total of several hundred hours [25,26,27,28,29,30]. A 10-kW CLC unit has been constructed for solid fuels [19].

2.4 The CLC reactor system

The CLC units used for the experiments presented in this thesis were designed as interconnected fluidized beds, with the oxygen-carrier particles acting as bed material. Fluidization offers a large contact area between gaseous and solid phase, and the use of interconnected fluidized beds is a proven technology for moving particles between reaction chambers.

The amount of material needed in the fuel reactor depends on the rate of reaction between the oxygen carrier and the fuel. Similarly, the bed mass in the air reactor is determined by the rate of particle oxidation.

The two factors determining the size of the solids flux are (a) oxygen needed for oxidation of the fuel, and (b) heat needed to sustain the desired reaction temperature, in the case of an endothermic reaction between particles and fuel.

The solids flux determines the difference in conversion of particles leaving and returning to the air reactor, i.e. how much of the available oxygen in the particles that is consumed in the fuel reactor. The degree of oxidation of the particles, also called particle conversion, X, is defined as the ratio of the amount of available oxygen present in the carrier and the amount of available oxygen present in the carrier when fully oxidized,

$$X = \frac{m_{actual} - m_{red}}{m_{ox} - m_{red}} \tag{7}$$

where m_{actual} is the actual mass of the carrier in its partially oxidized state, m_{ox} is the mass of the sample when fully oxidized, and m_{red} the mass of the sample in the fully reduced form. The particle conversion in the air reactor, X_{AR}, is larger than that in the fuel reactor, X_{FR}, during normal combustion conditions. The difference in particle conversion,

$$\Delta X = X_{AR} - X_{FR}, \tag{8}$$

hence becomes a function of the particle circulation; increasing the solids flux in the reactor system leads to a decrease in ΔX.

Gas leakages between the air and fuel reactors have to be minimized. Leakages from the fuel reactor to the air reactor would lead to CO_2 escaping into the atmosphere and would thus decrease carbon capture efficiency, whereas a leakage of air to the fuel reactor would dilute the CO_2 stream with nitrogen, which might result in extra costs for CO_2 purification. The installation of particle seals between the air and fuel reactors is an effective way of preventing gas leakages.

2.5 Process studies

A number of literature studies have investigated the possibility to combine power cycles with the chemical-looping system. These process simulations have been performed using different types of oxygen carriers and natural gas or synthesis gas as fuel. Reviews of the literature in this area can be found in the doctoral theses of Wolf [31] and Naqvi [32]. The process studies demonstrate that it is theoretically possible to achieve high thermal efficiencies using CLC integrated with CO_2 capture. However, if very high efficiencies are to be reached using gaseous fuels, combined cycle processes involving pressurized fluidized beds would have to be used. It should be pointed out that the temperatures normally used in combined cycles are higher than those at which oxygen carriers usually have been tested.

2.6 CLC using NiO-based oxygen carriers and natural gas as fuel

Nickel-based oxygen carriers have a number of advantages, the most important of which are high melting temperature and high rate of reaction with gaseous fuels. R_0 for Ni/NiO is also relatively high (0.21). On the other hand, nickel is expensive and more toxic than other metals identified as suitable as oxygen carriers.

Nickel oxide and fuel (methane), and nickel and oxygen react ideally according to:

Fuel reactor: $4\ NiO + CH_4 \rightarrow 4\ Ni + 2\ H_2O + CO_2$ (9)
$\Delta H_{1000°C} = 133.6$ kJ/mole CH_4

Air reactor: $2\ Ni + O_2 \rightarrow 2\ NiO$ (10)
$\Delta H_{1000°C} = -468.5$ kJ/mole O_2

The reaction between NiO and methane is endothermic, and consequently there will be a temperature drop in the fuel reactor. When reactions (9) and (10) are combined, the remaining components represent conventional combustion of methane with oxygen:

$CH_4 + 2\ O_2 \rightarrow CO_2 + 2\ H_2O$ (11)
$\Delta H_{1000°C} = -803.4$ kJ/mol CH_4

As mentioned in the introduction, oxygen carriers based on nickel cannot completely convert methane to H_2O and CO_2. There will be small amounts of CO and H_2 present in the product gas [33]. The amounts of incombustible gases are functions of the temperature in the fuel reactor and can be calculated thermodynamically using minimization of Gibbs free energy. Here, this calculation was carried out using HSC Chemistry 5.1 with 100% CH_4 over an excess of NiO. The gaseous species included in the calculation were CH_4, CO_2, CO, H_2O, H_2 and O_2, and the solid phases included were C, NiO and Ni. Table 1 shows equilibrium fractions of CO and H_2.

	T (°C)			
	650	750	850	950
CO (%)	0.22	0.40	0.65	0.98
H_2 (%)	0.87	1.02	1.16	1.31

Table 1. Equilibrium fractions of CO and H_2 during combustion with CH_4 after condensation of H_2O.

Nickel acts as a catalyst in steam reforming of natural gas:

$$C_nH_{2m} + n\ H_2O \rightarrow n\ CO + (n + m)\ H_2. \quad (12)$$

Through this steam reforming mechanism, nickel contributes to the oxidation of the natural gas, which explains why it is beneficial to keep the solids circulation low when operating a chemical-looping combustor with a NiO-based oxygen carrier. As explained above, ΔX is a measure of the amount of available oxygen in the oxygen carrier. Low circulation means that X_{FR} is low, which in turn means that many Ni-sites are available for steam reforming. Hence, the solids circulation rate affects the conversion of the natural gas. In addition, Ni-sites may also catalyze pyrolysis, i.e. reaction (5).

2.7 Purpose of work

The oxygen carrier is the key component in chemical-looping technology, and the large-scale application of CLC is still dependent upon the availability and performance of oxygen carriers. The purpose of the work presented here was to investigate the feasibility of making a good oxygen carrier at a reasonable production cost by using commercially available raw materials and commercial preparation methods. The work focuses primarily on the long-term performance of oxygen carriers in continuous CLC operation. The effects on particles of long-term exposure to a CLC environment cannot be otherwise evaluated.

3. Experimental

Detailed descriptions of the two chemical-looping combustors used in the experiments can be found in papers I and II (10-kW unit) and paper III (300-W unit).

The fuel used in the experiments here presented was natural gas, which is composed of approximately 90% methane, 6% ethane, 3% higher hydrocarbons, and 1% N_2 and CO_2. The lower heating value of the fuel is 39.6 MJ/m_n^3. The fuel load is per default reported as the fuel power (e.g. 10 kW), which is defined on thermal basis as the product of the lower heating value and the (normal) volumetric flow according to

$$P_{th} = H_i \dot{V}_{fuel} . \tag{13}$$

3.1 Comparison of 10 kW and 300 W units

Both units utilize the concept of interconnected fluidized beds with an air reactor and a fuel reactor where the gas velocity in the air reactor provides the driving force for particle circulation. Separation of particles from the gas flow is achieved by a cyclone in the 10-kW unit and by simply expanding the cross-section above the air reactor in the 300-W unit. The 10-kW unit has a weir in the fuel reactor which determines the solids inventory, whereas the inventory of the fuel reactor in the smaller unit is determined by (a) the total solids inventory and (b) the height of a water column, through which the pressure difference – and hence the relative bed height – between the air and fuel reactors can be altered. Particle seals are used in both systems to prevent gas leaks between the reactors.

The smaller reactor system is placed inside an oven, which makes operation more convenient: the heating is faster and hence the start-up period shorter. The oven is easily opened and requires no removal of insulation, which makes the whole reactor system easily accessible, a feature that (a) facilitates exchange of particle inventory, and (b) means that technical problems can be quickly addressed. This is an obvious advantage in comparison to the 10 kW unit.

In the larger unit, it is possible to calculate the actual circulation by a heat balance over the fuel reactor. In paper III, the temperature difference between the air and fuel reactors in the

300-W unit is used as a measure of circulation. However, it is an approximate method that only provides a relative measure of circulation.

The superficial velocity used in the reactor system is approximately 0.15 m/s for the reacted gas in the fuel reactors of both the 10-kW unit and the 300-W unit, assuming a temperature of 850°C, whereas the velocity in the air reactor, after compensating for the oxygen depletion in the combustion air due to reaction, differs between the reactor systems:

- in the 10-kW unit, the typical superficial velocity (1000ºC and $\lambda = 1.25$) is 2.5 m/s in the riser and 0.7 m/s in the air reactor,
- in the 300-W unit, the typical velocity (850 ºC and $\lambda = 1.3$) is 0.7 m/s in the upper part of the air reactor.

Leakages of gas between the air and fuel reactors are very small in the 10-kW unit. In fact, they are below the detection limit. In the 300-W unit, however, there are leakages in both directions. The extent of these leakages was investigated in paper III and it was shown that the leakage from the fuel to the air reactor is about 5% of the added carbon, whereas the leakage flow in the opposite direction is much smaller, 0-0.2% of the added air, which could oxidize a maximum of 0.2% of the added fuel.

Due to attrition and fragmentation of particles, fine material is continuously produced during CLC operation. In order to estimate the particle life time, the loss of fines (LoF) is a useful parameter. It is defined as the fractional loss of small particles per unit time, or:

$$LoF = \frac{m(\text{elutriated particles} < 45\ \mu\text{m during } \Delta t)}{\Delta t \cdot m(\text{total solids inventory})}\ [\text{h}^{-1}] \qquad (14)$$

The amount of fines produced can not be determined in the 300-W unit, due to the small solids inventory. However, the 300-W unit is not designed for long-term evaluations of particles, and hence the loss of fines is a measure more pertinent to tests in the 10-kW unit. It is plausible that the loss of fines is smaller in the 300-W unit since (a) porous discs are used for gas distribution instead of nozzles, and (b) the gas velocity in the air reactor is lower.

3.2 Oxygen carriers used in the experiments

Four different NiO-based oxygen carriers were used in the experiments: one particle produced

by spin-flash drying (N-IFP, paper I), two spray-dried particles (N-VITO and N-VITOMg, paper II and III), and one impregnated particle (N-CSIC, paper III). The important characteristics of the oxygen carriers used in the study are summarized in table 2. Apparent density is measured on particles sized 125-180 μm and calculated assuming a void between particles of 37%. The crushing strength is measured on particles of size 180-212 μm. The GRACE particle [34,35], which was used in CLC operation in a 10-kW unit for more than 100 h with very high conversion of fuel [25], has been included for comparison.

Table 2. Characteristics of the oxygen carriers used in the experiments and the GRACE particle.

Denotation used in this study	Active material	Fraction of active material ($\%_{mass}$)	Support material	Production method	Crushing strength (N)	BET surface area (m^2/g)	Apparent density (kg/m^3)	Manu-facturer
N-IFP	NiO	60	$NiAl_2O_4$	Spin-flash drying	5.3		4400	IFP
N-VITO	NiO	40	$NiAl_2O_4$	Spray-drying	2.3	0.7	3600	VITO
N-VITOMg	NiO	40	$NiAl_2O_4$ (~42%) and $MgAl_2O_4$ (~18%)*	Spray-drying	2.0		3250	VITO
N-CSIC	NiO	18	α-Al_2O_3	Hot impregnation	4.8		2340	CSIC
GRACE	NiO	40	$NiAl_2O_4$	Freeze-granulation	2.5	0.4	3800	

*assuming that all added MgO reacted with Al_2O_3.

It is important to point out that, unlike the GRACE particle, the IFP- and VITO-particles were prepared by commercial – i.e. more economically feasible – production methods. Furthermore, in the case of the VITO-particles, the starting materials used were commercially available materials, and not high-purity substances. N-CSIC is an impregnated oxygen carrier that was used in a mixed batch of oxygen carriers in one test in the 300-W unit in order to improve the methane conversion.

SEM images of fresh particles (i.e. particles not subjected to CLC) can be seen in figure 6. The physical appearance of N-VITOMg (not shown) is very similar to that of N-VITO.

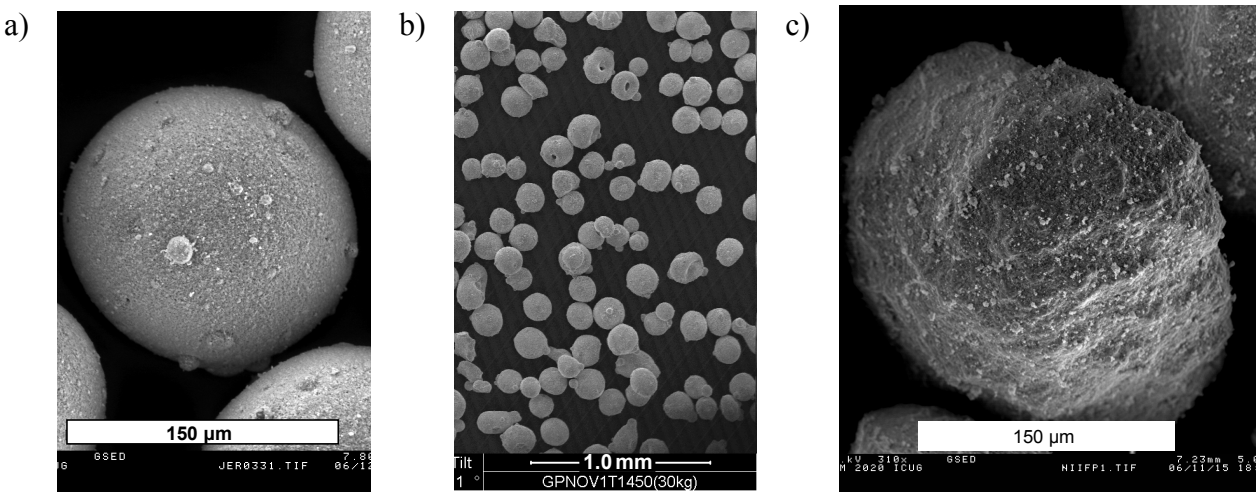

Figure 6. (a) and (b) are SEM images of fresh N-VITO; (c) shows fresh N-IFP.

The minimum fluidization and terminal velocities (u_{mf}, u_t) shown in table 3 were calculated according to relations by Kunii and Levenspiel [36]. Values for sphericity, ϕ, are based on SEM images of the particles and are therefore somewhat uncertain. The minimum fluidization voidages, ε_{mf}, are estimations for a loosely packed bed with particles of indicated sphericity, as suggested by Kunii and Levenspiel. The average particle diameters are calculated from the particle size distribution of respective oxygen carrier.

Particle	ϕ	ε_{mf}	$\bar{d}_p$ (µm)	u_t (m/s)	u_{mf} (m/s)
N-IFP	0.8	0.50	130	0.70	0.015
N-VITO	0.9	0.45	135	0.65	0.010
N-VITOMg	0.9	0.45	135	0.60	0.010
N-CSIC	0.8	0.50	180	0.70	0.015

Table 3. Terminal and minimum fluidization velocities for the particles used in the study. u_t is calculated for air at 1000ºC and u_{mf} is calculated for a mixture of CO_2 and steam at a ratio of 1:2, corresponding to full oxidation of methane, at 850ºC.

3.3 Estimating the solids circulation

The solids circulation determines the difference in particle conversion between the fuel and air reactor. A low circulation rate means that the conversion difference is high, and thus, the particles in the fuel reactor will contain considerable amounts of metallic Ni. As described above, this will have implications for the fuel conversion, since Ni-sites catalyze steam reforming.

Neither in the 10-kW unit nor in the 300-W unit can the solids flux be directly measured. However, for a specific oxygen carrier circulating in the 10-kW unit, the solids flux can be

expressed as a function of the gas velocity and the pressure drop at the top of the riser. According to Johansson et al. [37], the following correlation can be used to calculate the net solids flux for a specific unit geometry:

$$G_s = \rho_{exit}(u - u_t) = -\frac{1}{g}\frac{dp}{dh}(u - u_t), \quad (15)$$

where u is the superficial velocity, u_t is the terminal velocity of an average sized particle and ρ_{exit} is the particle density at the riser exit. Since it is not possible to obtain solid samples from the top of the riser, u_t is based on the average particle size. The applicability of this expression depends on (a) the actual value of u_t at the top of the riser, (b) accuracy in pressure drop measurement in the upper part of riser, and (c) the ratio of solids externally recirculated to that internally separated at the top of the riser.

For the 10-kW unit, the solids circulation calculated by equation (15) is believed to give a significant overestimation. Nevertheless, it provides a useful means for comparing particle circulations during the entire test period. G_s multiplied with the cross sectional area of the riser is referred to as circulation index, although it is a non-dimensionless property with units kg/min.

Particle circulation in the 10-kW unit can also be calculated by comparing the temperatures of particles entering and exiting the fuel reactor. Since the reaction in the fuel reactor is endothermic for NiO-based particles, there is a temperature drop which is related to the magnitude of the solids flux; a low solids flux leads to a sharp temperature decrease and vice versa. This temperature difference was used to estimate the circulation in papers I and II. A detailed description of the method, including assumptions and simplifications, is presented in paper II.

3.4 Data evaluation

Oxygen and the carbon containing gases are continuously measured on-line, whereas hydrogen is measured only intermittently. Carbon monoxide, methane, hydrogen and carbon dioxide concentrations are presented as fraction of total carbon from the fuel reactor according to

$$f_i = \frac{x_i}{x_{CO_2} + x_{CO} + x_{CH_4}}, \tag{16}$$

where i represents CO_2, CO, CH_4 and H_2, and x is the molar fraction of the substance indicated by the sub-script in dry exit gas from the fuel reactor. The measured concentrations of CO, CO_2, CH_4 and H_2 are somewhat lower due to mixing with nitrogen from the particle seals.

4. Results and discussion

In papers I and II, the 10 kW unit is used to study the effects of long-term CLC operation on oxygen-carrier particles. In paper III, the 300 W unit is used to evaluate two spray-dried particles, individually and mixed, with the purpose of finding the optimally performing batch with respect to fuel conversion.

4.1 Papers I and II: long-term tests in 10-kW reactor system

Paper I evaluates the performance of N-IFP and paper II that of N-VITO and N-VITOMg. Prior to the experiments accounted for in papers I and II, the Chalmers 10 kW unit had been used for testing of the GRACE-particle, and the results from those tests will be used here for comparison.

4.1.1 Duration of fuel operation

The GRACE-particle was tested for 105 h; N-IFP was subjected to 160 h of operation; and the VITO-particles were used for > 1000 h of operation with fuel in the 10-kW reactor system.

Of the 1016 h of fuel operation achieved with the VITO-particles, the first 405 h were accomplished using a single batch of N-VITO. The last 611 h were achieved using a $50/50_{mass}$-mixture of (i) N-VITO-particles used for 405 h, and (ii) fresh N-VITOMg. Thus, at the conclusion of the test series, approximately half of the particles in the reactor system had been subjected to > 1000 h of chemical-looping combustion, whereas the other half had been used for 611 h. The idea behind using a mixed oxide system of these particular oxygen carriers originated from findings that the addition of MgO or the use of $MgAl_2O_4$ has a profound effect on the methane conversion [38]. However, the oxygen transport capacity is relatively low for this type of oxygen carrier, especially at lower temperatures. Hence, the mixture of these two particles may result in a more optimal system, in comparison to utilizing the oxygen carriers alone.

4.1.2 Fuel conversion

Generally, conversion of the natural gas improves with increasing fuel-reactor temperature and decreasing rate of particle circulation. This has been observed for all particle batches. For the GRACE-particle and N-IFP, the fraction of CO exiting the fuel reactor followed the

thermodynamical equilibrium quite closely, whereas for the VITO-particles, CO fractions were slightly above equilibrium.

Table 4 shows optimum performance of the different particles at T_{FR} = 800-850ºC. Here, the hydrogen fraction is obtained assuming that the water-gas shift reaction,

$$CO + H_2O \leftrightarrow H_2 + CO_2, \tag{17}$$

is at equilibrium and that the ratio H_2O/CO_2 = 1.85, which is true when oxidation of the natural gas is complete, since the H/C-ratio is 3.7, as previously stated. The equilibrium constant, K, is obtained from HSC Chemistry 5.1.

The combustion efficiency is calculated according to

$$\eta_{comb} = 1 - \frac{H_{i,CO}\dot{V}_{CO} + H_{i,CH4}\dot{V}_{CH4} + H_{i,H2}\dot{V}_{H2}}{H_{i,fuel}\dot{V}_{fuel}}, \tag{18}$$

where H_i is the lower heating value and $\dot{V}$ is the volumetric flow (m_n^3/s).

Table 4. Optimum performance of oxygen carriers used in 10-kW unit at T_{FR} = 800-850ºC.

	P_{th} (kW)	T_{FR} (C)	K	f_{CH4} (%)	f_{CO} (%)	f_{CO2} (%)	f_{H2} (%)	η_{comb} (%)
GRACE	10	800	1.06	0.15	0.4	99.45	0.78	99.5
N-IFP	11	850	0.89	0.35	0.65	99.0	1.07	99.1
N-VITO	10	840	0.92	0.9	1	98.1	1.71	98.2
N-VITO & N-VITOMg	10	850	0.89	0.23	1.26	98.5	2.08	98.7

For the GRACE-particle, the highest fuel conversion was obtained at 800ºC. At this temperature, the optimum solids circulation was reached.

During normal stable operation, the fuel-reactor temperature is tightly linked to the solids circulation. When the temperature in the air reactor is 1000ºC, which is the normally used temperature, the fuel-reactor temperature is usually 800-900ºC. It is possible to investigate lower temperatures at start-up, and also by changing the temperature of the incoming particles, i.e. by decreasing the temperature in the air reactor. This latter option, however, is

not normally used, since it requires substantial cooling flows to remove heat evolved in the exothermic reaction.

Operation with the GRACE-particle below 800ºC was reported to result in an increase of CO, but this might have been an effect of low circulation, i.e. insufficient supply of oxygen [25]. With N-IFP, temperatures as low as 660ºC were investigated, and it was found that CO followed the equilibrium. Using the mixed VITO-batch, the fuel reactor was operated < 650ºC with little CH_4 in the fuel-reactor exit gas, but a lot of CO. As in the case with the GRACE-particle, this might have been an effect of low circulation.

4.1.3 Loss of fines

The loss of fines was used to calculate the expected particle life time for the GRACE-particle, the IFP-particle, and the mixed VITO-batch. The expected lifetimes for the GRACE- and IFP-particles were 40000 h and 4500 h, respectively. A lot of fines were produced during operation with N-IFP, which was evident both during handling of the particles and by studying the mass balance. Nevertheless, it is possible that a fraction of the fines may have escaped through the filter bags, where elutriated material from the air reactor is collected. Prior to the VITO-runs, the filter bags were replaced with new ones that had lower cut-off diameter. The collection and handling of fines produced in the VITO-runs followed a meticulous procedure, and it is believed that the calculated expected lifetime, 33000 h, is a reliable estimation as far as mechanical degradation is concerned.

4.1.4 Agglomeration

Sintering of particles is a complex process which is influenced primarily by temperature and chemical environment [39]. Gas velocity and mixing conditions in the fuel reactor also affects sintering behaviour of particles. A low velocity implies more physical contact between particles.

The GRACE-particle showed no signs of agglomeration during operation in the 10 kW unit. N-IFP agglomerated during sub-stoichiometric (λ = 0.8) operation. The operation with N-VITO resulted in the formation of agglomerates on a few occasions. Massive agglomeration occurred when the fuel feed was unintentionally decreased.

4.1.5 Reactivity and mechanical strength

Similar observations were made for the GRACE and VITO-particles concerning mechanical strength: a slight increase was observed as an effect of operation. The reactivity of the GRACE- and IFP-particles did not change during operation, whereas the reactivity for the N-VITO and the mixed VITO-batch actually increased during an initial period of time (approximately 50 h).

4.1.6 Particle conversion and circulation

For N-IFP, the rate of circulation was calculated to 2-3 kg/min at 11 kW, which would correspond to $\Delta X = 0.2$.

For the mixed VITO-batch, the rate of circulation was calculated to 2-4 kg/min at 10 kW. This circulation was classified as "moderate" to "high", and the corresponding $\Delta X = 0.14$-0.27. The method based on a heat balance over the fuel reactor could not be used to obtain the rate of particle circulation at "low" circulation because the requirement of minor temporal changes in the fuel-reactor bed temperature could not be met.

In order to obtain the particle conversion at low circulation, the fuel feed was cut and replaced with air following an experiment at low circulation, while simultaneously, fluidization in the particle seals was terminated, which effectively stopped the circulation of particles. Hence the amount of oxygen needed for complete particle oxidation was obtained, and X_{FR} could be calculated, which, combined with a knowledge of X_{AR} (0.98), resulted in $\Delta X = 0.4$. A more detailed description of the procedure is given in paper II.

4.2 Paper III: comparison of oxygen carriers

Spray-dried particles were investigated in a continuous 300-W reactor system. An attempt to optimize the oxygen-carrier performance by mixing two different spray-dried Ni-particles was conducted. Here, the reference particle, N-VITO, was combined with N-VITOMg. The former had good oxygen-transport capability while the latter had very good methane-conversion characteristics, as described earlier.

Prior to the experiments carried out in the 300-W reactor system, smaller batches of particles were tested batch-wise in a laboratory reactor. These reactivity investigations were conducted

in a fluidized-bed reactor of quartz, and the two spray-dried particles were evaluated individually and mixed. The investigations indicated that mixing of the two oxygen-carrier particles can be beneficial for fuel conversion.

The findings from the batch experiments were evaluated in a 300-W chemical-looping combustor at three temperatures; 750°C, 850°C and 950°C. In general, fuel conversion increased, as expected, with (a) decreased circulation, and (b) increased fuel-reactor temperature. The operation with N-VITO was somewhat unstable, and the fuel conversion was unsatisfactory at $T_{fuel\ reactor}$ = 750°C, but good at the higher temperatures. With the mixture of the two spray-dried particles, operation was stable and, in comparison to the operation with only N-VITO, fuel conversion improved at all three temperatures, especially at 750°C. At low circulation, the fraction of unconverted methane was < 0.1% both at 850°C and 950°C.

Moreover, a third, NiO-based impregnated oxygen carrier was introduced into the mixture in order to improve the methane conversion even further. This particle, composed of 18%$_{mass}$ NiO on α-Al_2O_3, was prepared by CSIC in Spain [40]. Excellent conversion of the fuel was obtained at relatively high circulation with this three-particle mixture.

5. Conclusions

In order to bring the CLC technology to the commercial level, it is important to operate continuous CLC units for long periods of time with oxygen carriers which can be produced with materials available at reasonable cost and which are produced with commercial methods. Although there have been several investigations in continuous reactors earlier, the duration of the tests were often limited and often particles were produced with non-commercial and expensive methods. Hence, this thesis has focused on long-term experiments in a 10-kW chemical-looping combustor. The most important finding presented in this thesis is the successful long-term operation (> 1000 h) using NiO-based particles manufactured by spray-drying of commercial raw materials.

A 300-W CLC unit was used to investigate the possibility to optimize the performance of oxygen carriers by using mixed oxygen carrier batches, and results showed that such optimization was possible.

The main conclusions of the investigations in this thesis are given below.

5.1 Long-term tests in the 10-kW reactor system

5.1.1 Paper I: N-IFP

- An oxygen carrier produced by spin-flash drying was evaluated during 160 h of fuel operation. High fuel conversion to CO_2 and H_2O was achieved. The exit gas stream from the fuel reactor contained typically 0.7% CO, 0.3% CH_4 and approximately 1.3% H_2.
- Investigations of the relationship between CH_4 and circulation confirmed previously presented theories that a large solids flux leads to increased methane concentrations and vice versa.
- No decrease in reactivity was seen during the test period.
- The loss of fines was larger than that observed in previous testing in the CLC prototype. The estimated particle life time was 4500 h.

5.1.2 Paper II: N-VITO and N-VITOMg

- Oxygen-carrier particles prepared from commercially available raw materials by spray-drying were used for > 1000 h of combustion.

- 405 h of fuel operation were accomplished using N-VITO, a particle with NiO ($40\%_{mass}$) as active component and $NiAl_2O_4$ as inert. Another 611 h of operation were accomplished using a mixture of the used N-VITO particles in combination with a similar particle, N-VITOMg. The reason for mixing the two particles was to optimize the performance with respect to fuel conversion.
- In general, fuel conversion increased, as expected, with (a) decreased circulation, and (b) increased fuel-reactor temperature. Compared to the operation with only N-VITO, fuel conversion was improved using the oxygen-carrier mixture, although the fraction of CO was higher. Using the oxygen-carrier mixture, the methane fraction was typically 0.4-1% and the typical combustion efficiency was 98%.
- Agglomeration of particles occurred on a few occasions. The agglomerates were soft, and could be crushed and re-introduced into the reactor system.
- No decrease in reactivity was seen during the test period. During an initial period, the reactivity increased.
- The loss of fines decreased slowly throughout the test period. An estimated particle lifetime of 33000 h was calculated from the loss of fines.

5.2 Comparison of oxygen carriers (paper III)

The oxygen carriers N-VITO and N-VITOMg were evaluated in batch fluidized-bed experiments, individually and mixed, and the mixture turned out to perform optimally. In order to confirm the results obtained in the batch reactor, N-VITO and a mixture of the two particles were evaluated in the 300-W unit:

- The operation with N-VITO was somewhat unstable, and the fuel conversion was unsatisfactory at $T_{fuel\ reactor} = 750°C$, but good at the higher temperatures.
- With the mixture of the two spray-dried particles, operation was stable and, in comparison to the operation with N-VITO, fuel conversion improved at all three temperatures, especially at 750°C. At low circulation, the fraction of unconverted methane was < 0.1% both at 850°C and 950°C.
- Furthermore, a third, NiO-based impregnated oxygen carrier was introduced into the mixture in order to improve the methane conversion even further. Excellent conversion of the fuel was obtained at relatively high circulation with this three-particle mixture.

References

[1] Statens energimyndighet. Energiläget 2007.

[2] IPCC. 2007. IPCC Fourth Assessment Report (AR4). Working Group I: The Physical Science Basis.

[3] National Oceanic and Atmospheric Administration (NOAA), Earth System Research Laboratory: Global Monitoring Division. (http://www.esrl.noaa.gov/)

[4] Harvey, D. 2000. *Global Warming: The Hard Science*. Pearson Education Limited.

[5] IPCC. 2005. IPCC Special Report: Carbon Dioxide Capture and Storage.

[6] Mattisson, T., Lyngfelt, A. 2001. Applications of chemical-looping combustion with capture of CO2. Proceddings of the 2nd Nordic Minisymposium on Carbon Dioxide Capture and Storage, Göteborg, Sweden.

[7] Mattisson, T., Zafar, Q., Lyngfelt, A., and Gevert, B. 2004. Integrated hydrogen and power production from natural gas with CO_2 capture. 15th World Hydrogen Energy Conference, Yokohama, 27th June-2nd July, 2004.

[8] Zafar, Q. 2005. *Investigation of oxygen carrier materials for Chemical-Looping Reforming*, Licentiate Thesis, Department of Chemical and Biological Engineering, Chalmers University of Technology, Göteborg.

[9] Johansson, R. 2003. *Integrerad vätgas- och kraftproduktion utan utsläpp av koldioxid – tillämpning av chemical-looping combustion*, Master Thesis, Chalmers University of Technology, Göteborg, Sweden.

[10] Rydén, M. 2008. *Hydrogen production from fossil fuels with carbon dioxide capture, using chemical-looping technologies*, PhD Thesis, Department of Energy and Environment, Division of Energy Conversion, Chalmers University of Technology, Göteborg, Sweden.

[11] de Diego, L. F., Ortiz, M., Adánez, J., García-Labiano, F., Abad, A., Gayán, P. 2008. Synthesis gas generation by chemical-looping reforming in a batch fluidized bed reactor using Ni-based oxygen carriers. *Chemical Engineering Journal* Volume 144, Issue 2, Pages 289-298.

[12] Lewis, W. K., Gilliland, E. R. 1954. Productions of pure carbon dioxide. US Patent No. 2,665,972.

[13] Richter, H., Knoche, K. 1983. Reversibility of combustion processes. ACS Symp. Ser. 235, Washington, D.C., 71-85.

[14] Ishida, M., Zheng, D., Akehata, T. 1987. Evaluation of a chemical-looping-combustion power-generation system by graphic exergy analysis. *Energy* 12: 147-154.

[15] Ishida, M. and Jin, H. 1994. A new advanced power-generation system using chemical-looping combustion. *Energy* Vol. 19. No. 4. pp. 415-422.

[16] Lyngfelt, A., Leckner, B., Mattisson, T. 2001. A fluidized-bed combustion process with inherent CO_2 separation - application of chemical-looping combustion. *Chemical Engineering Science* 56:3101-3313.

[17] Johansson, M., Mattisson, T., Rydén, M. and Lyngfelt, A. 2006. Carbon Capture via Chemical-Looping Combustion and Reforming. *International Seminar on Carbon Sequestration and Climate Change*, Rio de Janeiro, Brazil, 24-27 October 2006.

[18] Mattisson, T., and Lyngfelt, A. 2001. Capture of CO2 using chemical-looping combustion. First Biennial Meeting of The Scandinavian-Nordic Section of the Combustion Institute, Göteborg, April 18-20, 2001, pp. 163-168.

[19] Berguerand, N., Lyngfelt, A. 2008. Design and operation of a 10 kW_{th} chemical-looping combustor for solid fuels – Testing with South African coal. *Fuel* 87:2713-2726.

[20] Jerndal, E., Mattisson, T., and Lyngfelt, A. 2006. Thermal Analysis of Chemical-Looping Combustion. *Chemical Engineering Research and Design* 84**:**795-806.
[21] Cho, P., Mattisson, T. and Lyngfelt, A. 2004. Comparison of iron-, nickel-, copper- and manganese-based oxygen carriers for chemical-looping combustion. *Fuel* 83:1215-1225.
[22] Ishida, M., Yamamoto, M., Ohba, T. 2002. Experimental results of chemical-looping combustion with $NiO/NiAl_2O_4$ particle circulation at 1200 ºC. *Energy Conversion and Management* 43:1469-1478.
[23] de Diego, L. F., García-Labiano, F., Adánez, A., Gayán, P., Abad, A., Corbella, B. M., Palacios, J. M. 2004. Development of Cu-based oxygen carriers for chemical-looping combustion. *Fuel* 83:1749-1757.
[24] Villa, R., Cristiani, C., Groppi, G., Lietti, L., Forzatti, P., Cornaro, U., Rossini, S. 2003. Ni based mixed oxide materials for CH_4 oxidation under redox cycle conditions. *Journal of Molecular Catalysis A: Chemical*. Volumes 204-205:637-646.
[25] Lyngfelt, A., and Thunman, H. Construction and 100 h of operational experience of a 10-kW chemical looping combustor. Chapter 36 in *Carbon Dioxide Capture for Storage in Deep Geologic Formations - Results from the CO_2 Capture Project, Volume 1 – Capture and Separation of Carbon Dioxide From Combustion Sources.* Ed.: Thomas, D. Elsevier Science, London 2005, pp. 625-646.
[26] Johansson, E., Mattisson, T., Lyngfelt, A., Thunman, H. 2006. A 300 W laboratory reactor system for chemical-looping combustion with particle circulation. *Fuel* 85:1428–1438.
[27] Ryu, H. J., Bae, D. H., and Jin, G. T. 2003. Effect of temperature on reduction reactivity of oxygen carrier particles in a fixed bed chemical-looping combustor. *Kor J Chem Eng* 20:960–966.
[28] de Diego, L. F., García-Labiano, F., Gayán, P., Celaya, J., Palacios, J. M., Adanez, J. 2007. Operation of a 10 kW_{th} chemical-looping combustor during 200 h with a CuO-Al_2O_3 oxygen carrier. *Fuel* 86:1036-1045.
[29] Kolbitsch, P., Pröll, T., Bolhar-Nordenkampf, J., Hofbauer, H. 2008. Operating experience with chemical looping combustion in a 120kW dual circulating fluidized bed (DCFB) unit. GHGT-9: 9th International Conference on Greenhouse Gas Control Technologies, 16-20 November 2008.
[30] Bolhar-Nordenkampf, J., Pröll, T., Kolbitsch, P, Hofbauer, H. 2008. Performance of a NiO-based oxygen carrier for chemical looping combustion and reforming in a 120kW unit. GHGT-9: 9th International Conference on Greenhouse Gas Control Technologies, 16-20 November 2008.
[31] Wolf, J. 2004. CO2 mitigation in advanced power cycles, PhD Thesis, Department of Chemical Engineering and Technology. Royal Institute of Technology, Stockholm, Sweden.
[32] Naqvi, R. 2006. Analysis of Natural Gas-fired Power Cycles with Chemical Looping Combustion for CO2 Capture, PhD Thesis, Department of Energy and Process Engineering, Norwegian University of Science and Technology, Trondheim, Norway.
[33] Mattisson, T., Johansson, M., and Lyngfelt. A. 2006. The use of NiO as an oxygen carrier in chemical-looping combustion. *Fuel* 85:736-747.
[34] Lyngfelt, A., Kronberger, B., Adanez, J., Morin, J.-X., and Hurst, P. 2005. The GRACE project. Development of oxygen carrier particles for chemical-looping combustion. Design and operation of a 10 kW chemical-looping combustor. *Greenhouse Gas Control Technologies* 7:115-123 (*7th International Conference on Greenhouse Gas Control Technologies*, Vancouver, Canada, 5th-9th September 2004).

[35] Johansson, M., Mattisson, T. and Lyngfelt, A. 2006. The use of $NiO/NiAl_2O_4$ particles in a 10 kW chemical-looping combustor. *Ind Eng Chem Res* 45:5911-5919.
[36] Kunii, D., Levenspiel, O. 1991. *Fluidization Engineering*. Reed Publishing Inc., Stoneham.
[37] Johansson, E., Lyngfelt, A., Mattisson, T. and Johnsson, F. 2002. A circulating fluidized bed combustor system with inherent CO_2 separation - application of chemical looping combustion. *7th Int. Conf. on Circulating Fluidized Beds*, Niagara Falls, Ontario, May 5-7, 2002, 717-724.
[38] Jerndal, E., Mattisson, T., Thijs, I., Snijkers, F., Lyngfelt, A. 2008. NiO particles with Ca and Mg based additives produced by spray-drying as oxygen carriers for chemical-looping combustion. 9th International Conference on Greenhouse Gas Control Technologies, 16 - 20 November 2008. Accepted for publication.
[39] Sehested, J. 2003. Sintering of nickel steam-reforming catalysts. *Journal of catalysis* 271:417-426.
[40] Dueso, C., de Diego, L. F., García-Labiano, F., Gayán, P, Abad, A., Adánez, J. 2008. Methane Combustion in a 500 W_{th} Chemical-Looping Combustion System Using an Impregnated Ni-based Oxygen Carrier. Submitted for publication.

Paper I

available at www.sciencedirect.com

ScienceDirect

journal homepage: www.elsevier.com/locate/ijggc

160 h of chemical-looping combustion in a 10 kW reactor system with a NiO-based oxygen carrier

Carl Linderholm [a,*], *Alberto Abad* [b], *Tobias Mattisson* [a], *Anders Lyngfelt* [a]

[a] *Department of Energy and Environment, Energy Technology, Chalmers University of Technology, 41296 Göteborg, Sweden*
[b] *Instituto de Carboquímica (CSIC), Department of Energy and Environment, Miguel Luesma Castán 4, Zaragoza 50018, Spain*

ARTICLE INFO

Article history:
Received 3 August 2007
Received in revised form
10 January 2008
Accepted 3 February 2008
Published on line 2 April 2008

Keywords:
Chemical-looping combustion
Oxygen carrier
Fluidized bed

ABSTRACT

Chemical-looping combustion, CLC, is a technology with inherent separation of the greenhouse gas CO_2. The technique uses an oxygen carrier made up of particulate metal oxide to transfer oxygen from combustion air to fuel. In this work, an oxygen carrier consisting of 60% NiO and 40% $NiAl_2O_4$ was used in a 10 kW CLC reactor system for 160 h of operation with fuel. The first 3 h of fuel operation excepted, the test series was accomplished with the same batch of oxygen carrier particles. The fuel used in the experiments was natural gas, and a fuel conversion to CO_2 of approximately 99% was accomplished. Combustion conditions were very stable during the test period, except for the operation at sub-stoichiometric conditions. It was shown that the methane fraction in the fuel reactor exit gas was dependent upon the rate of solids circulation, with higher circulation leading to more unconverted methane. The carbon monoxide fraction was found to follow the thermodynamical equilibrium for all investigated fuel reactor temperatures, 660–950 °C. Thermal analysis of the fuel reactor at stable conditions enabled calculation of the particle circulation which was found to be approximately 4 kg/s, MW. The loss of fines, i.e. the amount of elutriated oxygen carrier particles with diameter <45 μm, decreased during the entire test period. After 160 h of operation the fractional loss of fines was 0.00022 h^{-1}, corresponding to a particle life time of 4500 h.

1. Introduction

1.1. *Chemical-looping combustion*

A large number of techniques for CO_2 capture have been proposed and investigated for large scale power production applications, but most of these techniques have the disadvantage of requiring huge amounts of energy for the CO_2 separation, resulting in a substantial power plant efficiency decrease. A CO_2 separation technology without such an energy penalty would obviously be of great interest.

In traditional combustion the fuel is in direct contact with air. In 1987, Ishida et al. presented a novel combustion concept they called chemical-looping combustion, where the traditional combustion would be divided into two gas–solid reactions: oxidation of metal by air and reduction of metal oxide by fuel. However, a similar process was patented already in 1954 by Lewis and Gilliand.

Two interconnected reaction chambers, or reactors, are needed for the process, one for reduction and the other for oxidation of the metal/metal oxide particles. By circulating the particles between these reactors, a continuous system for combustion of fuel with inherent CO_2 separation is achieved,

* *Corresponding author at*: Energiteknik, Hörsalsvägen 7B, Chalmers University of Technology, 41296 Göteborg, Sweden. Tel.: +46 31 772 1443; fax: +46 31 772 3592.
E-mail address: carl.linderholm@chalmers.se (C. Linderholm).
1750-5836/$ – see front matter
doi:10.1016/j.ijggc.2008.02.006

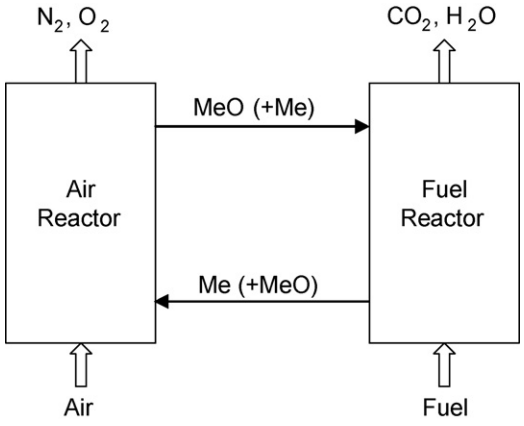

Fig. 1 – Chemical-looping combustion, CLC. By simply condensing the water produced in the fuel reactor, pure CO_2 is obtained.

see Fig. 1. After a simple H_2O condensation step, pure CO_2 is obtained from the fuel reactor exhaust gas stream.

Two interconnected fluidized beds have an advantage over alternative designs, because the process requires good contact between gas and solids as well as a flow of solid material between the two reactors (Lyngfelt et al., 2001).

Assuming that the metal/metal oxide used is Ni/NiO and that the fuel is methane, the reactions in respective reactor are as follows,

$$\text{Fuelreactor}: \quad 4NiO + CH_4 \rightarrow 4Ni + 2H_2O + CO_2 \quad \Delta H_{1000\,^\circ C} = 133.6\,\text{kJ/mol} \tag{1}$$

$$\text{Airreactor}: \quad 2Ni + O_2 \rightarrow 2NiO \quad \Delta H_{1000\,^\circ C} = -468.5\,\text{kJ/mol} \tag{2}$$

The reaction between NiO and natural gas is endothermic, and consequently there will be a temperature drop in the fuel reactor. However, the net heat release over the entire system is the same as for conventional combustion:

$$CH_4 + 2O_2 \rightarrow CO_2 + 2H_2O \quad \Delta H_{1000\,^\circ C} = -803.4\,\text{kJ/mol} \tag{3}$$

1.2. *Oxygen carrier*

The key component in CLC technology is the oxygen carrier. Several metal/metal oxide pairs have been investigated for potential use as oxygen carriers in CLC, e.g. Fe_2O_3/Fe_3O_4 (e.g. Cho et al., 2001), Cu/Cu_2O (e.g. de Diego et al., 2004), Mn_3O_4/MnO (e.g. Cho et al., 2004) and Ni/NiO (e.g. Jin et al., 1999). Johansson et al. (2006a) reports 84 original publications with experimental work on oxygen carriers for CLC. A small number of publications investigate the possibility to use pure metal oxides, i.e. natural ores, as oxygen carriers (Mattisson et al., 2001a). Most studies on oxygen carriers have been made using active metal oxides combined with inert material, such as NiO supported on $NiAl_2O_4$. Several production methods have been reported in the literature, e.g. sol–gel and dissolution methods (Ishida et al., 1996), mechanical mixing (Ryu et al., 2001; Adánez et al., 2004), spray-drying (Ishida et al., 2002), co-precipitation (Villa et al., 2003; de Diego et al., 2004), surfactant mediated synthesis (Song et al., 2003), freeze-granulation (Cho et al., 2004; Mattisson et al., 2004) and impregnation (de Diego et al., 2005; Adánez et al., 2006a). In general, the resulting particulate oxygen carrier has a porous structure with a large surface area, thus increasing the accessibility of the reacting gases to the metal oxide. However, the optimal method for large-scale oxygen carrier preparation remains an open issue.

An oxygen carrier that is to be used in a continuously operated CLC environment has to meet a number of requirements, the most important of which are suitable properties for use in a fluidized-bed reactor and sufficient rates of oxidation and reduction. These rates in combination with the oxygen transfer capacity of the carrier govern the amount of bed mass in the reactors and the needed circulation rate of the oxygen carrier, as reported by Lyngfelt et al. (2001) and Abad et al. (2007b). Ideally the fuel will be fully converted to CO_2 and H_2O, but some metal/metal oxide systems, e.g. NiO/Ni, which was used in this study, have thermodynamic limitations on fuel conversion, leading to the presence of small amounts of H_2 and CO (Mattisson and Lyngfelt, 2001b; Jerndal et al., 2006). Other important characteristics of the oxygen carrier are resistance to attrition and fragmentation and avoidance of agglomeration. Furthermore, cost, health issues and environmental concerns need be considered, as do melting temperatures of the compounds used and heat balances of the fuel reactions for the cases where the reaction with fuel is endothermic.

To check the suitability of the synthesized oxygen carriers, the majority of tests have been performed in laboratory batch reactors, for instance in thermogravimetric analysers (TGA) or laboratory fluidized-bed reactors. In those tests the particles are exposed alternately to air and fuel. However, it is only possible to simulate a chemical-looping system to a certain extent. In order to gain a more adequate understanding of the behaviour and usefulness of the particles in this process, tests are needed in a real system where the particles are continuously circulated between an air reactor and a fuel reactor. Few continuous reactor systems have been reported (Ryu et al., 2004; Lyngfelt et al., 2004; Adánez et al., 2006b; Johansson et al., 2006b,c; Abad et al., 2006, 2007a). The process has been successfully demonstrated in two different 10 kW chemical-looping combustor prototypes for natural gas combustion, the first was operated with fuel for more than 100 h using a nickel-based oxygen carrier (Lyngfelt and Thunman, 2005), and the second has been run with fuel for 120 h using a copper-oxide-based oxygen carrier (Adánez et al., 2006b).

1.3. *Objective*

The objective of this work was to check the suitability of a new Ni-based oxygen-carrier during long-time combustion in a 10 kW CLC system. The oxygen carrier was prepared by spin-flash, a commercially available technique used to produce particulate matter. Previous testing in the Chalmers 10 kW CLC unit has been accomplished using freeze-granulated particles. The combustion efficiency and the capacity of the

CLC technology to capture CO_2 were to be probed. Moreover, the lifetime of particles was to be estimated from a minimum of 100 h of fuel operation.

2. Experimental

2.1. 10 kW CLC prototype

Lyngfelt et al. (2001) proposed a design of a 10 MW chemical-looping combustor with interconnected fluidized beds where the particulate oxygen carrier acts as bed material. The proposed CLC system basically looked like a circulating fluidized bed with an extra bubbling fluidized bed after the cyclone. The 10 kW CLC prototype used in this study was designed and built in 2002/2003 within the EU-project GRACE (Lyngfelt et al., 2004; Lyngfelt and Thunman, 2005).

The prototype is composed of two interconnected fluidized-bed reactors, the fuel and the air reactor, a cyclone to separate gas and solid flow from the air reactor, and two loop seals, see Fig. 2. The gas velocity in the air reactor and riser provides the driving force for the circulation of particles between the two beds. Entrained particles are recovered in the cyclone and brought to the fuel reactor through a downcomer.

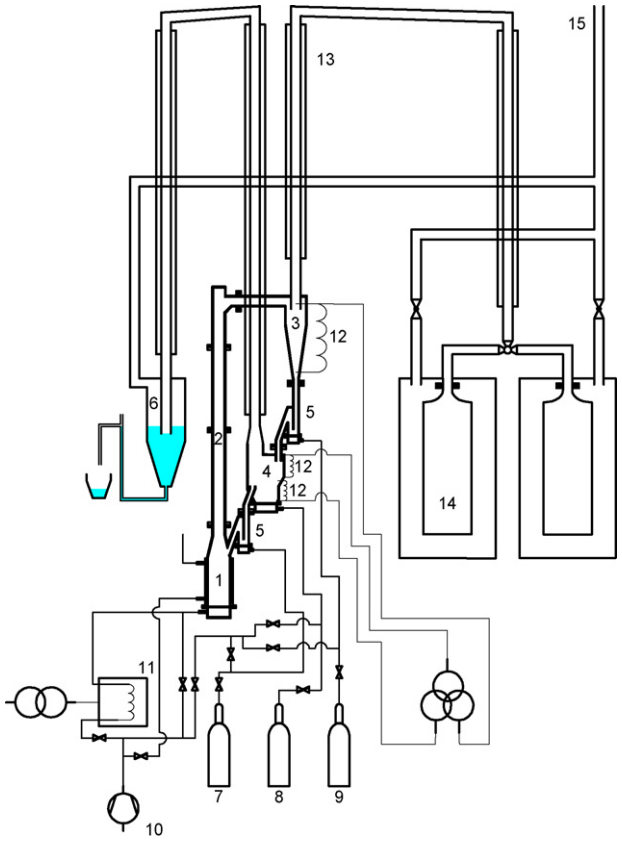

Fig. 2 – Drawing of prototype reactor system, also indicating the cooling and particle separation systems. (1) Air reactor, (2) riser, (3) cyclone, (4) fuel reactor, (5) upper and lower particle locks, (6) water seal, (7) nitrogen, (8) natural gas, (9) nitrogen, (10) air, (11) preheater, (12) heating coils, (13) finned tubes for cooling of gas streams, (14) filters and (15) connection to chimney.

The fuel reactor is a bubbling fluidized bed. Gravity is responsible for bringing the particles back to the air reactor. The entire reactor system is hanging on a scaffold and guided vertically using rails below the air and fuel reactors.

The two loop seals, or particle locks, are present in the loop in order to prevent gas leakage between the reactors: the high particle lock between the cyclone and fuel reactor, and the low particle lock between the fuel reactor and air reactor. Previous results have shown no indication of gas leakage between the reactors (Lyngfelt et al., 2004).

Nitrogen is normally used for particle lock fluidization. A part of this nitrogen escapes by the fuel reactor exit, diluting the CO_2 stream. In order to obtain a concentrated stream of CO_2 (not diluted with N_2) at the fuel reactor exit, two steam generators, providing the option to use water vapour for particle lock fluidization, have been installed. During the test series both particle locks were fluidized with nitrogen, except for a 2 h test run with water vapour.

The gas flows leaving the cyclone and fuel reactor are led through steel tubes which have fins on the outside to promote cooling. Following the cooling, the flow from the cyclone passes through large filter bags, where entrained particles are trapped. The filter weave cut off diameter is approximately 10 μm, and a fraction of the elutriated material may have escaped through the filter. The fuel reactor exit gas flow has a final steam condensation step in the form of a water seal, which also fills the function of trapping particles from the fuel reactor. An additional feature of the water seal is the possibility to control the pressure in the fuel reactor by adjusting the water level.

A supervision system has been installed to allow unmanned operation of the prototype. When the supervision system is activated, temperatures and gas concentrations in the air and fuel reactors must stay within certain intervals. The alarm will be triggered if the supervised parameters stray outside the pre-defined levels, meaning that the fuel gas will be cut and replaced with inert gas. The supervision system permits operation at combustion conditions during long periods of time, e.g. 24 h, with continuous natural gas feed.

2.1.1. Start-up and external heating and cooling options

The heating of the system is carried out using air as fluidizing agent in the air and fuel reactors. When the temperatures in respective reactor are high enough to begin fuel operation, air is replaced with nitrogen in the fuel reactor, and after a few minutes nitrogen is switched to fuel.

The incoming air to the air reactor can be preheated up to 1000 °C. The need for preheating during stable operation is due to heat losses in the system and depends on the air flow necessary to achieve proper circulation, i.e. particle size and density. The air reactor temperature is kept at 1000 °C with the aid of a Eurotherm Temperature Controller 2216e, which controls the air flow in the cooling jacket that encloses the air reactor.

For testing and time saving purposes it is desirable to have some external means of control over the fuel reactor temperature. Three homogenous Nikrothal 80 element wires with ceramic electric isolators wound around the fuel reactor provide such an option, which is used at start-up, and which can also be used to increase the temperature during normal

operation, i.e. in order to vary the temperature independently of the parameters that determine the fuel reactor temperature during normal operation, i.e. particle circulation, incoming particle temperature and fuel load.

During earlier runs carbon formation was observed in the fuel reactor wind box because the temperature was high enough for methane decomposition to occur. In order to avoid methane decomposition, the wind box has been equipped with an air cooling jacket.

2.1.2. Measurements

The gases leaving the reactors pass through cooling tubes after which a fraction of the gas is led to gas analysers where CO_2, CO, O_2 and CH_4 are continuously measured on-line. The carbon containing gases are measured using IR instruments and the oxygen is measured with paramagnetic technique. Hydrogen measurements are performed using gas chromatography.

Mass flow controllers are installed to feed fuel gas and air. Pressure measurements are used to supervise the bed heights and to evaluate particle flows as a function of operating conditions. The 10 kW unit uses 20 pressure transducers to measure the important pressure drops. A total of eight thermocouples monitor the temperatures in the system. Three thermocouples are placed in the fuel reactor, another two in the air reactor and the remaining ones are found in the cyclone, riser and air reactor cooling jacket.

Gas concentrations, temperatures, differential pressures and flows are logged every 10 s using the software InstruNet World.

2.1.3. Bed material and solids flux

After the first 3 h of operation, 3 kg particles were added to the reactor system. After this addition, the test series was accomplished with the same batch of particles. The total solids inventory was around 15 kg in the experiments.

The bed mass in the fuel reactor is given by the height of the overflow pipe. The amount of material present in the air reactor and riser depends on the total solids inventory and fluidization conditions.

The net solids flux determines the difference in conversion of particles leaving and returning to the air reactor, i.e. how much of the available oxygen in the particle flow is consumed in the fuel reactor (Lyngfelt et al., 2001). The degree of oxidation of the particles, henceforth termed particle conversion, X, is defined as the ratio of the amount of available oxygen present in the carrier and the amount of available oxygen present in the carrier when fully oxidized,

$$X = \frac{m_{\text{actual}} - m_{\text{fully red.}}}{m_{\text{fully ox.}} - m_{\text{fully red.}}}, \tag{4}$$

where m_{actual} is the actual mass of the carrier in its partially oxidized state. The particle conversion in the air reactor, X_{ox}, is larger than that in the fuel reactor, X_{red}, during normal combustion conditions. The difference in particle conversion,

$$\Delta X = X_{\text{ox}} - X_{\text{red}}, \tag{5}$$

hence becomes a function of the particle circulation; increasing the solids flux in the reactor system leads to a decrease in ΔX.

The solids flux, or particle circulation, cannot be directly measured in the 10 kW prototype. However, for a specific oxygen carrier in a specific unit geometry, the particle circulation is a function of the velocity of the air in the riser and the pressure drop in the riser. The following correlation can be used to provide a measure of the net solids flux (Johnsson et al., 1998),

$$G_s = \rho_{\text{exit}}(u - u_t) = -\frac{1}{g}\frac{dp}{dh}(u - u_t), \tag{6}$$

where u_t is the terminal velocity of an average sized particle. The solids circulation calculated by Eq. (6) is believed to give a significant overestimation, nevertheless it provides a useful means for comparing particle circulations during the entire test period. G_s multiplied with the cross sectional area of the riser will be referred to as circulation index, although in actuality it has the unit kg/min.

2.2. Oxygen carrier

The oxygen carrier particles used in the experiments were supplied by IFP (L'Institut Français du Pétrole). The particles were prepared by spin flash drying, and consist of 60%$_{\text{mass}}$ NiO and 40%$_{\text{mass}}$ $NiAl_2O_4$. The GRACE particles were based on the same active and support materials, but the mass ratio active/inert material for the GRACE particle was 40/60. A SEM image of a fresh particle, i.e. a particle not subjected to CLC environment, is shown in Fig. 3.

The apparent density of the carrier was measured on particles in the size range 125–180 μm and was found to be 4400 kg/m^3, assuming a void between particles of 37%. Voids inherent to the material are excluded for calculation of apparent density. The crushing strength was measured on particles in the size range 180–212 μm and the average of 20 measurements was 5.3 N, which can be compared to the crushing strength of the GRACE particle (Mattisson et al., 2008),

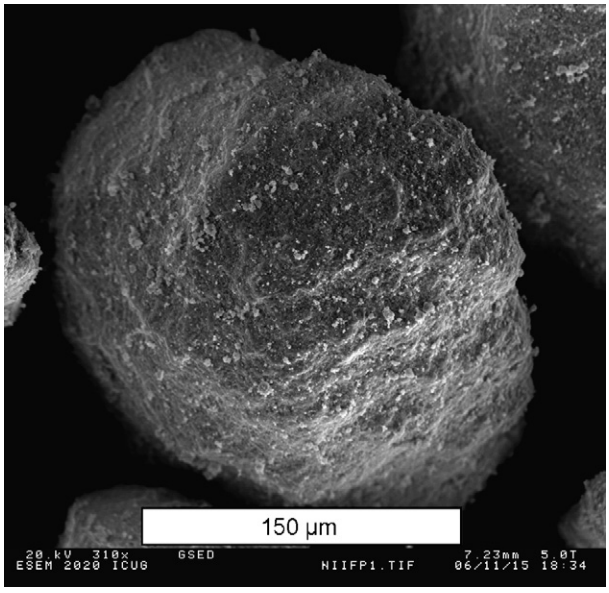

Fig. 3 – SEM image of fresh particle.

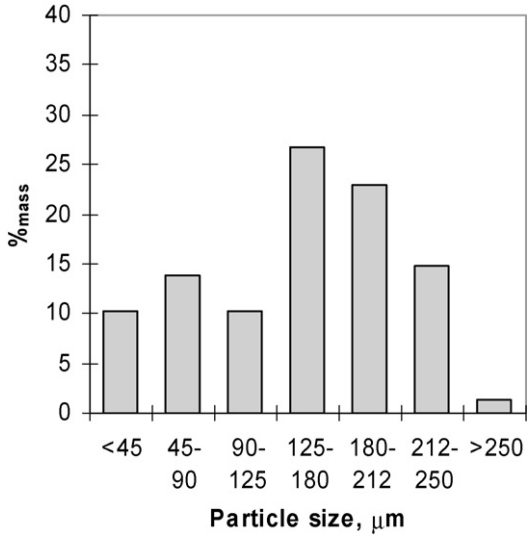

Fig. 4 – Particle size distribution of fresh material.

which was 2.5 N. The mean particle diameter was 132 μm. Fig. 4 shows the particle size distribution of the fresh material.

Minimum fluidization and terminal velocities were calculated using the correlations of Kunii and Levenspiel (1991). The minimum fluidization velocity in the fuel reactor at 850 °C during operation with fuel is 0.0054 m/s, and the terminal velocity in air at 1000 °C is 0.77 m/s using the average particle diameter.

2.3. *Fuel*

Natural gas was used as fuel in the experiments. The main constituent of the fuel is methane, but exact composition may vary over time. Table 1 shows the average composition of natural gas in October 2006 according to DONG Energy, Denmark. The lower heating value based on the average fuel composition is 39.6 MJ/m^3, which means that a fuel flow of 15.0 L_n/min corresponds to a thermal power of 10 kW. The H/C ratio of the fuel is 3.75, the oxygen consumption is 2.20 moles O_2 per mole fuel and the volume expansion is 3.26 mole product gas per mole fuel when fuel conversion is complete.

2.4. *Scope of the study*

An oxygen carrier produced by spin-flash drying has not previously been tested in a continuously operated CLC system. The GRACE particle was successfully used in the Chalmers 10 kW CLC prototype in 2003 for more than 100 h of stable operation with fuel (Lyngfelt et al., 2004; Lyngfelt and Thunman, 2005; Johansson et al., 2006d).

In the experiments with the GRACE particle, the carbon monoxide fraction in the fuel reactor exhaust gas was typically 0.5% at 800 °C, corresponding to the thermodynamical equilibrium fraction (at 800 °C), and the methane fraction was around 0.1%. Inevitably, the results with the spin-flash particle have to be compared to the GRACE results.

During the 2003 test series a possible correlation between methane fraction and particle circulation was identified.

Table 1 – Average composition of natural gas used in experiments

Species	Formula	Mole%
Methane	CH_4	89.78
Ethane	C_2H_6	5.82
Propane	C_3H_8	2.31
Isobutane	C_4H_{10}	0.39
n-Butane	C_4H_{10}	0.53
Isopentane	C_5H_{12}	0.12
n-Pentane	C_5H_{12}	0.08
Hexane+	C_6H_{14}	0.06
Nitrogen	N_2	0.27
Carbon dioxide	CO_2	0.62

However, at the time, the fuel reactor temperature was linked to the particle circulation, with higher circulation leading to higher fuel reactor temperature and vice versa. Consequently, it was not possible to rule out a temperature influence on the above-mentioned correlation. The fuel reactor exterior has since been equipped with heat wires providing a means of temperature control independent of particle circulation.

Below, the different aims of the study are summarized:

- independent variation of circulation and fuel reactor temperature to investigate relationship between CH_4 fraction and circulation;
- validate the CO fraction dependence on fuel reactor temperature for a large temperature span;
- variation of fuel load and its effect on fuel conversion;
- tests with steam fluidization of particle locks to obtain a high purity CO_2 stream;
- perform circulation calculations based on thermal analysis of the fuel reactor;
- long-term tests, >100 h of fuel operation, in order to estimate particle life time and investigate any changes in reactivity.

3. Results and discussion

The tests were run during 20 days. In total, the CLC unit was operated for 160 h with fuel.

The excess air ratio, λ, was 0.8–2.6, normally around 1.6.

3.1. *Fuel conversion*

Carbon dioxide, carbon monoxide, methane and hydrogen concentrations are presented as fraction of total carbon in the fuel reactor exit gas according to

$$f_i = \frac{x_i}{x_{CO_2} + x_{CO} + x_{CH_4}}, \quad (7)$$

where i represents CO_2, CO, CH_4 or H_2 and x is the molar fraction of the substance indicated by the subscript in dry exit gas from the fuel reactor. The measured concentrations of H_2, CO, CO_2 and CH_4 are somewhat lower due to mixing with nitrogen from particle locks.

In the experiments, carbon monoxide fractions were in the range of 0.3–1.0% and methane fractions 0.15–0.6%. The CO_2 fraction was around 99% during the entire test period, and is

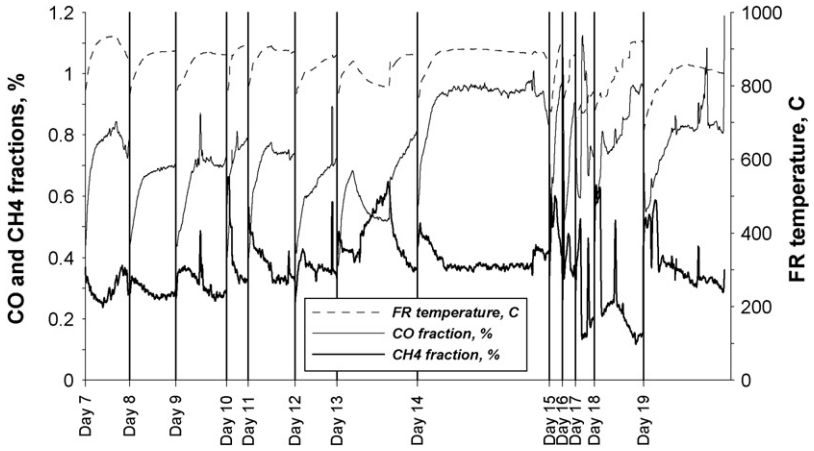

Fig. 5 – Temperature at the top of the fuel reactor, CO and CH_4 fractions versus time.

referred to as the fuel conversion to CO_2. Another way of expressing the fuel conversion is to compute the combustion efficiency from the heating values of the fuel and the remaining combustible gases, i.e. CO, CH_4 or H_2, in the fuel reactor exit gas. The combustion efficiency obtained in this way was 99.1% for a typical case at 800 °C with 0.5% CO, 0.4% CH_4 and 1.1% H_2 (the latter fraction is an assumption based on the thermodynamical NiO-equilibrium).

3.1.1. *CO and CH_4 fractions versus time*

Fig. 5 shows fuel reactor exit gas fractions of CO and CH_4 along with the fuel reactor temperature as a function of time, from day 7 to 19, corresponding to approximately 130 h of fuel operation. Start-up periods have been removed as well as a few shorter periods of measuring system malfunction. The relationship between the fuel reactor temperature and CO fraction is evident. Days 1–6 and 20 are not presented in Fig. 5, due to circulation problems days 1–4, fuel dilution with inert gas days 5 and 6, leading to very high concentrations of methane, see later section, and finally, on day 20, poor mixing in the fuel reactor as a consequence of a fuel gas distribution nozzle breaking loose from the bottom plate.

On days 14 and 19 operation was maintained overnight. Days 15–18 involved tests with varying fuel load, circulation and fuel reactor temperature. The last displayed measuring points in Fig. 5 shows the bolting CO-fraction resulting from the distribution nozzle coming loose from the bottom plate.

In summary, CO and CH_4 levels are relatively stable during the displayed test period. No loss in reactivity was observed during the operation time. The fluctuations that can be seen in Fig. 5 are mostly due to variations in temperature, circulation and fuel load.

Table 2 – Equilibrium concentrations of carbon monoxide and hydrogen during combustion with methane after condensation of H_2O

	T (°C)			
	650	750	850	950
CO (%)	0.22	0.39	0.64	0.97
H_2 (%)	0.87	1.01	1.15	1.29

3.1.2. *Dependence of CO, H_2 and CH_4 fractions on fuel reactor temperature*

When using a nickel-based oxygen carrier in CLC, it is not possible to obtain full conversion of the fuel due to a thermodynamical constraint. Small fractions of CO and H_2 will always be present, see Table 2, whereas the fraction of unconverted methane is theoretically very close to 0%. Fig. 6 displays CO fractions days 7–13 as well as equilibrium fractions of CO. Each cross represents the average of 15 measurements, i.e. 2.5 min. Only every tenth data point can be viewed in Fig. 6, i.e. 90% of the data has been removed for clarity. The relationship between the CO fractions and the equilibrium curve is evident. Fig. 6 also reveals methane fractions during the same test period. The circulation index

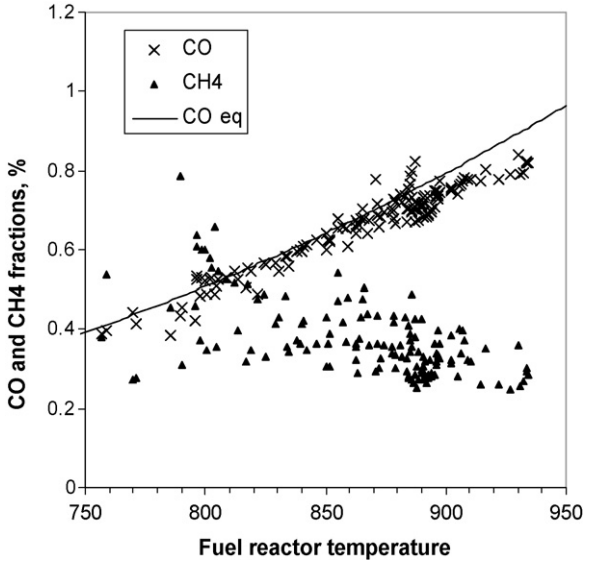

Fig. 6 – CO and CH_4 fractions versus fuel reactor temperature. The thermodynamic equilibrium curve for CO is also displayed.

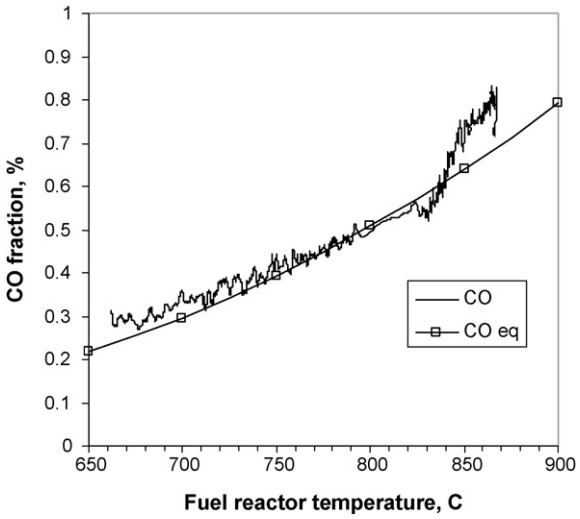

Fig. 7 – CO fraction versus fuel reactor temperature during 5 h on day 5. The thermodynamic equilibrium curve for CO is also displayed.

was never below 15 during these tests, and the excess air ratio was between 1.5 and 1.6.

Hydrogen measurements were performed on one occasion during 2 h. The hydrogen fraction was relatively stable at 1.5%. The temperature of the fuel reactor was kept at 800 °C and the CO and CH_4 fractions were 0.8 and 0.4% respectively, thus both CO and H_2 were above the equilibrium concentrations.

Interestingly, tests on days 5–6 at low fuel reactor temperatures, see Fig. 7, show that CO fractions follow the equilibrium curve. Methane fractions are significantly higher, 2–4%, during these tests, but this is a consequence of fuel gas dilution with nitrogen, which will be discussed in a later section.

3.1.3. *Dependence of CH_4 and CO fractions on particle circulation*

In order to investigate the relationship between fuel reactor temperature and CH_4 fraction, tests were performed at three different fuel reactor temperatures, 700, 800 and 900 °C, and two different particle circulation rates. The circulation index was calculated according to Eq. (6) and then averaged over 5 min. Test duration was approximately 40 min, except for the test at 700 °C with circulation index 15–20, which lasted a mere 15 min.

Fig. 8a–c display CO and CH_4 fractions versus circulation index during the tests. In all three figures it is obvious that lower circulation leads to lower CH_4 fractions and higher CO fractions.

The investigated correlation could be explained by the amount of metallic nickel present in the oxygen carrier. Lower circulation leads to increased oxygen turnover in the particles and consequently increased amounts of nickel in the particles in the fuel reactor. Since nickel acts as a catalyst in the reactions

$$CH_4 + H_2O \rightarrow CO + 3H_2 \quad (8)$$

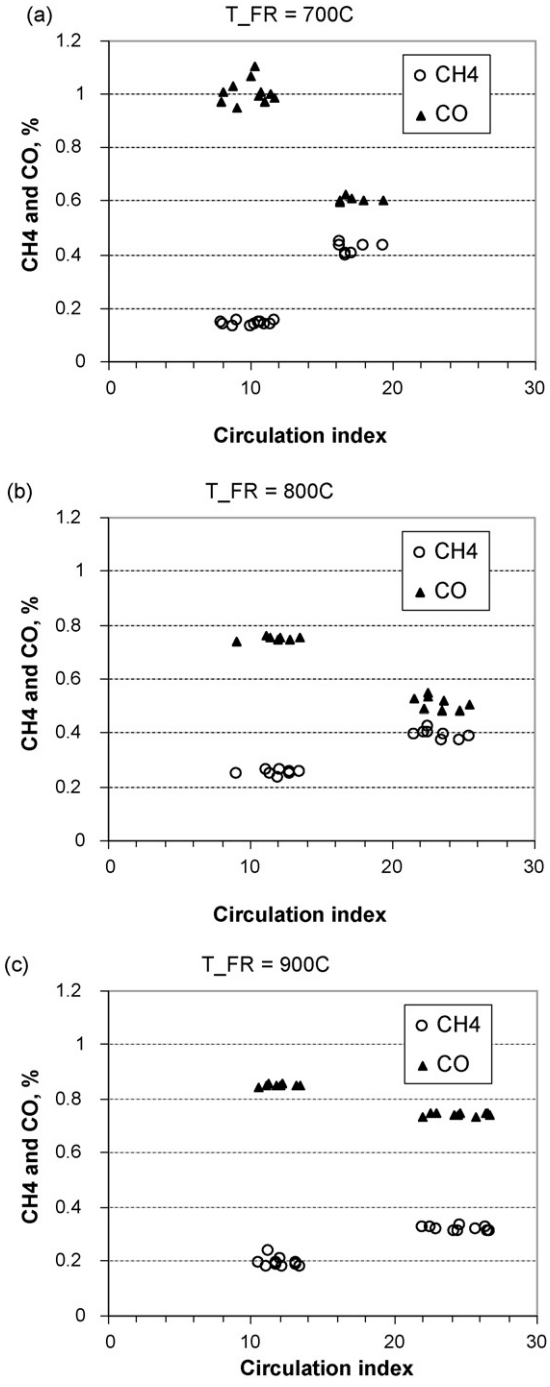

Fig. 8 – (a–c) CH_4 and CO fractions versus circulation index at (a) 700 °C, (b) 800 °C and (c) 900 °C.

and

$$CH_4 \rightarrow C + 2H_2 \quad (9)$$

it is expected that more nickel will lead to less CH_4.

Fig. 8a–c suggests a correlation between circulation and the quotient CO/CH_4. Data analysis investigating this relationship over the entire test period resulted in Fig. 9. The correlation is thus clear for all temperatures.

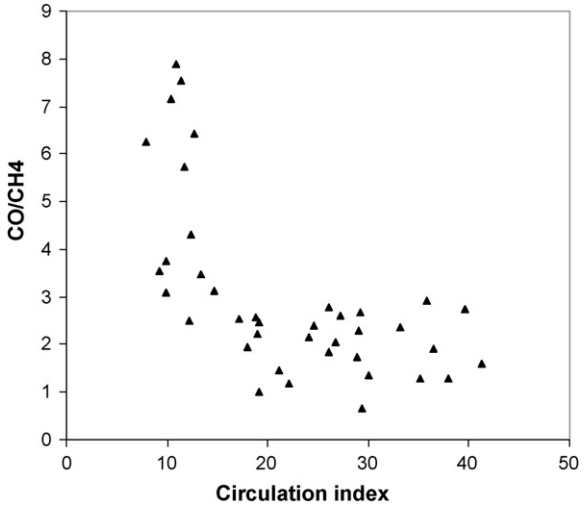

Fig. 9 – CO/CH_4-ratio versus circulation index.

3.1.4. *Increased fuel load*

A single test at increased fuel load, corresponding to 17 kW, was carried out during 3 h on day 15. At 17 kW the process was autothermal, i.e. no additional heating was necessary. No significant change in fuel conversion was observed. However, a thermal power of 17 kW requires larger air flows leading to increased circulation and consequently increased temperature in the fuel reactor, which translates to higher CO fraction. The fuel reactor temperature, and hence the CO fraction, kept increasing during the test, since there are no means of cooling the fuel reactor. The excess air ratio was 1.2 during the test at 17 kW.

3.1.5. *CH_4 fraction dependence on fuel dilution*

A few tests where the fuel reactor was fluidized with fuel gas and nitrogen simultaneously were performed in order to investigate the mixing in the fuel reactor.

Diluting the fuel with inert gas has a significant impact on the CH_4-fraction in the exit gas, as can be seen in Fig. 10. Decreasing the incoming fuel concentration leads to slower

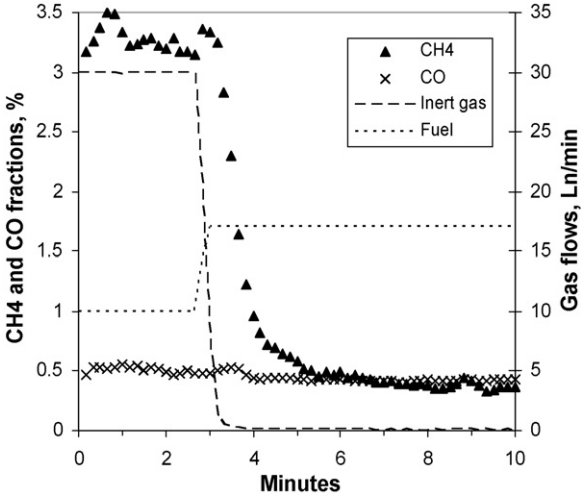

Fig. 10 – Effect of fuel gas dilution on methane conversion.

average reaction rate in the bed, but, in this case, the final conversion should be higher than that obtained when the fuel is not diluted because a smaller amount of fuel is fed. The increase in methane concentration could be due to different reasons. In this particular case, the inert gas will lead to larger gas velocities in the lower part of the bed thus decreasing the fuel residence time. It also means larger bubbles, with more methane present in the bubbles. More important, however, is probably that higher flow of methane will increase the fraction of catalytically active nickel in the particles.

Circulation and fuel reactor temperature were relatively constant during the test. It can also be mentioned that the test was repeated with very similar result.

3.1.6. *Steam fluidization of particle locks*

Steam was used to fluidize the particle locks on one occasion for approximately 2 h. No influence on fuel conversion or CO concentration could be observed. Typical concentrations were 94% CO_2, 0.9% CO and 0.15% CH_4. The fuel reactor temperature was 940 °C which means that the thermodynamically expected hydrogen concentration was 1.25%. Adding the nitrogen present in the fuel, the gas total amounts to approximately 97%. The deviation from 100% can be attributed to an error in the CO_2 measurements at very high concentrations of CO_2, which was demonstrated later by feeding pure CO_2 to the gas analyser, which then measured only 97%. It is important to point out that the instrument was calibrated between 0 and 80% CO_2 and trustworthy within this interval. When the particle locks were fluidized with nitrogen the CO_2 concentration stayed between 68 and 80%.

3.2. *Particle circulation estimation based on thermal analysis of fuel reactor*

When the heat wires around the fuel reactor are not in use, the single source of heat for the endothermic reaction is the particles coming from the air reactor. Adding the heat required for particle reduction with that for heating the incoming fuel and the heat loss through the insulation, the total amount of heat needed in the fuel reactor, $\dot{Q}_{FR}$, is obtained.

Three thermocouples monitor the temperature in the fuel reactor. One is in the bed, one is placed in the "roof", and one is used to measure the temperature of the incoming particles. Assuming that the particles leaving the reactor have the same temperature as the bed, the difference between particles entering and those leaving the fuel reactor, ΔT_{part}, is known.

Hence the particle mass flow can be calculated according to

$$\dot{m}_{part} = \frac{\dot{Q}_{FR}}{C_{p,part}\,\Delta T_{part}}, \tag{10}$$

where $C_{p,part}$ is obtained from the inert and active components of the oxygen carrier.

During stable operation with a fuel load corresponding to a thermal power of 11 kW the total heat loss from the reactor system is around 5 kW. There is some uncertainty regarding the magnitude of the heat loss from the fuel reactor. Here, it will be assumed that the heat loss from the fuel reactor is 1 kW, although halving or doubling this value has only a marginal effect on the result. The surface area of the fuel

reactor is merely 25% of the total surface area and the temperature is significantly lower than those of the air reactor, riser and cyclone. The heat of reaction, i.e. the heat necessary to reduce the particles, is 1.9 kW at a thermal power of 11 kW and a fuel reactor temperature of 850 °C. During the tests which form the basis for the calculations presented here, the temperatures in the fuel and air reactors were very stable. The temperature of the incoming particles was around 950 °C and ΔT_{part} was around 100 °C. Heating the incoming fuel to 850 °C requires approximately 0.7 kW.

The particle circulation obtained in this way is by a factor 10 smaller than the particle circulation index, thus in the order 2–3 kg/min, or 4 kg/s, MW. Combining this result with the oxygen demand at 11 kW and assuming that the particles leaving the air reactor are fully oxidized, it is possible to calculate the average difference in particle conversion, ΔX, which is found to be 0.2.

The drawback with the presented method is that it is reliable only when temperatures in the reactor system are stable during a long period of time.

3.3. Elutriation

Fig. 11 shows the loss of fines from the prototype as a function of the day when they were collected. Particles elutriated from the air reactor are collected in large filter bags and particles elutriated from the fuel reactor are collected in the water seal. The loss of fines is expressed as the amount of fine particles, diameter <45 μm, elutriated per hour divided by the total mass of particles in the reactor system. It can be noted that particles of all sizes are elutriated from the air reactor as an effect of poor cyclone efficiency, i.e. compared to large-scale cyclones. Particles having a diameter between 90 and 212 μm are re-introduced to the reactor system. Such additions of recycled material occurred on days 10, 14 and 19, prior to operation.

The air filter was not emptied after the first day of fuel operation due to the short operation period. Elutriation during the first 2 days was substantial as a consequence of not sieving the oxygen carrier prior to addition. Since 24% of the fresh material had a diameter less than 90 μm it not surprising that a large portion of this was elutriated during the first 2 days.

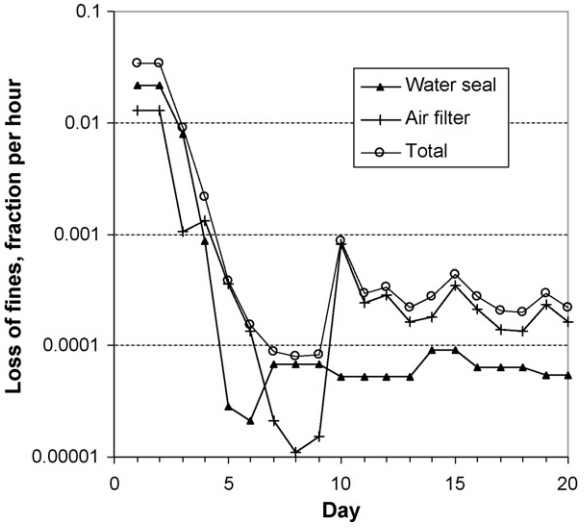

Fig. 11 – Loss of fines over the entire test period.

On day 10 it was found that fine material adhered to the filter bags and a different method for emptying the bags was adopted. Hence the calculated fractions elutriated prior to day 10 are too low and on day 10 too high.

On days 5 and 6 the amount of material elutriated to the water seal was very small and cannot be trusted with the same level of confidence as the other days. After day 6 particles elutriated to the water seal were not collected every day.

It should also be noted that on day 15 the system was run at 17 kW, resulting in larger gas velocities in both the air reactor and the fuel reactor, which may explain the enhanced loss of fines this day.

The elutriation towards the end of the test period should yield a reliable estimation of the particle life time, which was found to be 4500 h. This can be compared to the estimated particle life time of the GRACE particle, which was found to be 40,000 h (Lyngfelt et al., 2004).

3.4. Gas leakage

There was no detectable gas leakage between the reactors. No CO_2 was seen in the exit gas stream from the air reactor, thus there is no leakage from fuel reactor to the air reactor. In the opposite direction it is more difficult to measure leakage during operation with fuel, since the exit gas from the fuel reactor is usually diluted with N_2 from the particle locks. However, during the period of inert gas fluidization of fuel reactor and particle locks, which always precedes fuel operation, a leakage would easily be spotted as oxygen in the fuel reactor exit gas, and no such leakage was observed.

3.5. Carbon formation

Carbon formation on particles was below the detection limit during the tests. Carbon formation on particles would be manifested as CO_2 in the exit gas stream from the air reactor, and as mentioned in the previous section no CO_2 was observed. Each day at the end of fuel operation natural gas was replaced with nitrogen, which in turn was switched to air after 10–15 min. The introduction of oxygen in the fuel reactor produces a small CO_2 peak that can be integrated to give an estimation of the amount of carbon formed during fuel operation. Such calculations applied to a number of randomly chosen days show that a few grams of carbon was formed on each run. This carbon was probably formed in zones of poor mixing. For comparison, 9 g of carbon is added per minute at 10 kW.

3.6. Agglomerations, sub-stoichiometric runs and fuel reactor mixing

Operation on days 1–4 presented circulation problems due to the formation of particle agglomerates in the fuel reactor. The agglomeration occurred during unintentional runs at sub-stoichiometric air-to-fuel ratios, $\lambda \approx 0.8$. The reason for the sub-stoichiometric operation was a brand new, but poorly calibrated Bronkhorst mass flow controller, which was feeding almost twice the amount of fuel gas it was supposed to.

Fig. 12 – Agglomerate formed in the fuel reactor. The squares on the paper are 5 mm.

The exact mechanisms of particle agglomeration are not yet well understood. In the case of the present oxygen carrier, it is clear that the degree of oxidation has an influence on agglomeration; more reduced particles seem to form agglomerates easier. When it occurred, agglomeration was quite rapid and so massive that the circulation could not be maintained. Following the agglomeration on days 1–3, the fuel reactor had to be opened and the agglomerates crushed and re-introduced. The agglomerates were a few centimetres large and quite soft, see Fig. 12.

Other factors that may influence agglomeration behaviour are particle size and shape, and fuel reactor mixing conditions. The mixing in the fuel reactor was imperfect during the entire test series, which was demonstrated by introducing high pressure air through the pressure taps leading down to the fuel reactor bed. An air boost in the post-operation phase typically halved the oxygen concentration for 15–30 s, whereas in an ideally stirred reactor, it would increase. A small CO_2 peak would also follow the air boost.

On day 4, there were anew signs of agglomeration, but this time prompt action was taken: (a) the air-to-fuel ratio was increased, (b) nitrogen was introduced along with fuel gas in the fuel reactor in order to improve mixing conditions and (c) attempts to break the agglomerates by subjecting the fuel reactor to short high pressure air boosts through the pressure taps were made, and this time the agglomeration process seemed, at least partly, reversible. From day 5 and forward, there were no indications of agglomeration.

4. Conclusions

An oxygen carrier produced by spin-flash drying was evaluated in a continuous 10 kW chemical-looping combustor. 160 h of fuel operation was achieved with high fuel conversion to CO_2 and H_2O. The exit gas stream from the fuel reactor contained typically 0.7% CO, 0.3% CH_4 and approximately 1.3% H_2.

Investigations of the relationship between CH_4 and circulation confirmed previously presented theories that a large solids flux leads to increased methane concentrations and vice versa.

No decrease in reactivity was seen during the test period.

A method for calculation of the circulation based on a heat balance over the fuel reactor was presented. The typical solids flux at 11 kW was 4 kg/s, MW.

The loss of fines was larger than that observed in previous testing in the CLC prototype. The estimated particle life time was 4500 h.

There was no detectable gas leakage between the reactors. When steam was used as fluidization gas in particle locks, a concentrated stream of CO_2 was obtained.

Acknowledgements

This work was made within the EU-financed research project Enhanced Capture of CO_2 (ENCAP), SE56-2004-502666. The particles were supplied by Institut Français du Pétrole (IFP). The authors would like to acknowledge contributions from Nicolas Berguerand, Marcus Johansson, and Erik Jerndal.

REFERENCES

Abad, A., Mattisson, T., Lyngfelt, A., Rydén, M., 2006. Chemical-looping combustion in a 300 W continuously operating reactor system using a manganese-based oxygen carrier. Fuel 85, 1174–1185.

Abad, A., Mattisson, T., Lyngfelt, A., Johansson, M., 2007a. The use of iron oxide as oxygen carrier in a chemical-looping reactor. Fuel 86, 1021–1035.

Abad, A., Adánez, J., García-Labiano, F., de Diego, L.F., Gayán, P., Celaya, J., 2007b. Mapping of the range of operational conditions for Cu-, Fe-, and Ni-based oxygen carriers in chemical-looping combustion. Chem. Eng. Sci. 62, 533–549.

Adánez, J., de Diego, L.F., García-Labiano, F., Gayán, P., Abad, A., Palacios, J.M., 2004. Selection of oxygen carriers for chemical-looping combustion. Energy Fuels 18, 371–377.

Adánez, J., García-Labiano, F., de Diego, L.F., Gayán, P., Celaya, J., Abad, A., 2006a. Nickel-copper oxygen carriers to reach zero CO and H_2 emissions in chemical-looping combustion. Ind. Eng. Chem. Res. 45, 2617–2625.

Adánez, J., Gayán, P., Celaya, J., de Diego, L.F., García-Labiano, F., Abad, A., 2006b. Chemical-looping combustion in a 10 kW prototype using a CuO/Al_2O_3 oxygen carrier: effect of operating conditions on methane combustion. Ind. Eng. Chem. Res. 45, 6075–6080.

Cho, P., Mattisson, T., Lyngfelt, A., 2001. Reactivity of iron oxide with methane in a laboratory fluidized bed—application of chemical-looping combustion. In: Seventh International Conference on Circulating Fluidized Beds, Niagara Falls, Ontario, May 5–7, 2002, pp. 599–606.

Cho, P., Mattisson, T., Lyngfelt, A., 2004. Comparison of iron-, nickel-, copper- and manganese-based oxygen carriers for chemical-looping combustion. Fuel 83, 1215–1225.

de Diego, Luis, F., García-Labiano, F., Adánez, A., Gayán, P., Abad, A., Corbella, B.M., Palacios, J.M., 2004. Development of Cu-based oxygen carriers for chemical-looping combustion. Fuel 83, 1749–1757.

de Diego, L.F., Gayán, P., García-Labiano, F., Celaya, J., Abad, A., Adánez, J., 2005. Impregnated CuO/Al_2O_3 oxygen carriers for chemical-looping combustion: avoiding fluidized bed agglomeration. Energy Fuels 19, 1850–1856.

Ishida, M., Zheng, D., Akehata, T., 1987. Evaluation of a chemical-looping combustion power-generation system by graphic exergy analysis. Energy 12 (2), 147–154.

Ishida, M., Jin, H., Okamoto, T., 1996. A fundamental study of a new kind of medium material for chemical-looping combustion. Energy Fuels 10, 958–963.

Ishida, M., Yamamoto, M., Ohba, T., 2002. Experimental results of chemical-looping combustion with $NiO/NiAl_2O_4$ particle circulation at 1200 °C. Energy Conv. Manage. 43, 1469–1478.

Jerndal, E., Mattisson, T., Lyngfelt, A., 2006. Thermal analysis of chemical-looping combustion. Chem. Eng. Res. Des. 84, 795–806.

Jin, H., Okamoto, T., Ishida, M., 1999. Development of a novel chemical looping combustion: synthesis of a solid looping material of $NiO/NiAl_2O_4$. Ind. Eng. Chem. Res. 38, 126–132.

Johnsson, F., Vrager, A., Leckner, B., 1998. Solids segregation in a CFB-boiler furnace. In: Fan, L.-S., Knowlton, T. (Eds.), Fluidization IX. Engineering Foundation, pp. 757–764.

Johansson, M., Mattisson, T., Rydén, M., Lyngfelt, A., 2006a. Carbon capture via chemical-looping combustion and reforming. In: International Seminar on Carbon Sequestration and Climate Change, Rio de Janeiro, Brazil, 24–27 October.

Johansson, E., Mattisson, T., Lyngfelt, A., Thunman, H., 2006b. A 300 W laboratory reactor system for chemical-looping combustion with particle circulation. Fuel 85, 1428–1438.

Johansson, E., Mattisson, T., Lyngfelt, A., Thunman, H., 2006c. Combustion of syngas and natural gas in a 300 W chemical-looping combustor. Chem. Eng. Res. Des. 84 (A9), 819–827.

Johansson, M., Mattisson, T., Lyngfelt, A., 2006d. The use of $NiO/NiAl_2O_4$ particles in a 10 kW chemical-looping combustor. Ind. Eng. Chem. Res. 45, 5911–5919.

Kunii, D., Levenspiel, O., 1991. Fluidization Engineering. Reed Publishing Inc., Stoneham.

Lewis, W.K., Gilliand, E.R., Production of pure carbon dioxide. US Patent No. 2,665,972 (1954).

Lyngfelt, A., Leckner, B., Mattisson, T., 2001. A fluidized-bed combustion process with inherent CO_2 separation—application of chemical-looping combustion. Chem. Eng. Sci. 56, 3101–3313.

Lyngfelt, A., Kronberger, B., Adanez, J., Morin, J.-X., Hurst, P., 2004. The GRACE project. Development of oxygen carrier particles for chemical-looping combustion. Design and operation of a 10 kW chemical-looping combustor.In: Seventh International Conference on Greenhouse Gas Control Technologies, Vancouver, Canada, September 5–9.

Lyngfelt, A., Thunman, H., 2005. Construction and 100 h of operational experience of a 10 kW chemical looping combustor. In: Thomas, D. (Ed.), Carbon Dioxide Capture for Storage in Deep Geologic Formations—Results from the CO_2 Capture Project. Capture and Separation of Carbon Dioxide From Combustion Sources, vol. 1Elsevier Science, London, pp. 625–646 (Chapter 36).

Mattisson, T., Lyngfelt, A., Cho, P., 2001a. The use of iron oxide as an oxygen carrier in chemical-looping combustion of methane with inherent separation of CO_2. Fuel 80, 1953–1962.

Mattisson, T., Lyngfelt, A., 2001b. Capture of CO_2 using chemical-looping combustion. In: First Biennial Meeting of The Scandinavian-Nordic Section of the Combustion Institute, Göteborg, April 18–20, pp. 163–168.

Mattisson, T., Johansson, M., Lyngfelt, A., 2004. Multicycle reduction and oxidation of different types of iron oxide particles—application to chemical-looping combustion. Energy Fuels 18, 628–637.

Mattisson, T., Johansson, M., Lyngfelt, A. The reaction of $NiO/NiAl_2O_4$ particles with alternating methane and oxygen, Can. J. Chem. Eng., 2008, in press.

Ryu, H.J., Bae, D.H., Han, K.H., Lee, S.Y., Jin, G.T., Choi, J.-H., 2001. Oxidation and reduction characteristics of oxygen carrier particles and reaction kinetics by unreacted core model. Kor. J. Chem. Eng. 18 (6), 831–837.

Ryu, H.J., Jin, G.T., Yi, C.K., Choi, J.H., 2004. Demonstration of inherent CO_2 separation and no NO_x emission in a 50 kW chemical-looping combustor: continuous reduction and oxidation experiment. In: Seventh International Conference on Greenhouse Gas Control Technologies, Vancouver, Canada, Pergamon Press, London.

Song, K.S., Seo, Y.S., Yoon, H.K., Cho, S.J., 2003. Characteristics of the NiO/hexaaluminate for chemical-looping combustion. Kor. J. Chem. Eng. 20 (3), 471–475.

Villa, R., Cristiani, C., Groppi, G., Lietti, L., Forzatti, P., Cornaro, U., Rossini, S., 2003. Ni based mixed oxide materials for CH_4 oxidation under redox cycle conditions. J. Mol. Catal. A: Chem. 204/205, 637–646.

Paper II

Long-term integrity testing of spray-dried particles in a 10-kW chemical-looping combustor using natural gas as fuel

Carl Linderholm[*,1], Tobias Mattisson[1] and Anders Lyngfelt[1]
[1]Department of Energy and Environment, Chalmers University of Technology, 41296 Göteborg, Sweden

Abstract
Chemical-looping combustion, CLC, is a combustion concept with inherent separation of CO_2. The fuel and combustion air are kept apart by using an oxygen carrier consisting of metals/metal oxides. The oxygen carriers used in this study were prepared from commercially available raw materials by spray-drying. The aim of the study was to subject the particles to long-term operation (> 1000 h) with fuel and study changes in particles, with respect to reactivity and physical characteristics. The experiments were carried out in a 10-kW chemical-looping combustor operating with natural gas as fuel. 1016 h of fuel operation were achieved. The first 405 h were accomplished using a single batch of $NiO/NiAl_2O_4$-particles. The last 611 h were achieved using a $50/50_{mass}$-mixture of (i) particles used for 405 h, and (ii) a second batch of particles similar in composition to the first batch, but with an MgO additive. Thus, at the conclusion of the test series, approximately half of the particles in the reactor system had been subjected to > 1000 h of chemical-looping combustion. The reason for mixing the two batches was to improve the fuel conversion. Fuel conversion was better with the mixture of the two oxygen carriers than it was using only the batch of $NiO/NiAl_2O_4$-particles. The CO fraction was slightly above the equilibrium fraction at all temperatures. Using the oxygen-carrier mixture, the methane fraction was typically 0.4-1% and the combustion efficiency was around 98%. The loss of fines decreased slowly throughout the test period, although the largest decrease was seen during the first 100 h. An estimated particle lifetime of 33000 h was calculated from the loss of fines. No decrease in reactivity was seen during the test period.

1. Introduction
Chemical-looping combustion (CLC) is a combustion concept with inherent separation of CO_2. In 2003, the first operation of the NiO-based oxygen-carrier GRACE [1] in the Chalmers 10-kW prototype meant a break-through for the chemical-looping technology. It turned a paper concept into a novel technology and demonstrated not only successful operation of a continuous unit, but also excellent fuel conversion and small loss of fines from the reactor system. However, the GRACE particle was prepared from very pure raw materials using freeze-granulation, which would be an expensive production method for large-scale manufacture of particles. Furthermore, the duration of fuel operation was 100 h, which is more than long enough to demonstrate the viability of the CLC concept, but insufficient amount of time to investigate the effect on particles of long-term exposure to a real CLC environment and hence insufficient to make a reliable estimation of the particle lifetime.

The oxygen carrier particles used in the present study were prepared from commercially available raw materials and a commercial production method. The purpose of the study was to subject these particles to a CLC environment for > 1000 h and to (a) study the general behaviour of the particles, i.e. fuel conversion as a function of circulation and temperature of

the fuel reactor, (b) investigate any changes in particle reactivity, structure et cetera, and (c) monitor the loss of fines and estimate the particle lifetime. Changes in physical and chemical properties, i.e. (b), will be reported only partly here; Shulman et al. [2] has presented a more detailed evaluation of the used particles.

2. Technical background

2.1 Chemical looping combustion (CLC)

In conventional combustion, the fuel, e.g. natural gas, is in immediate contact with the oxidizing agent, e.g. air. In chemical-looping combustion conventional combustion is split into two gas-solid reactions; oxidation of metal by air and reduction of metal oxide by fuel. Ishida et al. [3] were the first to recognize the potential of chemical-looping combustion as a CO_2 capture technology, but the combustion concept was actually patented already in 1954 by Lewis and Gilliland [4] for the purpose of CO_2 production.

The CLC process requires two interconnected reaction chambers between which a solid, particulate material is circulated. The solid particles, called oxygen carrier, consist of metal oxide (MeO) that is alternately reduced and oxidized while looping in the reactor system. Hence a continuous system for combustion of fuel with inherent CO_2 separation is achieved, see figure 1. After condensing the water, pure CO_2 is obtained from the fuel reactor exhaust gas stream. Two interconnected fluidized beds have an advantage over alternative designs, because the process requires good contact between gas and solids as well as a flow of solid material between the two reactors [5].

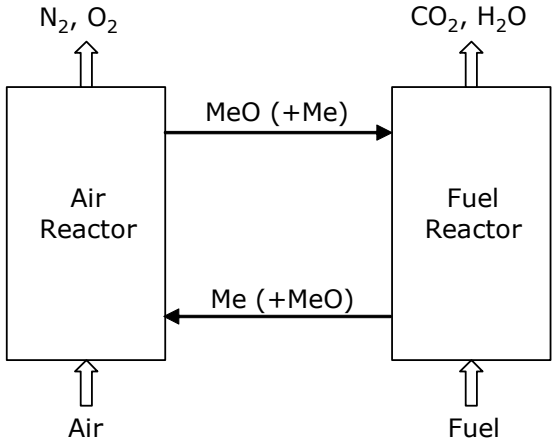

Figure 1. Conceptual layout of chemical-looping combustion. After condensing the water produced in the fuel reactor, pure CO_2 is obtained.

For a hydrocarbon fuel, i.e. natural gas, the chemical reactions taking place while the oxygen carrier circulates in the CLC reactor system can be described as follows,

$$\text{Fuel reactor:} \quad C_nH_m + (2n + \tfrac{1}{2}\, m)\, MeO \rightarrow n\, CO_2 + \tfrac{1}{2}\, m\, H_2O + (2n + \tfrac{1}{2}\, m)\, Me \qquad (1)$$

$$\text{Air reactor:} \quad Me + \tfrac{1}{2}\, O_2 \rightarrow MeO, \qquad (2)$$

and the net reaction in the reactor system thus becomes

$$C_nH_m + (n + \tfrac{1}{4}\, m)\, O_2 \rightarrow n\, CO_2 + \tfrac{1}{2}\, m\, H_2O, \qquad (3)$$

which is identical to conventional combustion. Consequently, the net heat release is also identical to conventional combustion. Reaction (2) is invariably highly exothermic, whereas reaction (1) can be either endo- or exothermic, depending on fuel and on the oxygen carrier.

Most of the work on chemical-looping technologies has been focused on the development and testing of oxygen carrier particles. The doctoral thesis by Johansson [6] provides an overview of work done in the field of oxygen carrier development. An oxygen carrier suitable for chemical-looping combustion is characterized by high rates of oxidation and reduction, high melting temperature, low tendency of attrition and fragmentation, low toxicity, low cost of raw materials and production and finally capability to convert the fuel entirely to CO_2 and H_2O.

In a comprehensive thermodynamical study [7], Jerndal et al. examined potential oxygen-carrier candidates and found that Fe_2O_3/Fe_3O_4, Cu_2O/Cu, Mn_3O_4/MnO and NiO/Ni were most suitable for CLC processes using natural gas as fuel. The oxygen carriers used in the present study were based on NiO, which, in spite of being toxic, expensive and burdened with a thermodynamical constraint [8], is a common choice due to its high reactivity and high melting points.

The major part of the experimental research done on oxygen carriers has been performed in laboratory batch reactors, where particles are subjected alternately to oxidizing and reducing conditions, thus simulating chemical-looping conditions. Tests in continuous chemical-looping systems are necessary to obtain a more comprehensive understanding of the behaviour of the particles.

The construction and testing of several different CLC prototypes has been reported in the literature. The 10-kW unit used in this study has previously been used for testing of two different nickel particles [9,10] for 105 h and 160 h of fuel operation, respectively, and one $Fe_2O_3/MgAl_2O_4$-particle [9] for 17 h. Very high fuel conversion was reported for both Ni-particles. Ryu et al. [11] reported results from a 50-kW chemical-looping combustor using methane and two types of particles. An oxygen carrier based on nickel was tested during 3.5 h with fuel conversion to CO_2 being approximately 98%, and another based on cobalt was tested during 25 h with a corresponding number of 97%. Adanez et al. [12] have demonstrated successful CLC operation in a 10-kW reactor system using a Cu-based oxygen carrier. Complete conversion of the fuel was accomplished using two particle sizes, each of which was tested for 60 h. Song and Kim [13] presented results from CLC experiments using an oxygen carrier based on NiO and Fe_2O_3 as active materials and bentonite as support. At a thermal power of 1 kW, very high conversion of the fuel, methane, was achieved. The successful operation of a 120-kW chemical-looping combustor was accomplished using natural ores [14] and spray-dried NiO-based particles [15]. On a smaller scale, a 300-W reactor system has been designed [16] and operated using a variety of oxygen carriers in combustion experiments [16,17,18,19,20] as well as reforming investigations [19,21]. A 10-kW CLC unit has been constructed for solid fuels [22]. Using an iron-titanium ore, ilmenite, as oxygen carrier, the unit has been operated with South African coal [22] and pet coke [23].

2.2 Particle conversion

The solids flux determines the difference in conversion of particles leaving and returning to the air reactor, i.e. how much of the available oxygen in the particles that is consumed in the fuel reactor [5]. The degree of oxidation of the particles, also called particle conversion, X, is defined as the ratio of the amount of available oxygen present in the carrier and the amount of

available oxygen present in the carrier when fully oxidized,

$$X = \frac{m_{actual} - m_{red}}{m_{ox} - m_{red}}, \quad (4)$$

where m_{actual} is the actual mass of the carrier in its partially oxidized state, m_{ox} is the mass of the sample when fully oxidized, and m_{red} the mass of the sample in the fully reduced form. The particle conversion in the air reactor, X_{AR}, is larger than that in the fuel reactor, X_{FR}, during normal combustion conditions. The difference in particle conversion,

$$\Delta X = X_{AR} - X_{FR}, \quad (5)$$

hence becomes a function of the particle circulation; increasing the solids flux in the reactor system leads to a decrease in ΔX.

2.3 Thermodynamic equilibrium fractions of CO and H_2

As mentioned in the introduction, oxygen carriers based on nickel cannot completely convert methane to H_2O and CO_2. There will be small amounts of CO and H_2 present in the product gas [24]. Table 1 shows equilibrium fractions of CO and H_2 for combustion with methane.

	T (°C)			
	650	750	850	950
CO (%)	0.22	0.40	0.65	0.98
H_2 (%)	0.87	1.02	1.16	1.31

Table 1. Equilibrium fractions of CO and H_2 during combustion with methane after condensation of H_2O.

2.4 The use of mixed NiO-based oxygen carriers in this study

In a study that was conducted in parallel to this one, the performance of a particle composed of 40%$_{mass}$ NiO and 60%$_{mass}$ $NiAl_2O_4$, here denoted N-VITO, was evaluated in batch tests and a 300-W chemical-looping reactor system [20]. Reactivity experiments in a batch fluidized bed reactor showed that N-VITO had excellent oxygen transport capacity, but with somewhat unsatisfactory methane conversion. Hence, measures were taken to improve the methane-conversion capability of the oxygen carrier. The addition of small amounts of MgO to the oxygen carrier was found to have a profound effect on the conversion capability of the particles. The MgO-doped particles will be referred to as N-VITOMg. However, the increased methane conversion was coupled to rather inferior oxygen transport in the particle, especially at lower temperatures, < 900°C. Thus, in order to achieve both good oxygen transport and methane conversion, the two particles were combined and investigated in batch experiments. The combination yielded a potent oxygen carrier mixture with the desired characteristics. Results acquired from operation of the batch reactor were confirmed in a continuous CLC reactor system. The outcome of these experiments resulted in the change of particle batches in the present study, i.e. from using a batch of only N-VITO particles for the first 405 h of operation, to using a mixed batch of used N-VITO and N-VITOMg.

3. Experimental

3.1 The 10-kW chemical-looping combustor

The 10-kW CLC unit used in this study was designed and constructed within the EU-project GRACE [1].

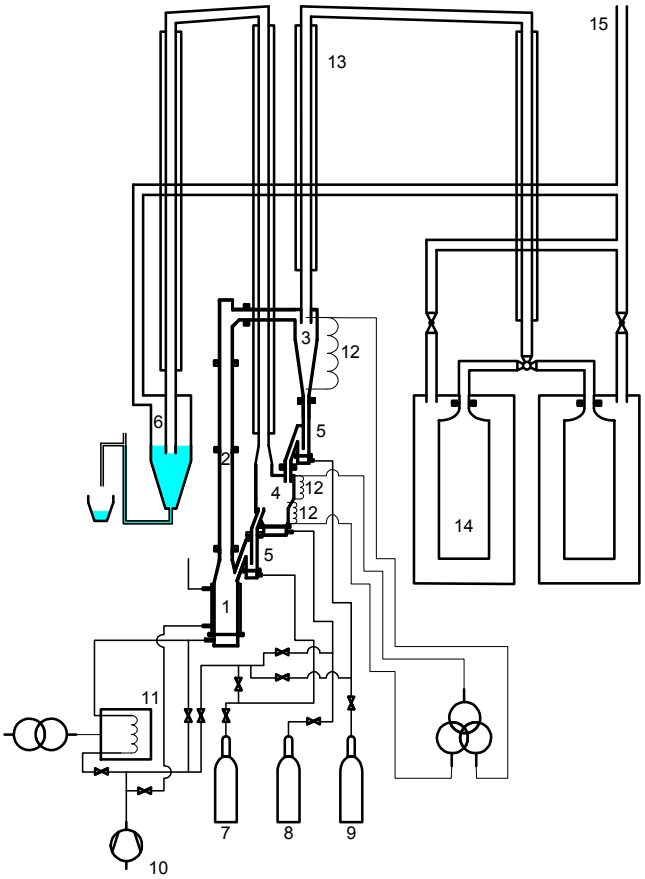

Figure 2. Layout of the Chalmers 10-kW chemical-looping combustor including cooling and particle separation systems. (1) air reactor, (2) riser, (3) cyclone, (4) fuel reactor, (5) upper and lower particle seals, (6) water seal, (7) nitrogen, (8) natural gas, (9) nitrogen, (10) air, (11) preheater, (12) heating coils, (13) finned tubes for cooling of gas streams, (14) filters and (15) connection to chimney.

The prototype is composed of two interconnected fluidized-bed reactors, the fuel and the air reactors, a cyclone to separate the flows of gas and particles from the air reactor, and two loop seals, see figure 2. The gas velocity in the air reactor and riser provides the driving force for particle circulation between the two beds. Entrained particles are recovered in the cyclone and brought to the fuel reactor via the upper particle seal. The fuel reactor is a bubbling fluidized bed. Particles are returned to the air reactor via the lower particle seal. Nozzles are used to distribute the gas in the fuel and air reactors, whereas 5-mm sintered quartz discs of porosity 1 are used as distribution plates in the particle seals. The entire reactor system is hanging on a scaffold and guided vertically using rails below the air and fuel reactors. The two loop seals are present in the system in order to prevent gas leakage between the reactors. Previous results have shown no indication of gas leakage between the reactors [9, 10].

For fluidization of the particle seals, nitrogen is the default option. Using nitrogen gives stable operation of the 10-kW unit, but dilutes the fuel reactor exit gas. In order to obtain a concentrated stream of CO_2 (not diluted with N_2) at the fuel reactor exit, there is an option to use steam for particle seal fluidization.

The gas flows leaving the cyclone and fuel reactor are led through steel tubes with fins on the outside to promote cooling. After cooling, the flow from the cyclone passes through a large

filter bag, where entrained particles are trapped. Switching between two filter bags during operation with fuel allows determination of the mass of elutriated particles for a specific period of time regardless of the duration of the test period; a useful option during long fuel runs. The fuel-reactor exit gas is led to a water seal, where most of the steam condenses. The water seal has two additional important properties; (a) to trap stray particles, i.e. fines, from the fuel reactor and (b) to provide the possibility to control the pressure in the fuel reactor by adjusting the water level.

A supervision system allows unmanned operation of the prototype. When the supervision system is activated, temperatures and gas concentrations in the air and fuel reactors must stay within certain intervals. Should the supervised parameters stray outside these intervals, the fuel gas will be cut and replaced with inert gas. The supervision system permits operation at combustion conditions during long periods of time, > 24 h, with continuous fuel feed.

3.1.1 External heating and cooling options

The heating of the system is carried out using air as fluidizing agent in the air and fuel reactors. When the temperatures in the reactors are high enough to begin fuel operation, air is replaced with nitrogen in the fuel reactor, and after a few minutes nitrogen is switched to fuel.

The incoming air to the air reactor can be preheated up to 1000°C. The need for preheating during stable operation is due to heat losses from the system and depends on the air flow necessary to achieve proper circulation, which is a function of the type of particle used, the fuel flow, and the total solids inventory. During normal operation, the air reactor temperature is kept at 1000°C with the aid of a Eurotherm Temperaure Controller 2216e, which controls the air flow in the cooling jacket that encloses the air reactor.

During this experimental series there were no external means of controlling the fuel-reactor temperature. Hence, the parameters determining the temperature of the fuel reactor during normal operation were solids flux, temperature of the incoming particles and fuel load.

3.2 Oxygen carriers

Two different oxygen carriers were used in these experiments. The important characteristics of the carriers are summarized in table 2. Apparent density is measured on particles sized 125-180 μm and calculated assuming a void between particles of 37%. The crushing strength is measured on particles of size 180-212 μm. The GRACE particle [1], which was used in CLC operation in the 10-kW unit for > 100 h with very high conversion of fuel, has been included for comparison.

Table 2. Characteristics of the oxygen carriers used in the experiments and the GRACE particle.

Denotation used in this study	Active material	Fraction of active material ($\%_{mass}$)	Support material	Production method	Crushing strength (N)	BET surface area (m^2/g)	Apparent density, (kg/m^3)
N-VITO	NiO	40	$NiAl_2O_4$	Spray-drying	2.3	0.7	3600
N-VITOMg	NiO	40	$NiAl_2O_4$ (~42%) and $MgAl_2O_4$ (~18%)*	Spray-drying	2.0		3250
GRACE	NiO	40	$NiAl_2O_4$	Freeze-granulation	2.5	0.4	3800

*assuming that all added MgO reacted with Al_2O_3.

SEM pictures of fresh particles (i.e. particles not subjected to CLC) can be seen in figure 3. It can be noted that a large fraction of the particles are donut-shaped. The physical appearance of N-VITOMg is very similar to that of N-VITO.

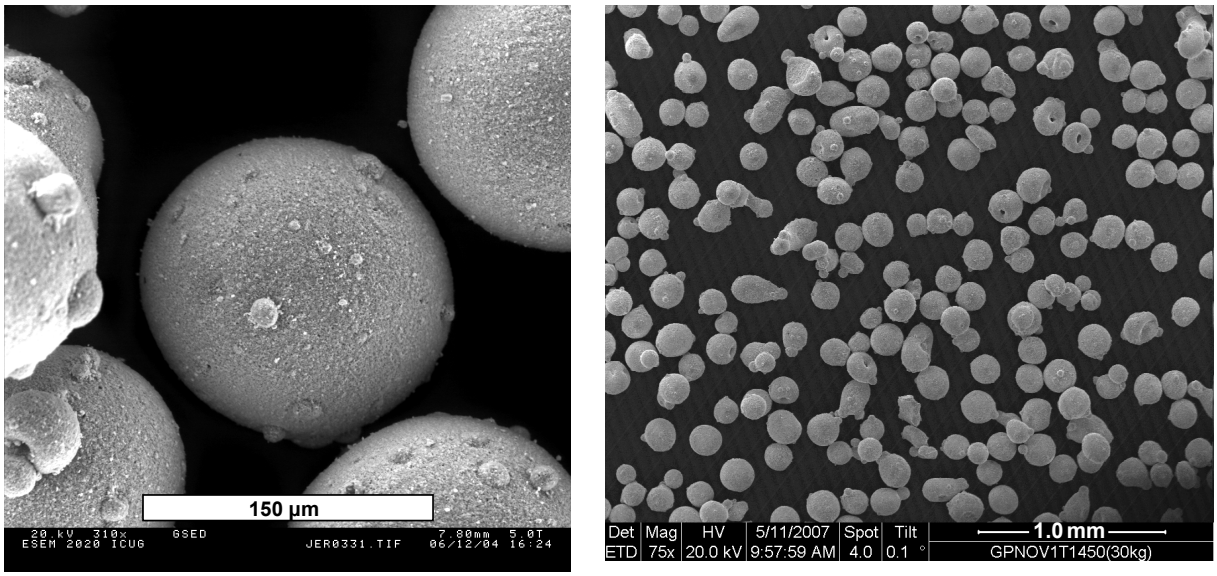

Figure 3. SEM images of fresh N-VITO particles.

The NiO used as raw material in the production of N-VITO and N-VITOMg was a refractory grade material from Novamet containing certain impurities; Co (≈1%), Cu (≈1%), Fe (≈0.5%). For the preparation of N-VITO a water-based slurry containing NiO, Al_2O_3 and small amounts of organic binder and dispersants was mixed, milled and pumped to the nozzle of the spray-dryer. The spray-dried material was sieved to obtain the right particle size distribution and sintered at 1450°C for 4 h. N-VITOMg was prepared in a similar fashion from a slurry that also contained 5% MgO and using a lower sintering temperature, 1400°C. A more detailed description of the particle preparation is presented by Jerndal et al. [25]. The particle size of N-VITO and N-VITOMg was 90-212 µm. The particle size distribution of N-VITO is shown in figure 4. The particle size distribution of N-VITOMg is very similar to that of N-VITO.

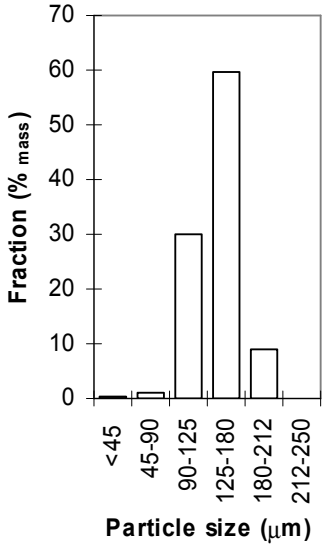

Figure 4. Particle size distribution of fresh N-VITO.

The minimum fluidization and terminal velocities (u_{mf}, u_t) shown in table 3 were calculated according to relations by Kunii and Levenspiel [26]. Values for sphericity, ϕ, were established from SEM images and are therefore somewhat uncertain. The minimum fluidization voidages, ε_{mf}, are estimations for a loosely packed bed with particles of indicated sphericity, as suggested by Kunii and Levenspiel. The average particle diameters, $\overline{d}_p$, are calculated from the particle size distribution.

Table 3. Terminal and minimum fluidization velocities for the particles used in the study. u_t is calculated for air at 1000°C, and u_{mf} is calculated for a mixture of CO_2 and steam at a ratio of 1:2, corresponding to full oxidation of methane, at 850°C.

Particle	ϕ	ε_{mf}	$\overline{d}_p$ (μm)	u_t (m/s)	u_{mf} (m/s)
N-VITO	0.9	0.45	135	0.65	0.010
N-VITOMg	0.9	0.45	135	0.60	0.010

The actual superficial velocity in the reactor system is approximately 0.15 m/s for the reacted gas in the fuel reactor (at 850°C) and approximately 2-3 m/s in the riser (at 1000ºC).

3.3 Fuel

Natural gas was used as fuel in all tests. The main constituent of the fuel is methane, and the average H/C ratio is 3.7. Oxygen consumption is 2.2 moles O_2 per mole fuel when fuel conversion to CO_2 and H_2O is complete, and the volume expansion due to reaction is 3.3 per mole fuel. Table 4 shows the average composition of natural gas in August, 2007 according to DONG Energy, Denmark. The lower heating value is 39.6 MJ/m_n^3 based on the average fuel composition.

Table 4. Average composition of natural gas used in the experiments.

Species	Formula	Mole-%
Methane	CH_4	89.51
Ethane	C_2H_6	5.92
Propane	C_3H_8	2.36
Isobutane	C_4H_{10}	0.40
n-butane	C_4H_{10}	0.56
Isopentane	C_5H_{12}	0.13
n-pentane	C_5H_{12}	0.08
Hexane+	C_6H_{14}	0.06
Nitrogen	N_2	0.28
Carbon dioxide	CO_2	0.71

3.4 Estimating the solids circulation

The solids flux cannot be directly measured in the 10-kW prototype. However, for a specific oxygen carrier in a specific unit geometry, the solids flux can be expressed as a function of the gas velocity and the pressure drop at the top of the riser. According to Johansson et al. [27], the net solids flux for a specific unit geometry can be expressed as

$$G_s = \rho_{exit}(u - u_t) = -\frac{1}{g}\frac{dp}{dh}(u - u_t), \qquad (6)$$

where u is the superficial velocity, u_t is the terminal velocity of an average sized particle and ρ_{exit} is the particle density at the riser exit. Since it is not possible to obtain solid samples from the top of the riser, u_t is based on the average particle size. The applicability of this expression depends on (a) the actual value of u_t at the top of the riser, (b) accuracy in pressure drop measurement in the upper part of riser, and (c) the ratio of solids externally recirculated to that internally separated at the top of the riser.

For the 10-kW unit, the solids circulation calculated by equation (6) is believed to give a significant overestimation. Nevertheless, it provides a useful means for comparing particle circulations during the entire test period. G_s multiplied with the cross sectional area of the riser is referred to as circulation index, although it is a non-dimensionless property with units kg/min.

Another way to express the solids circulation is by comparing the temperatures of particles entering and exiting the fuel reactor. Since the reaction in the fuel reactor is endothermic for NiO-based particles, there is a temperature drop which is related to the magnitude of the solids flux; a low solids flux leads to a sharp temperature decrease and vice versa. This temperature difference can be used as a measure of circulation if

(a) fuel power is constant,
(b) the temperature of the fuel reactor experiences only minor temporal changes (e.g. 2ºC/h),
(c) the incoming particles are the only source of heat, i.e. there is no external heating of the fuel reactor,
(d) the fuel reactor is well mixed, i.e. without temperature gradients and stagnant zones, and
(e) the thermocouples provide accurate information about the particle temperatures.

This temperature difference can be used to calculate the actual circulation rate of particles, as has been shown in a previous study [10]. The particles have to supply heat to (i) the incoming natural gas, which has to be heated to the reaction temperature, (ii) the endothermic reaction – full fuel conversion is assumed, and (iii) the heat loss through the insulation. The energy balance of the fuel reactor can thus be expressed as

$$\dot{m}_{solids}\,(T_{solids,in} - T_{FR})\,c_{p,solids} = \dot{V}_{fuel}\left(\int_{T_{amb}}^{T_{FR}} c_{p,ng}\,dT + \Delta h_r^{T_{FR}}\right) + \dot{Q}_{loss}, \qquad (7)$$

where

- $\dot{m}_{solids}$ (kg/s) is the mass flow of incoming particles; the mass decrease in the fuel reactor is neglected,
- $T_{solids,in}$ (ºC) is the temperature of incoming particles,
- T_{FR} (ºC) is the temperature of the fuel reactor,
- $c_{p,solids}$ (kJ/kg, ºC) is the specific heat of solids, which is assumed to be constant at $T_{average} = (T_{solids,in} + T_{FR})/2$; $c_{p,solids}$ is calculated for completely oxidized particles,
- $\dot{V}_{fuel}$ ($\mathrm{m_n^3/s}$) is the flow of natural gas,
- $c_{p,ng}$ ($\mathrm{kJ/m_n^3}$, ºC) is the specific heat of the natural gas,
- $\Delta h_r^{T_{FR}}$ ($\mathrm{kJ/m_n^3}$) is the heat of reaction at T_{FR},

- $\dot{Q}_{loss}$ (kW) is the heat loss through the insulation, which is assumed to be 0.75 kW. During stable operation at 10 kW the total heat loss from the system is 4-5 kW, and since the temperature in the air reactor and riser are higher than that of the fuel reactor and considering also that the surface area of the fuel reactor is a mere 25% of the total surface area of the reactor system, a heat loss from the fuel reactor of 0.5-1 kW is likely.

An additional prerequisite if the method is to be used to calculate the circulation rate is that all operational parameters have remained unchanged for a long period (e.g. 4 h) preceding the evaluation.

3.5 Measurements

The two gas streams leaving the air and fuel reactors pass through cooling tubes after which a fraction of each gas stream is led first through a small filter, where any entrained fines are removed, and then to a cooling device where most of the remaining steam is condensed. Finally, the two gas streams enter the analysers, SICK MAIHAK S710, where CO_2, CO, O_2 and CH_4 are continuously measured on-line. The carbon containing gases are measured using NDIR absorption, and the oxygen is measured using the paramagnetic sensor OXOR-P. The gas analyzers are calibrated with air, nitrogen, and a mixed gas composed of 10 ± 0.1% CO, 10 ± 0.1% CH_4 and CO_2. The tolerance of the IR instruments is 1% of the ideal value of the measurement range, which for CO and CH_4 means that a measured concentration of, for example, 0.7% translates to an actual concentration within the range 0.6-0.8%. Calibration of the gas analysers was conducted once or twice every week when the prototype was in operation. Hydrogen measurements were performed using gas chromatography (Varian Micro-GC).

Natural gas, nitrogen and air are fed to the 10-kW prototype using El-flow mass flow controllers from Bronkhorst. The measurement error is small, < 1% of measurement range with standard calibration. Steam was supplied to the particle seals using two Cellkraft Precision Evaporators E-1000.

Pressure measurements are used to supervise the bed heights and to evaluate particle flows as a function of operating conditions. The important pressure drops are measured using 20 pressure transducers from Honeywell of types 143PC03D, 143PC01D, 163PC01D36 and 163PC01D75, all of which measure differential pressures.

A total of eight thermocouples of type K monitor the temperatures in the unit. Three thermocouples are placed in the fuel reactor, another two in the air reactor and the remaining ones are found in the cyclone, riser and cooling jacket of the air reactor.

The elemental analysis performed on particles after the conclusion of the experimental series was performed at SP Technical Research Institute. The samples were dissolved in hot acid, and the determination of the elements was performed using ICP-OES (with a Perkin Elmer Optima 5300 DV).

3.6 Logging and data evaluation

Using the software InstruNet World, temperatures, differential pressures, incoming gas flows and gas concentrations were logged every ten seconds. For evaluation of data, 30 measurements (5 minutes) were averaged.

Carbon monoxide, methane, hydrogen and carbon dioxide concentrations presented below are given as fraction of total carbon from the fuel reactor according to

$$f_i = \frac{x_i}{x_{CO_2} + x_{CO} + x_{CH_4}} \tag{8}$$

where i represents CO_2, CO, CH_4 and H_2, and x is the molar fraction of the substance indicated by the sub-script in dry exit gas from the fuel reactor. The measured concentrations of CO, CO_2, CH_4 and H_2 are somewhat lower due to mixing with nitrogen from the particle seals.

Hydrogen was not continuously measured, but it was measured on several occasions during the test series. The hydrogen concentration, and the corresponding fraction, was also calculated for the entire test series. The calculation was made by combining an expression for the water-gas shift equilibrium,

$$K = \frac{[CO_2][H_2]}{[CO][H_2O]} = \frac{\dot{V}_{CO2}\dot{V}_{H2}}{\dot{V}_{CO}\dot{V}_{H2O}} \tag{9}$$

with molar balances of hydrogen and carbon over the fuel reactor. The equilibrium constant, K, was obtained using the software HSC Chemistry 5.1. Generally, the calculated concentration of hydrogen showed very good agreement with the measured concentration.

The combustion efficiency is calculated according to

$$\eta_{combustion} = 1 - \frac{H_{i,CO}\dot{V}_{CO} + H_{i,CH4}\dot{V}_{CH4} + H_{i,H2}\dot{V}_{H2}}{H_{i,fuel}\dot{V}_{fuel}}, \tag{10}$$

where H_i is the lower heating value and $\dot{V}$ is the volumetric flow (m_n^3/s).

4. Results

Experiments were carried out during 15 weeks. The typical duration of uninterrupted operation with fuel was 75 h and thus the unit was operated overnight on 40 occasions. Tests with fuel were performed during a total of 1016 h, 405 of which were performed using only N-VITO, while the remaining 611 h were accomplished using a mixture of equal mass shares of the used N-VITO and N-VITOMg. Hence, at the end of the test series, half the material had been used in CLC operation for > 1000 h; the other half had been used for 611 h.

The fuel power was 10 kW during 982 h. The fuel conversion during these experiments is described below. The air ratio, λ, was 1.17 – 1.46, and the air reactor temperature was normally 1000ºC.

The unit was operated at 5-8 kW for 31 h due to problems with the fuel feed. Most of this time, the fuel reactor was co-fluidized with nitrogen in order to keep the fluidization velocity constant. If the velocity in the fuel reactor is reduced, there is a risk of inadequate mixing and also of back-mixing of particles to the wind-box. The fuel conversion at reduced fuel power was similar to that at 10 kW.

The combustor was operated at 15 kW for 3 h using the oxygen-carrier mixture. The increased air flow led to excessively high circulation rates. It was difficult to bring down the circulation sufficiently to achieve good fuel conversion. The methane fraction was around 2% and CO was slightly above the thermodynamical equilibrium. The temperature of the fuel reactor kept increasing throughout the tests due to the excessive circulation.

4.1 Fuel conversion at 10 kW

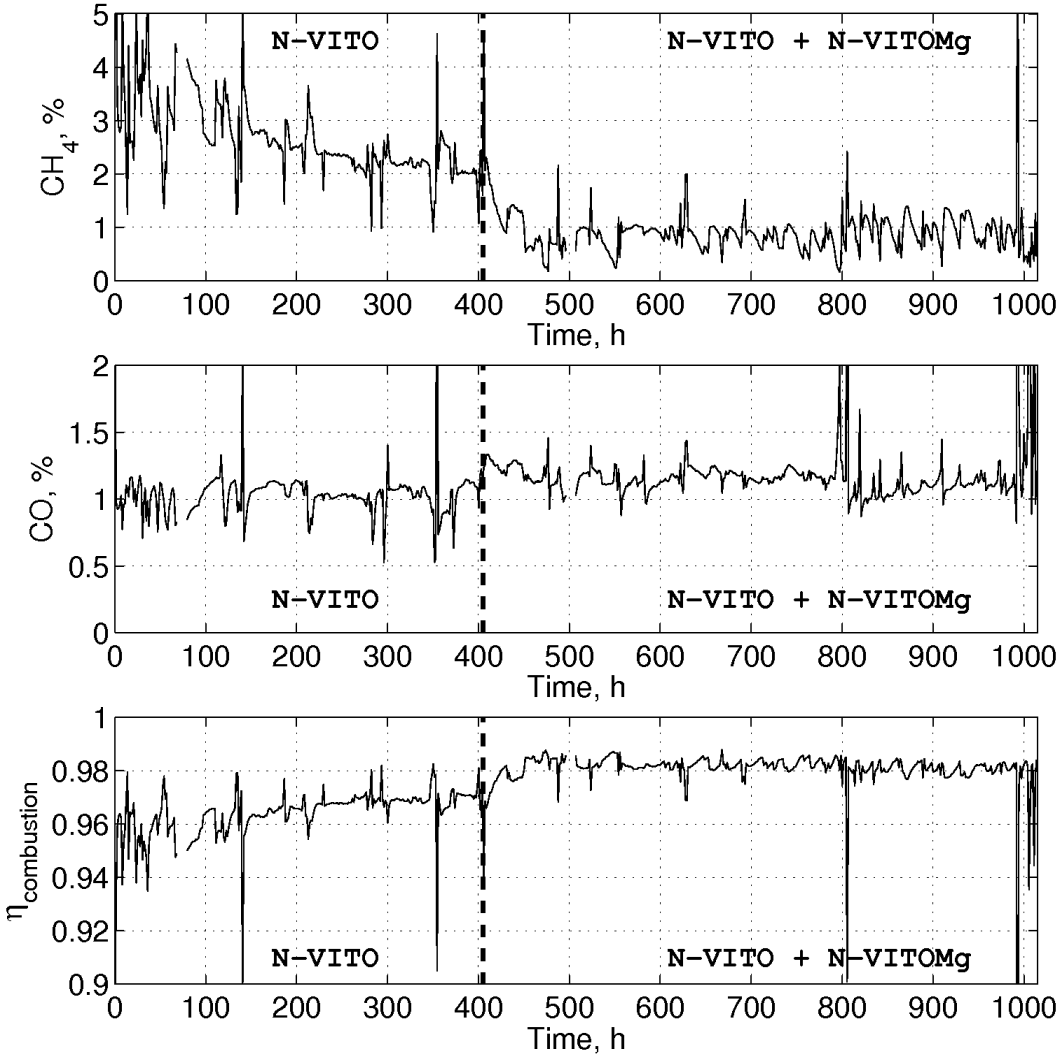

Figure 5. Fractions of CH_4 and CO plotted along with the combustion efficiency against time.

Figure 5 provides an overview of the entire experimental series with respect to fractions of CH_4 and CO and the combustion efficiency. Here, for reasons of clarity, only every 500th data point is plotted in each graph, i.e. less than one data point per hour. Each data point is the average of five minutes of operation. The broken line at 405 h separates the operation with only N-VITO from the operation with the mixture of N-VITO and N-VITOMg. On each of the three graphs, there are two gaps, at approximately 70 h and 500 h, corresponding to periods of approximately 9 hours (per gap) during which data was lost due to software malfunction.

The combustion efficiency, $\eta_{combustion}$, was almost identical to the CO_2 yield, f_{CO2} (not shown).

From figure 5 it is clear that the use of the mixture of two oxygen carrier particles leads to improved combustion efficiency and fuel conversion compared to the operation with only N-VITO. It is especially evident that the methane fraction decreases after an initial transition period of 35-50 h, during which time the fuel conversion improved. The CO fraction is somewhat higher using the oxygen-carrier mixture. For both oxygen-carrier systems, the CO fractions are above the equilibrium, and CO is also higher than what has been observed in previous testing with nickel-based oxygen carriers in the 10-kW unit [9,10].

4.1.1 Effect of temperature

Figure 6 depicts fractions of CH_4 and CO as functions of the temperature in the fuel reactor. This particular series was conducted during a 30-h period when the unit was operated with only N-VITO particles. The circulation was high and relatively constant (22 < circulation index < 28) throughout the test period.

The actual CO fractions are higher than those expected from the thermodynamical equilibrium (also shown in figure). However, the temperature dependence of CO is clearly illustrated.

As is evident from figure 6, an increase in temperature results in a decrease in the outlet CH_4 fraction. This is expected since the rate of gas-solid reactions usually increases with temperature. The circulation index actually increased somewhat as the temperature increased in figure 6. An increased circulation index usually results in a higher fraction of unconverted methane [10], and hence the effect of temperature on methane conversion is probably greater than that shown in the figure.

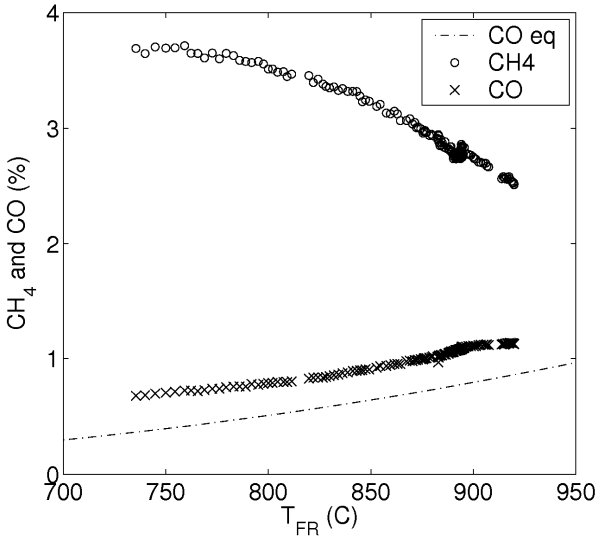

Figure 6. Fractions of CO and CH_4 and equilibrium fraction of CO as functions of temperature.

4.1.2 Effect of circulation

Figure 7 illustrates the dependence of CH_4 on circulation, and it can be seen that the best conversion of methane is obtained at the lowest circulation. This effect of circulation on fuel conversion is associated with the amount of metallic nickel on particles in the fuel reactor. As explained above, ΔX is a function of the solids circulation. Low circulation means that X_{FR} is low, which in turn means that there is a high amount of metallic nickel in the particles. This is an important aspect since metallic nickel acts as a catalyst in steam reforming of natural gas,

$$C_nH_m + n\,H_2O \rightarrow n\,CO + (n + \tfrac{1}{2}m)\,H_2, \quad (11)$$

as well as pyrolysis,

$$C_nH_m \rightarrow n\,C + \tfrac{1}{2}\,m\,H_2. \quad (12)$$

Hence, the solids circulation affects the conversion of the natural gas. It is believed that reaction (11) is important in CLC since there is a high partial pressure of H_2O in the fuel reactor.

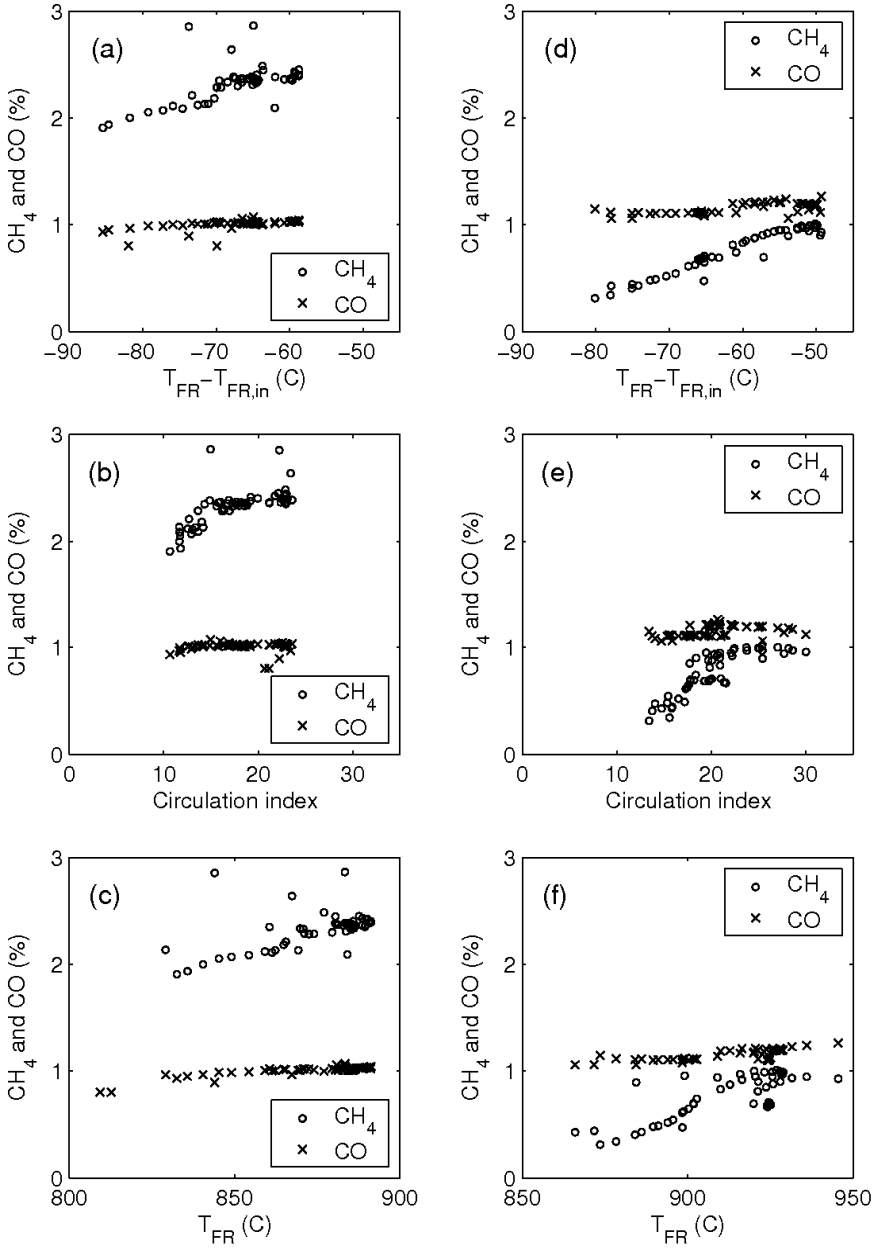

Figure 7. The effect of circulation on fractions of CH_4 and CO. 7 a-c show data from operation with N-VITO, and 7 d-f show data from operation with N-VITO + N-VITOMg.

Figures 7 a-c show data from one week of operation, or approximately 72 h, using N-VITO, and figures 7 d-f show data from another week of operation, approximately 75 h, using the mixture of N-VITO and N-VITOMg. Figures 7 a and d display CH_4 and CO as functions of the temperature difference in the fuel reactor, which is a measure of particle circulation, as

described in the experimental section; 7 b and e also show CH_4 and CO as functions of circulation, but using the so-called circulation index instead of the temperature difference; 7 c and f describe the temperature in the fuel reactor during the tests. Note the difference in temperature on the x-axes of figures 7 c and f, which is a result of lower circulation being used with N-VITO (7 b: circulation index = 10 – 22) compared to N-VITO + N-VITOMg (7 e: circulation index = 12 – 30), and a lower circulation will result in lower temperatures in the fuel reactor.

It has been established above (figure 6) that decreasing the temperature of the fuel reactor has an adverse effect on methane conversion. Nevertheless, in figure 7 the best fuel conversion is obtained at the lower temperatures. However, this is an effect of the connection between circulation and temperature; when circulation is decreased, the temperature in the fuel reactor decreases as well.

In general, the relationship between the fraction of methane and circulation is clearer for the oxygen-carrier mixture than it is for only N-VITO. The difficulties in demonstrating the circulation dependence of CH_4 using N-VITO were associated with problems reaching sufficiently low circulation, which could only be achieved by reducing the solids inventory.

Two tests at very low circulation (circulation index ≈ 5) were performed using N-VITO. The fraction of CH_4 was brought down to around 0.9%, CO was around 1% and the fuel-reactor temperature 840ºC. However, at these low rates of circulation, CO becomes very sensitive to circulation due to the limited supply of oxygen.

4.1.3 Hydrogen

Hydrogen was measured on a number of occasions. The fractions of hydrogen were closely associated with the fractions of CO and were always very close to the fractions calculated from the water-gas shift equilibrium. Figure 8 shows fractions of unburnt gases as a function of temperature during a low-circulation test with a duration of 8 h. "H2 calc" is calculated from the water-gas shift equilibrium as described above.

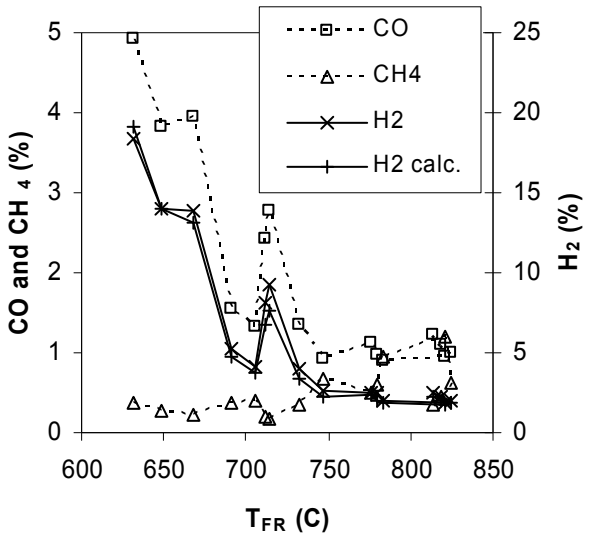

Figure 8. Fractions of CO, CH_4, H_2 and calculated fractions of H_2 using water-gas shift equilibrium.

4.2 Gas leakage

There was no detectable gas leakage between the reactors. No CO_2 was seen in the exit gas from the air reactor, and thus there is no leakage from the fuel reactor to the air reactor that could be detected with the NDIR-absorption instruments. In the opposite direction, i.e. from the air reactor to the fuel reactor, it is more difficult to measure leakage during operation with fuel, since the exit gas from the fuel reactor is usually diluted with N_2 from the particle seals. However, during the period of inert gas fluidization of the fuel reactor and particle seals, which always precedes fuel operation, a leakage would easily be spotted as oxygen in the fuel reactor exit gas, and no such leakage was observed.

Leakages can also be detected during operation with fuel if steam is used to fluidize the particle seals. Steam was used for a total of 11 h in the particle seals, which are normally fluidized with nitrogen. The operation of the unit was not disturbed when steam was introduced in the seals.

If there was no gas leakage from the air reactor to the fuel reactor, there should be no other gases in the exit gas from the fuel reactor but CO_2, H_2, CH_4, CO and a small amount of N_2 originating from the natural gas. Nevertheless, the total of these gases during operation with steam in the particle seals does not add up to the expected 100%, as can be seen in table 5. However, the deviation from 100% is within the measurement error.

Table 5. Dry gas concentrations during operation with steam (averages of one hour of stable operation).

Species	Conc. (%)	Measurement method
CO_2	94.5	IR
H_2	2.4	GC
CH_4	0.95	IR+GC
CO	1.20	IR+GC
N_2 (from fuel)	0.25	(see table 4)
Σ	99.3	

4.3 Carbon formation

Carbon formation on particles was below the detection limit during the tests. Carbon formation on particles would be manifested as CO_2 in the exit gas from the air reactor during operation. At the conclusion of each period of fuel operation, i.e. usually once a week, natural gas was replaced with nitrogen, which in turn was switched to air after 10-15 minutes. The introduction of oxygen in the fuel reactor produces a small CO_2 peak that can be integrated to give an estimation of the amount of carbon formed during fuel operation. Such calculations showed that a few grams of carbon were formed on each run. It is not clear where carbon is formed, but it would be expected to be in the lower parts of the bed or possibly in the wind box or pressure taps. Tests of material extracted from the lower particle seal found no solid carbon deposited on the particles. These particles had $X = 0.6$ and should be representative of particles in the fuel reactor during low circulation.

4.4 Circulation and ΔX

The circulation rate of particles can be calculated according to equation (7). The circulation obtained this way was 2-4 kg/min, or 3.3-6.6 kg/s, MW, which corresponds to $\Delta X = 0.14$-0.27. These numbers are pertinent to operation at medium to high circulation. The method

was not applicable during experiments at low circulation due to inability to meet the requirement of minor temporal changes of the fuel-reactor bed temperature.

An evaluation of the particle conversion at low circulation was performed by terminating fluidization in the particle seals and introducing air to the fuel reactor, following an experiment at low circulation. Normally, nitrogen is introduced in the particle seals at the conclusion of a test.

The evaluation consisted of two parts; (a) oxidation of particles in the fuel reactor in order to estimate the mass of oxygen needed for complete oxidation of particles and subsequent opening of the fuel reactor in order to determine the mass of particles, and (b) using a small laboratory quartz reactor to oxidize a 15-g sample of particles, 125-180 μm, originating from the lower particle seal, where fluidization was terminated and the degree of oxidation should be very similar to that measured in the fuel reactor. The particle conversions determined this way were: $X_{FR} = 0.59$; and $X_{LPS} = 0.60$.

X_{AR} was evaluated using elutriated particles in the size range 125-180 μm. Evaluation of these particles should provide accurate information about the particle conversion of particles entering the fuel reactor. It can be argued that these particles are in contact with air for longer periods of time, since they have to pass through the cooling tubes as described in the experimental section. However, the temperature in these tubes falls rapidly to levels at which no particle oxidation will occur. More importantly, the time that the particles spend in the cooling tubes is short in comparison to the residence time in the air reactor and riser. Determination of X_{AR} was made on five samples covering the entire test period. On average, $X_{AR} = 0.98$, which means that, at low circulation, $\Delta X \approx 0.4$.

4.5 Effect on particles of 1016 h of operation with natural gas

N-VITO particles initially added to the reactor system were in the size range 90-212 μm. After 405 h, the reactor system was opened and emptied. The particles were sieved and small fractions of < 90 μm and > 212 μm were removed. Equal mass shares of the used N-VITO and fresh N-VITOMg were introduced into the reactor system.

The crushing strength of N-VITO after 405 h of fuel operation was 2.3 N, i.e. the same as for fresh particles. For particles at t = 1016 h, the crushing strength of reduced particles ($X = 0.6$) was 2.1 N, whereas oxidized particles had a crushing strength of 2.5 N, i.e. a slight increase. No difference in density between fresh and used particles was observed.

Below follows a “macro-scale” evaluation of the effect on the particles, with focus on the mass balance of particles. For a more detailed, particle-scale analysis, the reader is referred to Shulman et al [2].

4.5.1 Loss of fines and estimated lifetime of oxygen carrier

Particles are continuously lost to the air filters through elutriation. Ideally, only fines, i.e. particles < 45 μm, would be elutriated. As an effect of poor cyclone efficiency, compared to large-scale cyclones, particles of all sizes are continuously elutriated to the air filter. Table 6 summarizes how the different particle sizes collected in the filters and the water seal are defined and the actions that were taken with each fraction during the long-term testing.

Table 6. Elutriated particles: definition and action taken during long-term testing.

Size range (μm)	Defined as / action taken
< 45	Fines / not recycled
45-90	Not fines / not recycled
90-212	Not fines / recycled
>212	Practically non-existent

The rate of elutriation is much higher to the air filters than to the water seal. The small amounts of material > 90 μm that are elutriated to the water seal are dried and recycled.

The loss of fines (*LoF*), which is a useful measure when estimating the lifetime of particles, is calculated as

$$LoF = \frac{m(\text{elutriated particles} < 45\ \mu m \text{ during } \Delta t)}{\Delta t \cdot m(\text{total solids inventory})}\ [h^{-1}], \qquad (13)$$

where Δt is a period of time, typically 24 h for the air filters and 75 h for the water seal. Figure 9 shows the loss of fines and total solids inventory as functions of the time of operation. For the calculation of the loss of fines, it has been assumed that the mass of the total solids inventory in the reactor system was constant at 15 kg. The reason for the jagged appearance of the curve showing the total solids inventory is the recycling of elutriated material, occurring normally once a week during the first 560 h, and a little more frequently thereafter. At about t = 600 h, it is believed that particles began adhering to the walls of the fuel reactor, as will be discussed below. Hence, the amount of circulating material during 600 h < t < 810 h is actually smaller than that implied by the total solids inventory. At t = 810 h, the reactor system was opened and the wall deposits, almost 2 kg, were removed, crushed and sieved. Sieved particles 90-212 μm were recycled. It can be seen in the figure that the total solids inventory starts to decrease at t = 810 h.

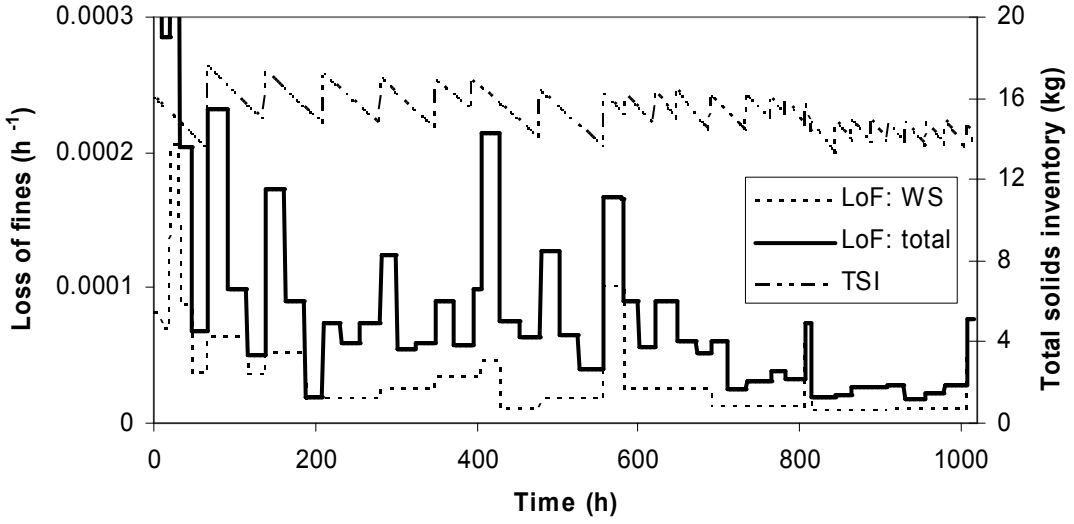

Figure 9. *LoF* and total solids inventory (TSI) as functions of the time of operation. WS: water seal.

LoF at the end of the experimental series can be used to estimate the particle lifetime. Here, the expected particle lifetime is based on the last 100 h of operation, during which time 22 g of fines were collected in the water seal and 20.5 g of fines were encountered in the air filters.

Assuming that the mass of the total solids inventory was 14 kg during this period, the loss of fines is 0.003% h^{-1}, which corresponds to a particle lifetime of 33000 h.

4.5.2 Mass balance

If predictions about particle lifetime based on *LoF* are to be reliable, it is necessary that the mass of added and recycled particles equals that of elutriated and extracted particles, i.e. that there are no mass flows unaccounted for.

16 kg of N-VITO were added at the start of the experiments. After 65 h of operation, the total solids inventory had decreased – due to elutriation – to the extent that sufficient circulation could no longer be sustained. Elutriated particles had to be recycled, a procedure that cannot be carried out during operation with fuel, and which is preferably done at cold conditions. In order to allow consecutive operation with fuel for > 70 h, an additional 2 kg of particles were added at t = 65 h. For several weeks, it was enough to recycle particles once a week, e.g. every 75 h. At a later stage of the test series, during operation with the oxygen-carrier mixture, particles had to be recycled on a daily basis due to decreased amount of circulating material. This decrease was caused by (a) continuous particle degradation and the associated accumulative loss of fines, (b) deposition of particles on the fuel-reactor interior, a phenomenon which was most pronounced during 600 h < t < 810 h and which is accounted for below, (c) leakage, occurring more or less simultaneously with the particle deposition. As a consequence, the recycling of material had to be performed during hot conditions in order to minimize the length of the fuel stop.

At t = 405 h, the reactor system was opened and particles were sieved and weighed. The mass balance showed that approximately 300 g were unaccounted for. A part of this mass decrease could be explained by a reduction of *X*, i.e. reduced amount of oxygen in the particles.

At t = 1016 h, the reactor system was once again opened and, this time, as is shown in table 7, the mass of encountered particles was actually somewhat larger than that added. The explanation for this must be that the reactor system was not properly emptied at t = 405 h.

Table 7. Mass balance of particles for the last 611 h (with mixed batch). "IN" shows the mass of added material at t = 405 h, and also from which vessel the already used N-VITO particles had been extracted. "OUT" shows extracted and elutriated material. AR: air reactor; FR: fuel reactor; LPS: lower particle seal; UPS: upper particle seal.

IN

Particle type and vessel of extraction	**m (g)**
N-VITO (used for 405 h)	8250
• *AR*	*5936*
• *LPS*	*916*
• *UPS*	*779*
• *FR*	*619*
N-VITOMg (fresh)	8265
SUM	**16515**

OUT

Vessel	**Time of recovery (h)**	**Size (µm)**	**Mass (g)**
AR	1016	(all)	4054.5
LPS	1016	(all)	885.5
LPS, windbox	1016	(all)	929.5
LPS, downcomer	1016	(all)	559.5
UPS	1016	(all)	2483
UPS, windbox	1016	(all)	903
FR	1016	(all)	4245
FR, wall deposits	1016	(all)	124
FR	810	(all)	1063.5
Filters	Intermittently	125-180	120
Filters	1016	90-212	437
Filters	Continuously	< 45	372.5
Filters	Continuously	45-90	104
Water seal	Continuously	< 45	187
Leaks	1016	(all)	75
SUM			**16543**

It can be noted in table 7 that there is a rather large amount of material in the upper particle seal. This may be explained by the shut-down procedure at the conclusion of the test series. Here, the fuel feed was terminated and fluidization of the particle seals was stopped simultaneously. The flow of air in the air reactor was decreased but was still high enough to maintain some carry-over from the riser to the cyclone and thus resulting in an excessive amount of particles in the upper particle seal (or more accurately, in the cyclone leg), as well as the large amount of material in the downcomer between fuel reactor and the lower particle seal. Fluidization of the fuel reactor also continued until the reactor system had cooled.

The wind boxes of both particle seals were full of particles at the conclusion of the test series, as can be seen in table 7. The explanation for this is that the gas distribution plates, which are made of sintered quartz, broke at t = 582 h (LPS) and t = 695 h (HPS). However, the functionality of the seals remained.

The explanation to why "LPS" is separated from "LPS, downcomer" in table 7 is that the material in the downcomer was extracted from above, i.e. from the fuel reactor. This was done in order to obtain a sample of particles representing those of the fuel reactor during operation with fuel, i.e. the particles in the lower particle seal, where fluidization was terminated at the same time as the fuel was cut and replaced with nitrogen. The particles in the downcomer

might have been oxidized in the fuel reactor during post-fuel operation with air and then splashed into the downcomer.

Table 7 shows that a mass of 1063.5 g was extracted from the fuel reactor at t = 810 h and not recycled to the reactor system. This mass consisted of wall deposits and some agglomerates.

The particles elutriated "intermittently" (table 7) to the filters represent six samples that were elutriated on six different occasions, and that were saved for later analysis.

The conclusions to be drawn from the mass balance are that there are no mass flows or leakages unaccounted for, and that no fines escaped through the filters.

4.5.3 Micro-agglomerates

At the conclusion of the test series, it was observed that a substantial amount of particles, 673 g or 4%$_{mass}$ of the initially added mass, were > 212 µm. These were found predominantly in the air reactor, as can be seen in table 8. The high frequency of micro-agglomerates in the air reactor is explained by their size, which gives a higher terminal velocity and thus a higher tendency to fall back into the bed of the air reactor. In other words, the abundance of these particles in the air reactor does not necessarily provide any information about where they were formed. A light-microscope picture – shown in figure 10 – of these particles revealed clusters of oxygen-carrier particles that appear to have been fused together, possibly by molten material, as figure 11 suggests.

There is a very distinct colour difference within a micro-agglomerate. In figure 11, the lighter area that looks like a melt and seems to connect two individual particles, appear golden or brownish and shiny in a light microscope, whereas the darker area has the original particle colour, i.e. dark green.

Table 8. Fractions of micro-agglomerates at t = 1016 h.

Vessel	Mass (g)	Fraction in vessel (%$_{mass}$)	Fraction of total oversize, >212 µm (%$_{mass}$)
Air reactor	463.5	11	69
Lower particle seal	75	3	11
Upper particle seal	37	1	5.5
Fuel reactor	97.5	2	14.5
Total	673	5	100

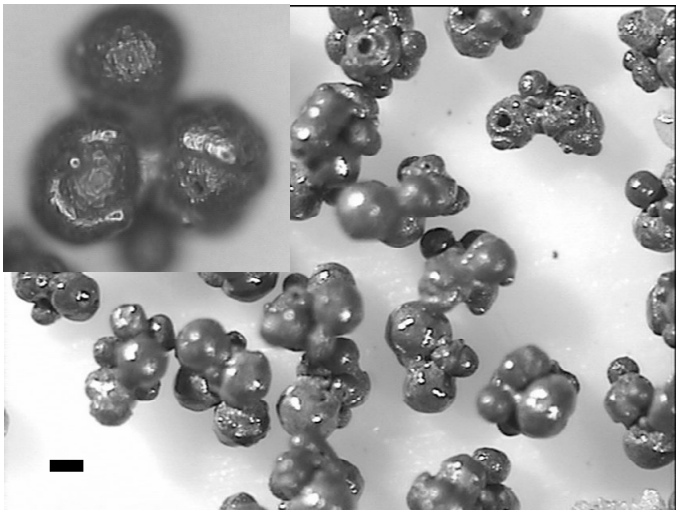

Figure 10. Light-microscope image of micro-agglomerates encountered in the air reactor upon opening after 1016 h of operation. The black line in the lower left corner represents 100 µm. The magnification of the inset (top left) is approximately twice that of the main picture.

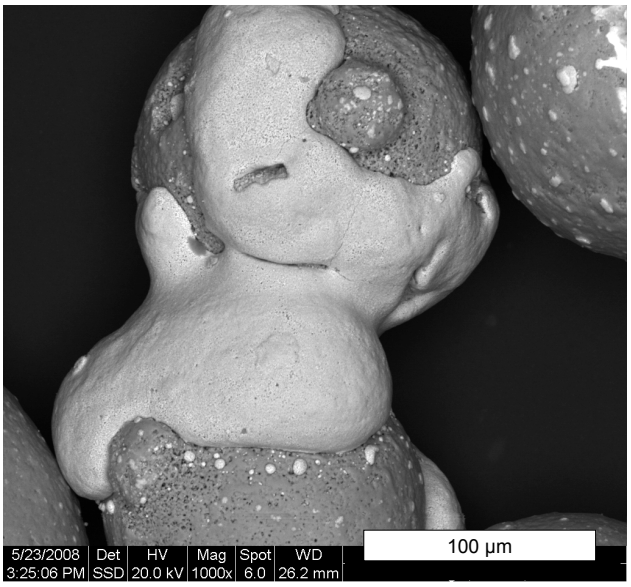

Figure 11. SEM image of micro-agglomerate.

Elemental analysis of the micro-agglomerates showed a very low occurrence of Mg, indicating that the majority of the particles forming the micro-agglomerates were N-VITO. It also revealed that the concentration of copper was > 50% higher than that found in fresh particles, fines, and used particles, which all had similar copper contents.

4.5.4 Agglomeration and wall deposits in the fuel reactor

Agglomeration sometimes occurs in the fuel reactor. The exact mechanisms that trigger agglomeration are not known, but it has been observed that agglomerates form during periods of poor mixing, and that the risk of agglomeration increases when the particle conversion is low [10]. The agglomerates can be quite large (> 5 cm) and are usually so soft that they can easily be crushed between fingers. Agglomerates formed in the fuel reactor are normally crushed and re-introduced into the reactor system, but some are saved for analysis.

At t = 65 h, circulation could not be maintained due to a large agglomerate being caught in the downcomer between the lower particle seal and the fuel reactor. The reactor system had to be

opened and the agglomerate was removed, crushed, sieved and re-introduced. It is not known why the agglomerate formed.

At t = 405 h, the 10-kW prototype had to be opened once again because of agglomerates impeding circulation. This time, massive agglomeration had occurred in the fuel reactor. This was most likely the effect of too low fuel flow during several hours, which led to poor mixing. This was associated with problems with the fuel-gas supply system.

At t = 810 h, the reactor system had to be opened due to insufficient material in circulation. This had two explanations; (i) a gasket had broken between the cyclone and the upper particle seal which resulted in leakage, and (ii) 1750 g particles were found to have adhered to the interior of the fuel reactor. These particle deposits had formed on walls that are not perpendicular; i.e. the middle section of the fuel reactor, which is conical, and the bottom plate around the nozzles. The wall deposits were scraped down from the walls, sieved, and particles within the size range 90-212 μm were returned to the reactor system. Elemental analysis of the wall deposits showed low occurrence of Mg, although higher than for the micro-agglomerates. Nevertheless, this indicates that the wall deposits mainly consisted of N-VITO. A few agglomerates were also found upon opening. Almost all of the particles that leaked out could be recovered and recycled.

At t = 1016 h, no agglomerates were encountered upon reactor opening, but 124 g of wall deposits.

It is important to point out that in a larger chemical-looping combustor the gas velocity in the fuel reactor would be higher and as a consequence it is expected that agglomeration would be much rarer. The superficial velocity in the fuel reactor of the 10-kW unit is around 0.15 m/s for the reacted gas at 850°C.

5. Discussion

Although there have been several investigations in continuous CLC units in the last decade, the durations of the tests have been rather limited. Furthermore, in many cases the materials have been prepared by methods that are not commercial. In this work, promising oxygen carriers have been investigated in a continuous 10-kW reactor in excess of 1000 h. The particles were prepared using commercial materials and production methods, and hence the work in this paper is a step towards taking the CLC technology to a new level of development. The experiments were successful and the used particles showed limited physical and chemical changes, see also the work of Shulman et al [2]. However, there were clear indications of agglomeration and formation of so-called ‘micro-agglomerates’ which need to be investigated further.

The use of the mixed oxide system showed clear advantages with respect to methane conversion.

No decrease in reactivity was seen during the experimental series. During the initial periods of operation, the performance of both batches actually seemed to improve. This is most evident with the oxygen-carrier mixture, where, during the first 35-50 h, there was a gradual decrease of CH_4 although all operating parameters and circulation remained constant. A possible explanation is that the reactivity N-VITOMg increases with number of cycle, i.e. the time spent in the reactor system, as shown by Jerndal et al. [25].

An elemental analysis of the Mg-content of the fines from the air reactor showed no major changes during the last 611 h. The mass fraction of Mg was between 1.6-2.1% of the total metal content. The corresponding numbers for N-VITO and N-VITOMg are 0% and 4.1%. This means that the rate of elutriation is similar for the two types of particles used. It was believed that the Mg-content of the fines would be higher, at least initially, since N-VITO had already been used in CLC operation for 405 h. It can be noted that the Mg-content was not analyzed after the first day of operation with the oxygen-carrier mixture, i.e. at t = 405+24 h, when it is likely that a higher Mg-content of the fines would have been found.

The result of the Mg-analysis provides important information since it suggests that N-VITOMg is no more sensitive to attrition than N-VITO. Combining this finding with the low Mg-content of the micro-agglomerates indicates that the estimated particle lifetime may be accurate for N-VITOMg but not for N-VITO, since the formation of micro-agglomerates should be taken into account for N-VITO, which would reduce its expected lifetime. However, the formation of micro-agglomerates is likely to be associated with the formation of large agglomerates or remnants of large agglomerates, which are not expected to form in a larger-scale fuel reactor using higher velocity, as discussed above. Moreover, it is possible that micro-agglomerates can be re-used as oxygen carriers after a simple crushing.

Since massive agglomeration occurred in the fuel reactor prior to opening at t = 405 h, only a small amount of particles from the fuel reactor was included in the mixed batch of oxygen-carrier particles. The fact that the majority of the N-VITO particles in the second batch originated from the air reactor implies that N-VITO particles were, on average, larger than the N-VITOMg particles, since there is an over-representation of large particles in the bottom bed of a CFB. The difference, however, should be small, and should not have any effect on the results.

6. Conclusions

Oxygen-carrier particles prepared from commercially available raw materials by spray-drying were used for > 1000 h in a 10-kW chemical-looping combustor. 405 h of fuel operation were accomplished using N-VITO, a particle with NiO ($40\%_{mass}$) as active component and $NiAl_2O_4$ as inert. Another 611 h of operation were accomplished using a mixture of the used N-VITO particles in combination with another particle, N-VITOMg, prepared similarly as N-VITO, but with a $5\%_{mass}$ addition of MgO in the raw materials, which should yield a combination of $NiAl_2O_4$ and $MgAl_2O_4$ constituting the inert. The reason for mixing the two particles was to optimize the performance with regards to fuel conversion. In general, fuel conversion increased, as expected, with (a) decreased circulation, and (b) increased fuel reactor temperature. Compared to the operation with only N-VITO, fuel conversion was improved using the oxygen-carrier mixture, although the fraction of CO was higher. For both batches, the CO fraction was slightly above the equilibrium fraction at all investigated temperatures. Using the oxygen-carrier mixture, the methane fraction was typically 0.4-1% and the combustion efficiency was around 98%.

The particle circulation was estimated on a few occasions from a heat balance over the fuel reactor during stable operating conditions and “medium” to “high” circulation. The calculated circulation was 2-4 kg/min, or 3.3-6.6 kg/s, MW, which corresponds to $\Delta X = 0.14 – 0.27$. An evaluation of the difference in particle conversion at low circulation showed that $\Delta X \approx 0.4$.

At the conclusion of the experimental series, micro-agglomerates were encountered primarily in the air reactor. Elemental analysis of these micro-agglomerates showed that they had a very low fraction of Mg, which implies that they were made up primarily of N-VITO.

No decrease in reactivity was seen during the test period. No gas leakage between the reactors was detected. Agglomeration of particles occurred on a number of occasions. The agglomerates were soft, and could be crushed and re-introduced into the reactor system.

The loss of fines decreased slowly throughout the test period. An estimated particle lifetime of 33000 h was calculated from the loss of fines.

Acknowledgements
This work was carried out within the EU-financed research-project CLCGP (Chemical-Looping Combustion CO2-Ready Gas Power), Contract Number 019800. The particles were supplied by VITO (Flemish institute for technological research) in Belgium. The authors would like to acknowledge very valuable contributions from Erik Jerndal, Nicolas Berguerand and Magnus Rydén.

Abbreviations and notation

AR	Air reactor
CFB	Circulating fluidized bed
CLC	Chemical-looping combustion
CSIC	Consejo Superior de Investigaciones Científicas
FR	Fuel reactor
GRACE	Grangemouth Advanced CO2 Capture Project
IPCC	Intergovernmental Panel on Climate Change
LoF	Loss of fines
LPS	Lower particle seal
Me/MeO	Metal/metal oxide
N-VITO	Spray-dried oxygen-carrier particles produced by VITO
N-VITOMg	Spray-dried oxygen-carrier particles produced by VITO
R_0	Oxygen ratio
SEM	Scanning electron microscopy
TSI	Total solids inventory
u_{mf}	Minimum fluidization velocity
UPS	Upper particle seal
u_t	Terminal velocity
VITO	Flemish institute for technological research
X	Particle conversion

References

[1] Lyngfelt, A., Kronberger, B., Adanez, J., Morin, J.-X., and Hurst, P. The GRACE project. Development of oxygen carrier particles for chemical-looping combustion. Design and operation of a 10 kW chemical-looping combustor. 7th International Conference on Greenhouse Gas Control Technologies, Vancouver, Canada, 5th-9th September 2004.
[2] Shulman, A., Linderholm, C., Mattisson, T., Lyngfelt, A. 2008. High Reactivity and Mechanical Durability of NiO/NiAl2O4 and NiO/NiAl2O4/MgAl2O4 Oxygen Carrier Particles used for over 1000 Hours in a 10 kW CLC Reactor. To be submitted for publication.
[3] Ishida, M. and Jin, H. 1997. CO2 recovery in a power plant with chemical looping combustion. *Energy Conversion and Management* 38:187-192.
[4] Lewis, W. K., Gilliland, E. R. 1954. Productions of pure carbon dioxide. US Patent No. 2,665,972.
[5] Lyngfelt, A., Leckner, B., Mattisson, T. 2001. A fluidized-bed combustion process with inherent CO_2 separation - application of chemical-looping combustion. *Chemical Engineering Science* 56:3101-3313.
[6] Johansson, M. 2007. *Screening of oxygen-carrier particles based on iron-, manganese- copper- and nickel oxides for use in chemical-looping technologies*, PhD Thesis, Department of Chemical and Biological Engineering, Environmental Inorganic Chemistry, Chalmers University of Technology, Göteborg, Sweden.
[7] Jerndal, E., Mattisson, T., and Lyngfelt, A. 2006. Thermal Analysis of Chemical-Looping Combustion. *Chemical Engineering Research and Design* 84:795-806.
[8] Mattisson, T., Johansson, M., and Lyngfelt. A. 2006. The use of NiO as an oxygen carrier in chemical-looping combustion. *Fuel* 85:736-747.
[9] Lyngfelt A, and Thunman, H. *Construction and 100 h of operational experience of a 10 kW chemical looping combustor*. Chapter 36 in Carbon Dioxide Capture for Storage in Deep Geologic Formations - Results from the CO2 Capture Project, Volume 1 – Capture and Separation of Carbon Dioxide From Combustion Sources, Ed.: Thomas, D. Elsevier Science, London 2005. pp. 625-646.
[10] Linderholm, C., Abad, A., Mattisson, T., Lyngfelt, A. 2008. 160 h of chemical-looping combustion in a 10 kW reactor system with a NiO-based oxygen carrier. *International Journal of Greenhouse Gas Control* 2:520-530.
[11] Ryu, H. J., Bae, D. H., and Jin, G. T. 2003. Effect of temperature on reduction reactivity of oxygen carrier particles in a fixed bed chemical-looping combustor. *Kor J Chem Eng* 20:960–966.
[12] Adánez, J., Gayán, P., Celaya, J., de Diego, L. F., García-Labiano, F., Abad, A. 2006. Chemical Looping Combustion in a 10 kW_{th} Prototype Using a CuO/Al_2O_3 Oxygen Carrier: Effect of Operating Conditions on Methane Combustion. *Industrial & Engineering Chemistry Research* 45:6075-6080.
[13] Son, S.R., Kim, S.D. 2006. Chemical-Looping Combustion with NiO and Fe_2O_3 in a Thermobalance and Circulating Fluidized Bed Reactor with Double Loops. *Industrial & Engineering Chemistry Research* 45:2689-2696.
[14] Pröll, T., Mayer, K., Bolhàr-Nordenkampf, J., Kolbitsch, P., Mattisson, T., Lyngfelt, A., Hofbauer, H. 2008. Natural minerals as oxygen carriers for chemical looping combustion in a dual circulating fluidized bed system. GHGT-9: 9th International Conference on Greenhouse Gas Control Technologies, 16-20 November 2008.
[15] Bolhàr-Nordenkampf, J., Pröll, T., Kolbitsch, P, Hofbauer, H. 2008. Performance of a NiO-based oxygen carrier for chemical looping combustion and reforming in a 120kW unit. GHGT-9: 9th International Conference on Greenhouse Gas Control Technologies, 16-20 November 2008.

[16] Johansson, E., Mattisson, T., Lyngfelt, A., Thunman, H. 2006. A 300 W laboratory reactor system for chemical-looping combustion with particle circulation. *Fuel* 85:1428–1438.
[17] Johansson, E., Mattisson, T., Lyngfelt, A., and Thunman, H. 2006. Combustion of Syngas and Natural Gas in a 300 W Chemical-Looping Combustor. *Chemical Engineering Research and Design* 84:819-827.
[18] Abad, A., Mattisson, T., Lyngfelt, A., and Rydén, M. 2006. Chemical-Looping Combustion in a 300 W Continuously Operating Reactor System Using a manganese-Based Oxygen Carrier. *Fuel* 85:1174-1185.
[19] Rydén, M., Lyngfelt, A., and Mattisson, T. Chemical-looping combustion and chemical-looping reforming in a circulating fluidized-bed reactor using Ni-based oxygen carriers. Accepted for publication in *Energy & Fuels.*
[20] Linderholm, C., Jerndal, E., Mattisson, T., Lyngfelt, A. 2008. Investigation of Ni-based mixed oxides in a 300 W chemical-looping combustor. Submitted for publication.
[21] Rydén, M., Lyngfelt, A., and Mattisson, T. 2006. Synthesis gas generation by chemical-looping reforming in a continuously operating laboratory reactor. *Fuel* 85:1631-1641.
[22] Berguerand, N., Lyngfelt, A. 2008. Design and operation of a 10 kW_{th} chemical-looping combustor for solid fuels – Testing with South African coal. *Fuel* 87:2713-2726.
[23] Berguerand, N., Lyngfelt, A. 2008. The use of petroleum coke as fuel in a 10 kW_{th} chemical-looping combustor. *International Journal of Greenhouse Gas Control* 2:169-179.
[24] Mattisson, T., Johansson, M., and Lyngfelt. A. 2006. The use of NiO as an oxygen carrier in chemical-looping combustion. *Fuel* 85:736-747.
[25] Jerndal, E., Mattisson, T., Thijs, I., Snijkers, F., Lyngfelt, A. 2008. NiO particles with Ca and Mg based additives produced by spray-drying as oxygen carriers for chemical-looping combustion. 9th International Conference on Greenhouse Gas Control Technologies, 16 - 20 November 2008. Accepted for publication.
[26] Kunii, D., Levenspiel, O. 1991. *Fluidization Engineering*. Reed Publishing Inc., Stoneham.
[27] Johansson, E., Lyngfelt, A., Mattisson, T. and Johnsson, F. 2002. A circulating fluidized bed combustor system with inherent CO_2 separation - application of chemical looping combustion. *7th Int. Conf. on Circulating Fluidized Beds*, Niagara Falls, Ontario, May 5-7, 2002, 717-724.

Paper III

Investigation of NiO-based mixed oxides in a 300-W chemical-looping combustor

Carl Linderholm[*,1], Erik Jerndal[2], Tobias Mattisson[1] and Anders Lyngfelt[1]
[1]Department of Energy and Environment, Chalmers University of Technology, 41296 Göteborg, Sweden
[2]Department of Chemical and Biological Engineering, Chalmers University of Technology, 41296 Göteborg, Sweden

Abstract
Chemical-looping combustion, CLC, is a novel combustion concept with inherent separation of CO_2. This study evaluates the performance of spray-dried nickel-based oxygen carrier particles prepared from commercially available materials. The possibility to optimize the methane conversion while retaining the oxygen transport capacity by mixing different NiO-based oxygen carriers was evaluated and results showed that such optimization was indeed possible. Experiments were carried out in a batch reactor as well as in a continuous 300-W unit. Experiments in the batch reactor evaluated the performance of two different spray-dried particles, individually and mixed, at two different temperatures, 850°C and 950°C. The reference particle, referred to as N-VITO in this study, contained only NiO and $NiAl_2O_4$ while the other spray-dried particle was similar to the reference but contained a small amount of MgO as additive in the starting material. It was found that the reference particle had good oxygen-transport characteristics, but that methane conversion left room for improvement. The particle with MgO addition, on the other hand, showed excellent methane conversion, but poor oxygen transport capability, especially at the lower temperature. The $50/50_{mass}$-mixture of the two particles resulted in a potent oxygen-carrier batch with the desired qualities. Three experimental series were conducted in the 300-W CLC-unit; (i) using only the reference particle, (ii) using a mixture of the reference particle and the particle with MgO-addition, and (iii) using the previous mixed oxide system together with a small quantity of a high-surface impregnated oxygen-carrier based on NiO and Al_2O_3. It is shown that the methane conversion to CO_2 is dependent primarily on the solids flux in the reactor system, but also on the temperature in the fuel reactor. Results showed that the operation was more stable and that it was possible to obtain better fuel conversion when the mixtures of two or three different oxygen carrier particles were used. With these mixtures, the methane fraction could be brought down to < 0.1% while still maintaining a low CO fraction.

1. Introduction
During the last 200 years, the atmosphere has experienced a dramatic increase in CO_2 concentration due to the combustion of fossil fuels. CO_2 absorbs outbound infrared radiation in the atmosphere, thus playing an important role in the so-called greenhouse effect. The largely prevailing opinion of the scientific community is that the warming seen in the last 50 years can be explained by human activities, primarily by the release of CO_2 and other greenhouse gases to the atmosphere.

In order to turn the trend of increasing CO_2 emissions, drastic measures need to be implemented. There are heat and power production methods that do not utilize fossil fuels and that are

essentially carbon neutral. Nonetheless, in the near future it is very likely that society will remain highly dependent on fossil fuels. Hence arises a necessity to find a way of continuing to use fossil fuels while at the same time preventing the CO_2 from escaping into the atmosphere. When carbon containing energy sources are oxidized, CO_2 must be captured and subsequently stored, a concept commonly referred to as carbon capture and storage. It is feasible to implement CO_2 capture on sites of significant CO_2 production, e.g. power plants. CO_2 storage options include depleted gas and oil fields and aquifers. Since 1996 around 1 Mt CO_2 has been injected annually beneath the North Sea floor in the Utsira aquifer [1]. Other on-going major CO_2 storage projects include the Weyburn Enhanced Oil Recovery Project in Canada and the In Salah Natural Gas Project in Algeria.

A large number of techniques for CO_2 capture have been proposed and investigated for large scale power production applications, and most of these techniques have the disadvantage of requiring large amounts of energy for the CO_2 separation, resulting in a substantial decrease in power plant efficiency. A CO_2 separation technology without such an energy penalty would obviously be of great interest.

1.1 The CLC process and the oxygen carrier

In conventional combustion, the fuel, e.g. natural gas, is in immediate contact with the oxidizing agent, e.g. air. In chemical-looping combustion conventional combustion is split into two gas-solid reactions; oxidation of metal (or metal oxide) by air and reduction of metal oxide by fuel. This combustion concept was first presented by Ishida et al. [2] in 1987.

The primary reason why CLC has gained interest in recent years is that the CO_2 separation is inherent to the CLC process. However, this advantage aside, CLC technology actually offers at least a couple of benefits compared to conventional combustion; (a) flue gas from the air reactor, which is the bulk of the gas used in the process, is innocuous, consisting of nitrogen and excess oxygen, and (b) there is no or very little thermal NO_x formation since there is no flame and temperature is relatively moderate.

The process requires two interconnected reaction chambers between which a solid, particulate material is circulated. The solid particles, called oxygen carrier, consist of metal oxide (MeO) that is alternately reduced and re-oxidized while looping in the reactor system. Hence a continuous system for combustion of fuel with inherent CO_2 separation is achieved, see figure 1. After condensing the water, pure CO_2 is obtained from the exhaust gas of the fuel reactor. Two interconnected fluidized beds have an advantage over alternative designs, because the process requires good contact between gas and solids as well as a flow of solid material between the two reactors [3].

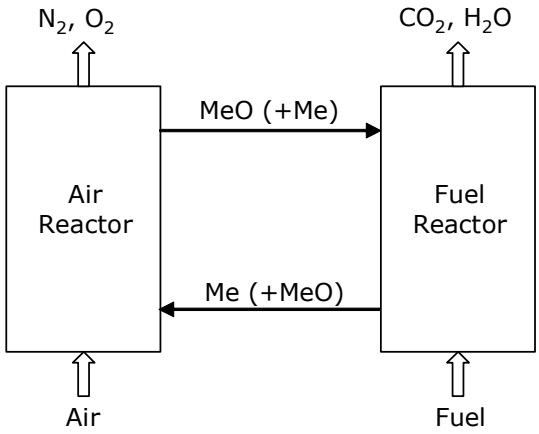

Figure 1. Chemical-looping combustion. After condensing the water produced in the fuel reactor, pure CO_2 is obtained.

For a hydrocarbon fuel, e.g. natural gas, the overall chemical reactions taking place while the oxygen carrier circulates in the CLC reactor system can be described as follows,

$$\text{Fuel reactor:} \quad C_nH_m + (2n + \tfrac{1}{2} m)\, MeO \rightarrow n\, CO_2 + \tfrac{1}{2} m\, H_2O + (2n + \tfrac{1}{2} m)\, Me \qquad (1)$$

$$\text{Air reactor:} \quad Me + \tfrac{1}{2}\, O_2 \rightarrow MeO, \qquad (2)$$

and the net reaction in the reactor system thus becomes

$$C_nH_m + (n + \tfrac{1}{4} m)\, O_2 \rightarrow n\, CO_2 + \tfrac{1}{2} m\, H_2O, \qquad (3)$$

which is identical to conventional combustion. Consequently, the net heat release is also identical to conventional combustion.

Reaction (2) is invariably highly exothermic, whereas reaction (1) can be either endo- or exothermic, depending on fuel and on what Me/MeO-pair is used as oxygen carrier [4]. When the reaction in the fuel reactor is endothermic, the solids circulation can be used to re-distribute heat released in the air reactor to the fuel reactor.

The ideal oxygen carrier is characterized by

- High rates of oxidation and reduction. This is necessary in order to minimize the size of the reaction chambers and the amount of needed material.
- Low tendency of attrition and fragmentation. It is desirable to minimize the production of fines and maximize particle lifetime.
- Sufficient oxygen ratio,

  $$R_0 = \frac{m_{ox} - m_{red}}{m_{ox}}, \qquad (4)$$

  where m_{ox} and m_{red} are masses of a fully oxidized and a fully reduced sample. A high R_0 is usually considered an advantage since more oxygen can be transported per unit mass of circulating material.
- High melting temperature in oxidized as well as reduced form. Materials

become soft when their melting temperature is approached. Operating a CLC system close to the melting temperature of the oxygen carrier might result in agglomeration.

- No or little solid carbon formation on particles. Solid carbon may form through pyrolysis,

  $$C_nH_m \rightarrow n\,C + \tfrac{1}{2}\,m\,H_2, \quad (5)$$

  or through the Boudouard reaction,

  $$2\,CO \rightarrow C + CO_2, \quad (6)$$

  and it is well established that both reactions can be catalyzed by metallic surfaces.
- Capability to convert the fuel entirely to CO_2 and H_2O.
- Low cost.
- Low toxicity both to humans and the environment.

Although natural ores can be used as oxygen carrier [5], most reported work on CLC has been accomplished using oxygen-carrier particles where the active component is combined with an inert material [6]. A thorough thermodynamic analysis of different active components [4] showed that carriers with Fe_2O_3/Fe_3O_4, Cu_2O/Cu, Mn_3O_4/MnO and NiO/Ni were most suitable for CLC processes using natural gas as fuel. Options for oxygen-carrier preparation include freeze-granulation [7], spray-drying [8], impregnation [9], co-precipitation [10], spin-flash drying [11] and a few others. Ideally, the produced particulate oxygen carrier should have a porous structure with a large surface area, thus increasing the accessibility of the reacting gases to the metal oxide.

Nickel-based oxygen carriers have a number of advantages, the most important of which are high melting temperature and high rate of reduction. R_0 for Ni/NiO is also relatively high (0.21). On the other hand, nickel-based oxygen carriers are burdened with a thermodynamical constraint [12], which means that there will always be small amounts of CO and H_2 in the fuel reactor exhaust gas. Furthermore, nickel is expensive and more toxic than other metals identified as suitable as oxygen carriers.

A number of chemical-looping combustors for gaseous fuel ranging from 0.3 – 50 kW_{th} have been designed and operated for a combined total of several hundred hours [13,14,15,16]. A 10-kW CLC unit has been constructed for solid fuels [17].

1.2 Purpose of study

The purpose of the study was to demonstrate the feasibility of making a good oxygen carrier at a reasonable production cost by using commercially available raw materials and a commercial preparation method. In the previous GRACE project [18] successful operation with a NiO-based oxygen carrier was demonstrated during 100 h in a 10 kW CLC reactor system. However, this oxygen carrier was produced using expensive raw materials of high purity. Moreover, the particles were produced by freeze-granulation, a method suitable for small particle batches but un-realistic for preparation of the amounts necessary for a commercial-sized CLC unit.

2. Experimental: 300-W unit

2.1 Experimental set up

The CLC reactor system used in these experiments is an improved version of the 300 W reactor designed by Johansson et al. [14] and the improvements were realised by Rydén et al. [19]. Figure 2 shows the experimental set up. The reactor is 200 mm high. The cross-sectional area of the fuel reactor measures 25×25 mm and the air reactor measures 25×40 mm at the bottom and 25×25 mm in the upper narrow part. The fluidization gases, air and natural gas, enter the air and fuel reactors via wind boxes that are separated from the reaction chambers by porous discs, which act as gas distributors. The gas velocity in the air reactor is high enough to entrain particles, a fraction of which falls into the downcomer of the upper particle seal, a J-type loop seal. The increased amount of particles in the downcomer leads to increased pressure which forces particles to enter the fuel reactor via the return orifice. Consequently, there is an increase in differential pressure over the fuel reactor bed, which in turn forces particles back to the air reactor via the lower particle seal, hence completing the particle loop. Both particle seals are fluidized with nitrogen. To ensure that particles from the air reactor are not entrained to the chimney along with the gas, there is a particle separation chamber above the reactor. The separation part is 240 mm high. The first 180 mm the separation chamber depth expands from an initial 25 mm to a maximum 105 mm, which is then constant the last 60 mm.

The reactor is placed in an electrically heated furnace, which is necessary in order to reach the desirable operating temperatures at start-up. Due to heat losses from the system, heat also needs to be supplied to the reactor system during normal operation with fuel. Two thermocouples are present in the reactor system; one in the air reactor and the other in the fuel reactor.

The exit gas stream from the fuel reactor is led to a water seal, which provides the possibility to increase the pressure in the fuel reactor by adjusting the height of the water column. This is done in order to minimize air leakage to the fuel reactor. The flue gases are cooled and led to gas analysers. CO_2, CO, CH_4 are measured using IR instrumentation. Paramagnetic sensors determine the oxygen content in the gases. Hydrogen was not measured during this test series. Bronkhorst mass flow controllers regulate all incoming gas flows.

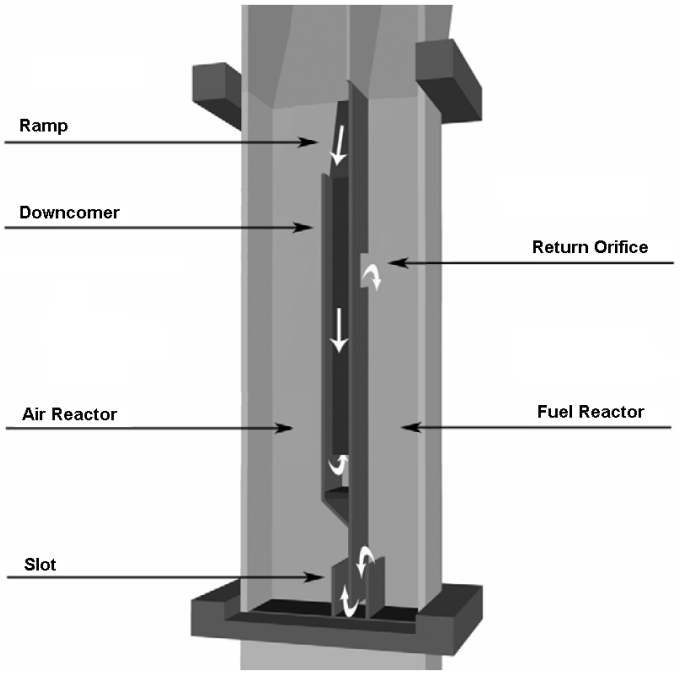

Figure 2. The 300-W CLC reactor system (bottom part). The slot is referred to as lower particle seal in the text.

2.2 Fuel

Natural gas was used as fuel in all tests. The main constituent of the fuel is methane, and the average H/C ratio is 3.7. Oxygen consumption is 2.2 moles O_2 per mole fuel when fuel conversion to CO_2 and H_2O is complete, and the volume expansion due to reaction is 3.3 per mole fuel. Table 1 shows the average composition of the natural gas according to DONG Energy, Denmark (August, 2007). The lower heating value based on the average fuel composition is 39.6 MJ / m_n^3.

Table 1. Average composition of natural gas used in the experiments.

Species	Formula	Mole-%
Methane	CH_4	89.51
Ethane	C_2H_6	5.92
Propane	C_3H_8	2.36
Isobutane	C_4H_{10}	0.40
n-butane	C_4H_{10}	0.56
Isopentane	C_5H_{12}	0.13
n-pentane	C_5H_{12}	0.08
Hexane+	C_6H_{14}	0.06
Nitrogen	N_2	0.28
Carbon dioxide	CO_2	0.71

2.3 Oxygen carriers

Three different oxygen carriers were used in these experiments: two spray-dried particles, N-VITO (the reference particle) and N-VITOMg and one impregnated particle, N-CSIC. The important characteristics of the oxygen carriers used in the study are summarized in table 2. Apparent density is measured on particles sized 125-180 μm and calculated assuming a void between particles of 37%. The crushing strength is measured on particles of size 180-212 μm. The GRACE particle [18, 20], which was used in CLC operation in a 10 kW unit for > 100 h with very high conversion of fuel [13], has been included for comparison.

Table 2. Characteristics of oxygen carriers used in the study and the GRACE particle.

Denotation used in this study	Active material	Fraction of active material ($\%_{mass}$)	Support material	Production method	Crushing strength (N)	BET surface area (m^2/g)	Apparent density (kg/m^3)	Manu-facturer
N-VITO/ Reference particle	NiO	40	$NiAl_2O_4$	Spray-drying	2.3	0.7	3600	VITO
N-VITOMg	NiO	40	$NiAl_2O_4$ (~42%) and $MgAl_2O_4$ (~18%)*	Spray-drying	2.0		3250	VITO
N-CSIC	NiO	18	α-Al_2O_3	Hot impregnation	4.8		2340	CSIC
GRACE	NiO	40	$NiAl_2O_4$	Freeze-granulation	2.5	0.4	3800	

*assuming that all MgO reacted with Al_2O_3.

SEM pictures of fresh particles (i.e. particles not subjected to CLC) can be seen in figures 3 a-c. No image of N-VITOMg is presented, but its physical appearance is very similar to that of N-VITO.

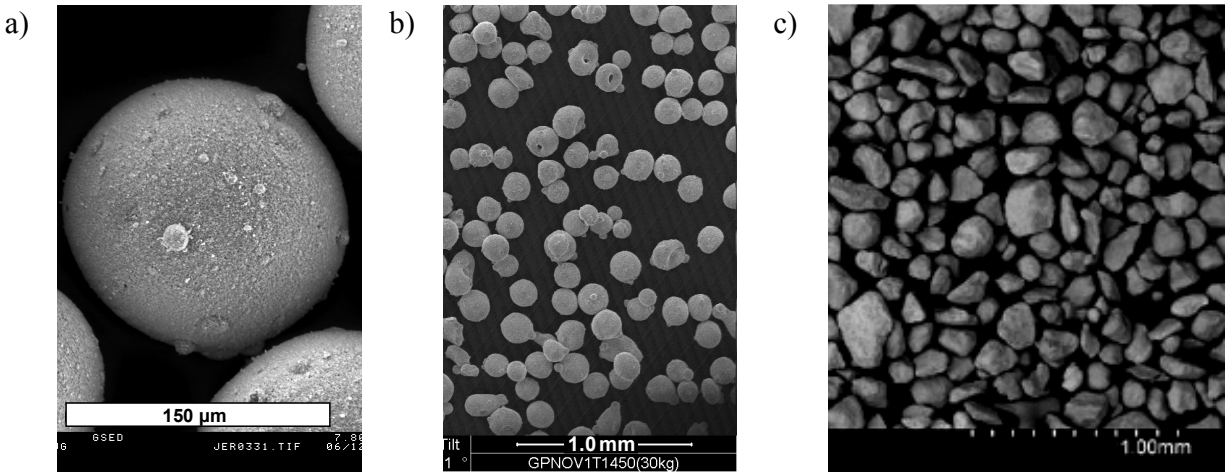

Figure 3. SEM images of oxygen carriers: a and b present fresh N-VITO; c shows fresh N-CSIC.

The NiO used as raw material in the production of N-VITO and N-VITOMg was a refractory grade material containing certain impurities; Co (≈1%), Cu (≈1%), Fe (≈0.5%). For the preparation of N-VITO a water-based slurry containing NiO, Al_2O_3 and small amounts of organic

binder and dispersants was mixed, milled and pumped to the nozzle of the spray-dryer. The spray-dried material was sieved to obtain the right particle size distribution and sintered at 1450°C for 4 h. N-VITOMg was prepared in a similar fashion from a similar slurry that also contained 5% MgO and using a lower sintering temperature, 1400°C. N-CSIC was prepared by CSIC in Spain using dry hot impregnation [21]. The particle size of N-VITO and N-VITOMg was 90-212 μm, and that of N-CSIC was 90-250 μm. The particle size distributions of N-VITO and N-CSIC are shown in figure 4. The particle size distribution of N-VITOMg is very similar to N-VITO.

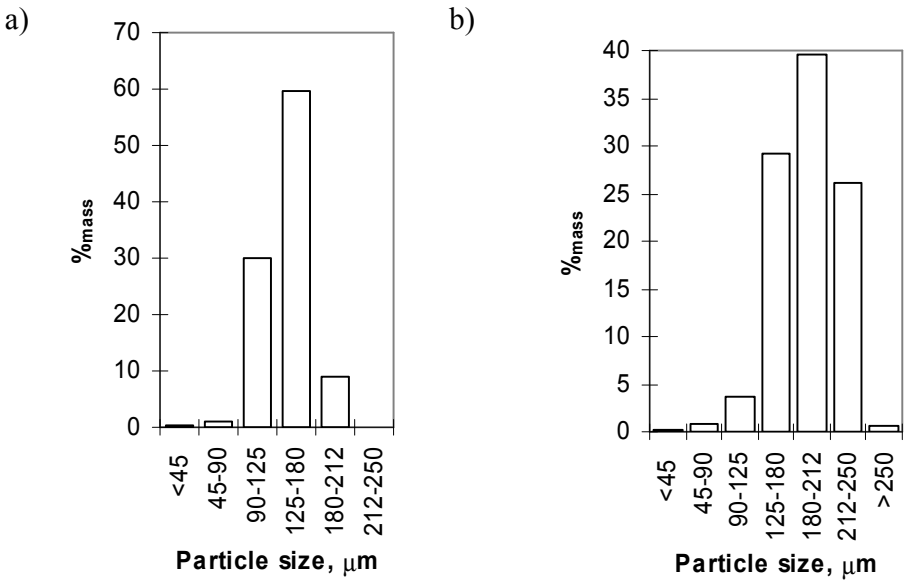

Figure 4. Particle size distribution of (a) fresh N-VITO, and (b) fresh N-CSIC.

The minimum fluidization and terminal velocities (u_{mf}, u_t) shown in table 3 were calculated according to relations by Kunii and Levenspiel [22]. Values for sphericity, ϕ, are assumed from SEM images and are therefore somewhat uncertain. The minimum fluidization voidages, ε_{mf}, are estimations for a loosely packed bed with particles of indicated sphericity, as suggested by Kunii and Levenspiel. The average particle diameters are calculated from the particle size distribution of respective oxygen carrier.

Table 3. Terminal and minimum fluidization velocities for the particles used in the study. The temperature used in the calculations is 850°C. u_t is calculated for air and u_{mf} is calculated for a mixture of CO_2 and steam at a ratio of 1:2, corresponding to full oxidation of methane.

Particle	ϕ	ε_{mf}	$\overline{d}_p$ (μm)	u_t (m/s)	u_{mf} (m/s)
N-VITO	0.9	0.45	135	0.65	0.010
N-VITOMg	0.9	0.45	135	0.60	0.010
N-CSIC	0.8	0.50	180	0.70	0.015

The superficial velocity actually used in the reactor system at 850°C is approximately 0.15 m/s for the reacted gas in the fuel reactor and approximately 0.65-0.80 m/s in the upper part of the air reactor.

2.4 Particle conversion and solids flux

The solids flux determines the difference in conversion of particles leaving and returning to the air reactor, i.e. how much of the available oxygen in the particle flow is consumed in the fuel reactor [3]. The degree of oxidation of the particles, also referred to as particle conversion, X, is defined as the ratio of the amount of available oxygen present in the carrier and the amount of available oxygen present in the carrier when fully oxidized,

$$X = \frac{m_{actual} - m_{red}}{m_{ox} - m_{red}}, \quad (7)$$

where m_{actual} is the actual mass of the carrier in its partially oxidized state, m_{ox} is the mass of the sample when fully oxidized, and m_{red} the mass of the sample in the fully reduced form. The particle conversion in the air reactor, X_{ox}, is larger than that in the fuel reactor, X_{red}, during normal combustion conditions. The difference in particle conversion,

$$\Delta X = X_{ox} - X_{red}, \quad (8)$$

hence becomes a function of the particle circulation; increasing the solids flux in the reactor system leads to a decrease in ΔX.

As stated above, ΔX is a measure of the amount of available oxygen in the oxygen carrier and consequently – in the case of nickel-based oxygen carriers such as those used in the present study – of the amount of metallic nickel present in the carrier. This is an important aspect since nickel acts as a catalyst in steam reforming of natural gas,

$$C_nH_m + n\ H_2O \rightarrow n\ CO + (n + ½m)\ H_2. \quad (9)$$

In this way, the solids circulation influences the conversion of the natural gas.

In summary, it is important to have sufficient particle circulation in order to provide oxygen for the fuel oxidation, and at the same time, if circulation is high, fewer nickel sites will be available for reforming and consequently the fraction of unconverted methane will be higher.

The solids circulation for a specific oxygen carrier in the 300-W unit depends on (a) the actual (hot) flow of gas in the air reactor and (b) the solids inventory in the air reactor, which is determined by the total solids inventory and, to a smaller extent, the pressure applied over the fuel reactor through the water column in the water seal, the height of which was kept constant in this study. Moreover, the flow of inert gas in the upper particle seal influences the circulation. This latter option to control the circulation was used on a few occasions when the air ratio, λ, was already low, and a further reduction in circulation was desired. It was later shown that very similar results could be obtained by reducing the total solids inventory instead of the flow in the upper particle seal.

There is no direct way of measuring solids circulation in the 300 W CLC unit. However, for a CLC system using a nickel-based oxygen carrier and natural gas as fuel, the reaction in the air

reactor is highly exothermic, whereas the reaction in the fuel reactor is endothermic, which gives rise to a temperature difference between the reactors, provided that no cooling air is circulating in the air reactor cooling jacket. This temperature difference can be used as a measure of circulation. It is an imperfect measure, the most evident flaw being the influence of the air ratio on the heat balance of the air reactor. However, for small variations in air flow, the effect on the temperature difference is marginal. Furthermore, when the total solids inventory is decreased in order to decrease particle circulation without changing the air flow, the inventory of the fuel reactor decreases as well, which might affect fuel conversion. During the experiments in this study, however, no adverse effects on fuel conversion were noted as the total solids inventory was reduced.

For a NiO-based oxygen carrier circulating in the 300-W unit at a specific fuel load with constant flows in the air reactor and the particle seals, the same amounts of heat are required and released in the fuel and air reactors (assuming complete conversion of the fuel to CO_2 and H_2O) regardless of the mass fraction of NiO in the carrier. Moreover, the support materials of the three different oxygen carriers used in the study have similar heat capacities, and NiO has similar heat capacity to the supports. Hence, it should be possible to use the temperature difference also to make circulation comparisons between the different batches used in the study.

2.5 Carbon deposition

As mentioned in the introduction, solid carbon can form on particles through methane decomposition and the Boudouard reaction. However, during normal CLC operation, no or very little carbon should form on particles, as long as the fuel reactor can be assumed to be well mixed. This has been demonstrated theoretically [12] and experimentally [13,23]. Estimating the amount of carbon formation on particles in the 300-W unit is complicated by the leakage flow from the fuel reactor to the air reactor. It is possible to get a qualitative indication of carbon deposition on particles by studying (a) the CO_2 transient in the air reactor following fuel termination and (b) CO formation in the fuel reactor during the same period, when nitrogen is used to fluidize the fuel reactor.

2.6 Leakage estimations

Experiments aiming to determine the amount of leakage from the air reactor to the fuel reactor can not be performed during fuel operation. Instead, these tests are carried out at operation temperatures prior to fuel operation. Air is used to fluidize the air reactor, nitrogen is used in the particle seals and CO_2 is the fluidizing agent in the fuel reactor. The flows and operating conditions used for these tests were as similar as possible to those used during fuel operation. The temperature in the reactor system was around 800°C. The flow of CO_2 in the fuel reactor was 0.80 L_n/min, which means that the size of the flow was between that of the unreacted flow of natural gas and the reacted gas flow consisting of CO_2 and H_2O. The leakage flow of air to the fuel reactor, $\dot{V}_{air\ leakage,\ AR->FR}$, was calculated according to

$$\dot{V}_{air\ leakage,\ AR->FR} = \frac{4.77[O_2]_{FR,meas}}{1-4.77[O_2]_{FR,meas}}\left(\dot{V}_{CO2,FR} - \dot{V}_{CO2,AR} + \frac{\dot{V}_{N2,UPS}}{2}\right), \qquad (10)$$

where $\dot{V}_{CO2,FR}$ is the flow of CO_2 in the fuel reactor and $\dot{V}_{CO2,AR}$ is the leakage flow of CO_2 from the fuel

reactor to the air reactor.

$$\dot{V}_{CO2,AR} = \frac{[CO2]_{AR,meas}}{1-[CO2]_{AR,meas}}(\dot{V}_{air} - 2.2\dot{V}_{fuel} + \dot{V}_{N2,LPS} + \frac{\dot{V}_{N2,UPS}}{2}), \qquad (11)$$

where $\dot{V}_{air}$ is the air flow and $2.2\dot{V}_{fuel}$ corresponds to the oxygen consumption, which is zero when no fuel is used.

The gas leakage from the fuel reactor to the air reactor is larger than that in the opposite direction. The leakage consists of CO_2, H_2O, and possibly also some unreacted natural gas.

$$CO_2 \ leakage = \frac{\dot{V}_{CO2,AR}}{1.134\dot{V}_{fuel}} \qquad (12)$$

The CO_2 leakage expressed in equation (12) relates the flow of CO_2 in the air reactor to the flow of total carbon added with the fuel. $\dot{V}_{CO2,AR}$ is defined in equation (11).

2.7 Experimental procedure

Each experimental session involved start-up, fuel operation and shut-down of the 300-W unit. The fuel operation comprised several experiments, the duration of which were 40 minutes to 2 h. The start of an experiment was defined at the time when the fractions of CO and CH_4 had stabilized, which occurred a few minutes after the desired fuel reactor temperature had been reached. The fuel reactor was kept at three different temperatures; 750°C, 850°C and 950°C, whereas the temperature of the air reactor was allowed to drift in accordance with the circulation and varied from [$T_{fuel\ reactor}$ + 10°C] to [$T_{fuel\ reactor}$ + 60°C]. Three oxygen carriers were used in three different compositions according to table 4. The thermal power used in the experiments was 315 W. The circulation was controlled by the total solids inventory, the air flow, and on a few occasions – as mentioned above – the flow of nitrogen in the upper particle seal. The total solids inventory was varied during the tests and ranged from 235-270 g for pure N-VITO and the 2-oxygen-carrier mixture, whereas the inventory was slightly higher, 250-280 g, for the 3-oxygen-carrier mixture. The initial inventory was at the high end of the interval and was then gradually decreased towards the low end in order to allow lower circulation. The air flow was 6-7.5 L_n/min, corresponding to λ = 1.2-1.5.

Table 4. Overview of the most important experiments performed in 300-W unit.

$T_{fuel\ reactor}$ (°C)	Composition of solids inventory ($\%_{mass}$)		
750	N-VITO, 100%	N-VITO, 50% N-VITOMg, 50%	
850	N-VITO, 100%	N-VITO, 50% N-VITOMg, 50%	
950	N-VITO, 100%	N-VITO, 50% N-VITOMg, 50%	N-VITO, 45.5% N-VITOMg, 45.5% N-CSIC, 9%

2.8 Data evaluation

Temperatures, differential pressures, incoming gas flows and gas concentrations are gathered every ten seconds and then averaged over 10 measurements. In figures 7-10 presented below, every 30th averaged measurement has been plotted, which means that each symbol corresponds to 5 minutes of operation.

Carbon monoxide, methane and carbon dioxide concentrations presented below are given as fraction of total carbon from the fuel-reactor outlet according to

$$f_i = \frac{x_i}{x_{CO_2} + x_{CO} + x_{CH_4}} \tag{13}$$

where i represents CO_2, CO, CH_4 and x is the molar fraction of the substance indicated by the sub-script in dry exit gas from the fuel reactor. The measured concentrations of CO, CO_2 and CH_4 are somewhat lower due to mixing with nitrogen from the particle seals. Hydrogen was not measured during these tests.

3. Experimental: batch experiments

Prior to the experiments carried out in the 300 W reactor system, smaller batches of particles were tested batch-wise in a laboratory reactor. These reactivity investigations were conducted in a fluidized bed reactor of quartz, with a length of 870 mm and an inner diameter of 22 mm. The reactor has a porous quartz disc placed 370 mm from the bottom.

Six experiments were performed at two temperatures using pure N-VITO, pure N-VITOMg or a mixture of the two particles, as summarized in table 5.

Table 5. Temperature and composition of batch used in the six experiments performed in batch reactor.

T (ºC)	Composition of solids inventory ($\%_{mass}$)		
850	N-VITO, 100%	N-VITOMg, 100%	N-VITO, 50%, N-VITOMg, 50%
950	N-VITO, 100%	N-VITOMg, 100%	N-VITO, 50%, N-VITOMg, 50%

15 g of bed material sized 125-180 µm was placed on the porous disc and heated in an inert atmosphere of N_2 to a desired reaction temperature of 950ºC or 850ºC. When the experimental temperature was reached, the particles were exposed alternately to 5% O_2 in N_2 and 100% CH_4, thus simulating the cyclic conditions of a chemical-looping combustion system. The low O_2 concentration was used to avoid a large temperature increase, due to the heat produced in the highly exothermic oxidation reaction. CH_4 was used during reduction since it is the major constituent in natural gas, and simplifies the experimental evaluation. Inert N_2 was introduced for 180 s to flush the system, and hence avoid reactions between oxygen and methane at transition between the oxidizing and reducing periods.

The gas from the reactor was led to an electric cooler, where the water produced in the reduction was condensed and removed, and then on to a Rosemount NGA-2000 gas analyzer where the concentrations of CO_2, CO, CH_4 and O_2 as well as the flow were measured.

The inlet gas flows used were 450 ml/min during reduction and inert periods and 1000 ml/min during oxidation periods.

The reactivity of the particles was calculated from the measured outlet concentrations and the gas flow. The particle conversion was calculated as a function of time for the reducing period as;

$$X_i = X_{i-1} - \int_{t_0}^{t_1} \frac{1}{n_o P_{tot}} \dot{n}_{out} (4 p_{CO_2,out} + 3 p_{CO,out} - p_{H_2,out}) dt \quad (14)$$

The particle conversion was also calculated during the oxidation period to verify that the oxygen carriers were completely oxidized;

$$X_i = X_{i-1} + \int_{t_0}^{t_1} \frac{2}{n_o P_{tot}} (\dot{n}_{in} p_{O_2,in} - \dot{n}_{out} p_{O_2,out}) dt \quad (15)$$

X_i is the conversion as a function of time for period *i*, X_{i-1} is the conversion after the preceding period, t_0 and t_1 are the times for the start and the finish of the period, n_o is the number of moles of active oxygen in the unreacted oxygen carrier, $\dot{n}_{in}$ and $\dot{n}_{out}$ are the molar flows of the gas going into and leaving the reactor after the water has been condensed and removed, P_{tot} is the total pressure and $p_{O_2,in}$, $p_{O_2,out}$, $p_{CO_2,out}$, $p_{CO,out}$ and $p_{H_2,out}$ are the partial pressures of incoming and outlet O_2 and outlet partial pressure of CO_2, CO and H_2 after the removal of H_2O. $p_{H_2,out}$ was not measured online but assumed to be related to the outlet partial pressure of CO and CO_2 through an empirical relation based on the equilibrium of the water-gas shift reaction;

$$CO + H_2O \leftrightarrow CO_2 + H_2 \quad (16)$$

Equation (13) was used to calculate the gas yield, or the conversion to CO_2, and also to quantify the amount of unreacted methane leaving the reactor.

4. Results: batch experiments

Figures 5 and 6 show gas yield as fuel conversion to CO_2 and fraction of unconverted fuel versus X. N-VITO defluidized at 950°C, which is the reason why CO_2 falls rapidly at $X \approx 0.28$. The reason why the CO_2 fraction at 850°C using N-VITOMg, depicted in figure 6, starts to decrease at much higher X can be explained by the strong oxygen-transport-capacity dependence on temperature of N-VITOMg. However, the conversion of methane is still good.

Note that with N-VITOMg the conversion to CO_2 decreases slightly with X also at 950°C. It should also be noted that, of the three oxygen-carrier systems, N-VITOMg has the highest fuel conversion to CO_2 at high X, N-VITO has the highest fuel conversion to CO_2 at low X, whereas

the mixture displays the highest CO_2 yield at "medium" particle conversion. This is most evident at 850°C, in figure 6, but manifested also at 950°C.

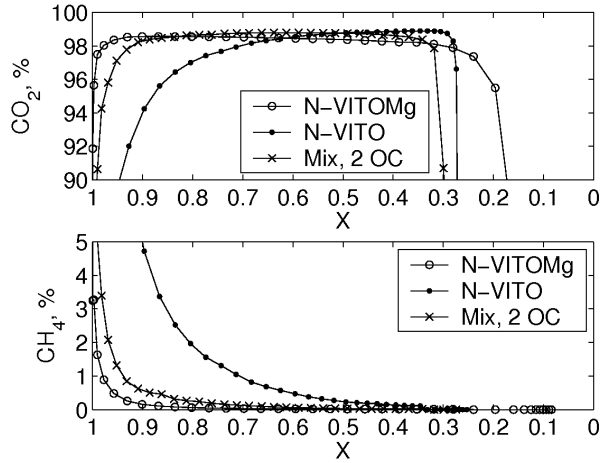

Figure 5. Gas yield and fraction of unconverted CH_4 at 950°C.

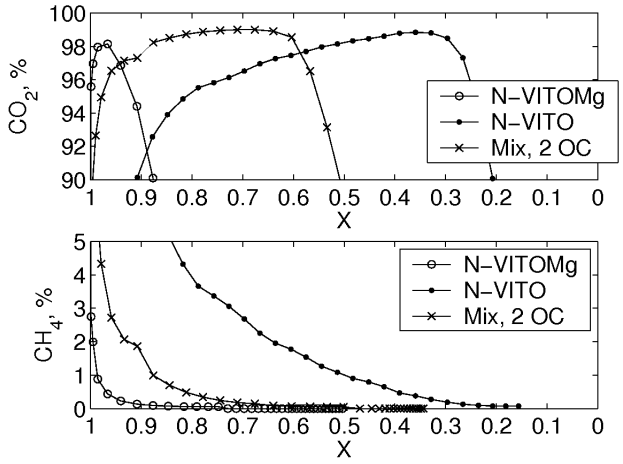

Figure 6. Gas yield and fraction of unconverted CH_4 at 850°C.

Thus, the laboratory batch tests indicate that mixing of the two oxygen carrier particles can be beneficial for fuel conversion.

5. Results: 300-W CLC unit

Experiments were conducted on 15 separate occasions. The total time of operation was 84 h, 25 of which were performed at 200 W. Tests at 200 W generally showed better conversion of the fuel along with lower and more stable CO fractions, but the results from these tests are not reported here. Results shown below are exclusively from experiments performed at 315 W. Each of the three oxygen-carrier compositions was run for approximately 20 h at 315 W.

For all three investigated particle mixtures, fuel conversion improved with (i) decreased circulation, and (ii) increased temperature.

The 3-oxygen-carrier mixture showed good fuel conversion at a relatively high circulation and

therefore a higher total solids inventory was used.

5.1 Fuel conversion

Figure 7 shows the fractions of CH_4 and CO plotted against the temperature difference of the fuel and air reactors using N-VITO. As described above, the temperature difference is an indication of the circulation rate of particles. The operation was not as stable as when the particle mixtures described below were used. Fractions of CH_4 exhibited the expected general relationship with circulation at 850°C and 950°C, whereas at 750°C the circulation dependence of methane could not be established. The fractions of CO showed some temperature dependence. However, there was some variation of CO at 850°C and 950°C which could not be attributed to any changes in operating conditions.

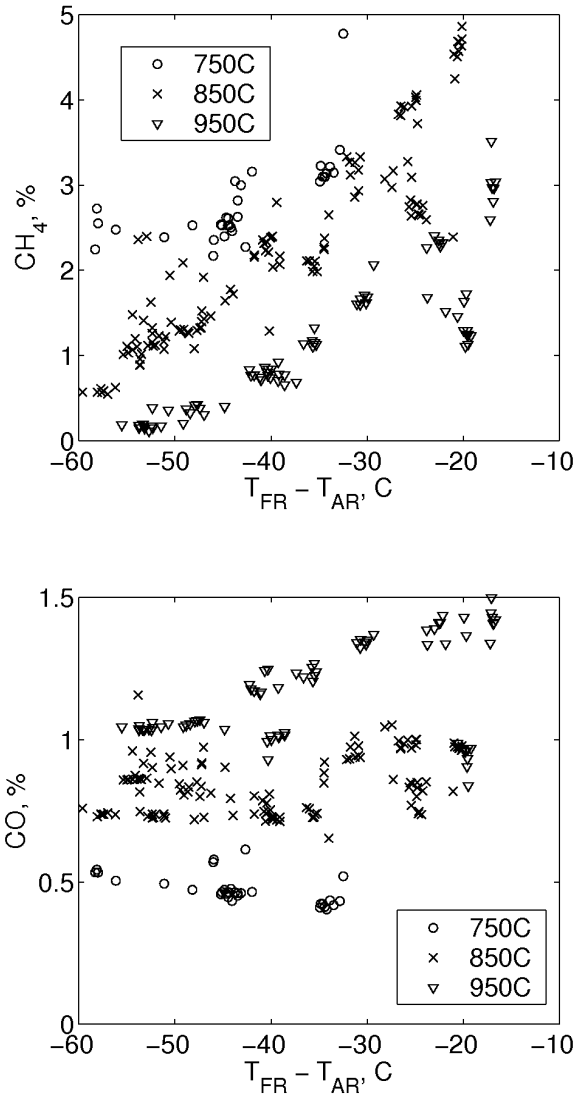

Figure 7. Fractions of CH_4 and CO using N-VITO.

Figure 8 shows data from operation with a mixture of two oxygen carriers, N-VITO and N-VITOMg, plotted similarly as figure 7. Here, the operation is stable, and it is possible to obtain

good conversion of the fuel even at 750°C. But in general the trend of the methane fraction is similar to that using the reference particle, N-VITO, with somewhat better conversion at low circulation for all temperatures.

Note how CO starts to increase as a function of circulation at very low recirculation rates at 750°C and 850°C, which is likely associated with the limited amount of oxygen available for reaction at these low recirculation rates.

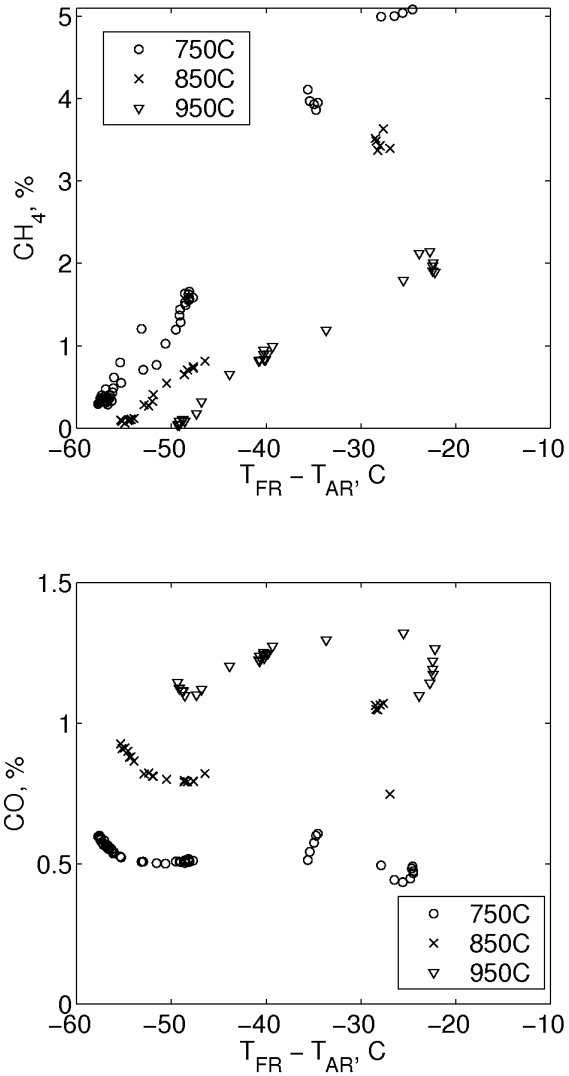

Figure 8. Fractions of CH_4 and CO using a mixture of N-VITO and N-VITOMg.

Figure 9 shows the CO and CH_4 fractions plotted versus the temperature of the fuel reactor for the 3-oxygen-carrier mixture. Equilibrium fractions of CO and H_2 are also plotted, and it is clear that the measured CO is close to equilibrium. The duration of the experiment was three hours and circulation was relatively high. The operation with the 3-oxygen-carrier mixture was in general very stable. This is particularly true for the CO fraction which does not display the same unexplainable variational behaviour that was the case primarily with N-VITO, but also with the 2-oxygen-carrier mixture.

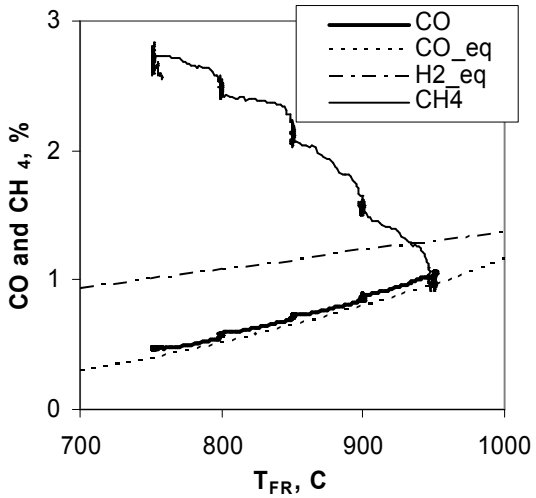

Figure 9. Fractions of CO and CH_4 using the three-particle mixture. Also shown are equilibrium fractions of CO and H_2.

Figure 10 compares the three oxygen carrier systems at a fuel reactor temperature of 950°C and varying circulation. It is evident that with the 3-oxygen-carrier mixture good fuel conversion is obtained at relatively high circulation. The $9\%_{mass}$-addition of impregnated particles clearly makes a difference with respect to methane conversion. It should be mentioned that the impregnated particles have a considerably higher surface area than the freeze granulated particles, and hence that there may be a relatively high active area available for catalyzed reactions.

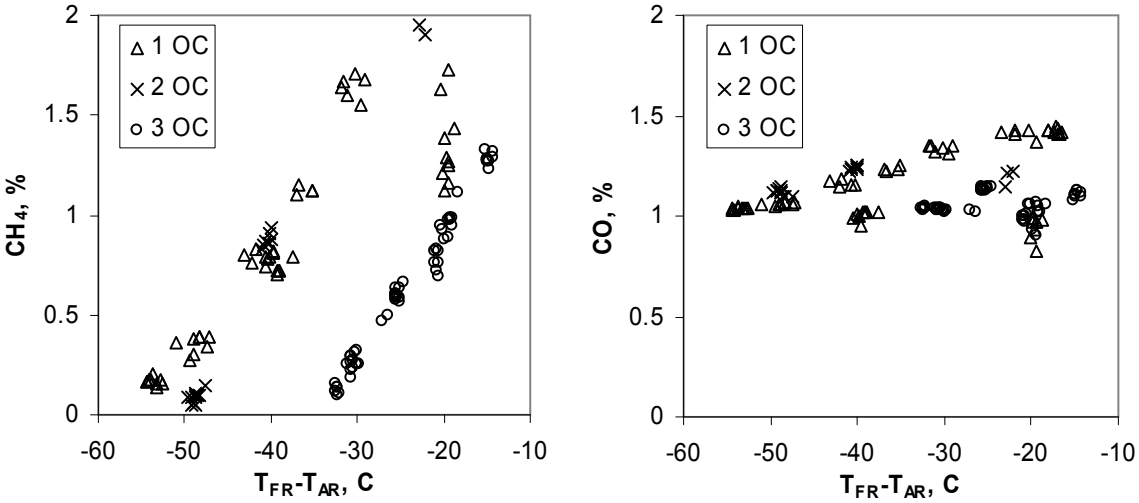

Figure 10. Fractions of CH_4 and CO for three sets of oxygen carrier compositions at $T_{fuel\ reactor}$ = 950°C.

5.2 Carbon formation and agglomeration

No formation of solid carbon could be observed during the experiments. This may not be surprising, considering that the experiments were conducted at relatively high gas yields to

carbon dioxide and water. Hence, the overall atmosphere in the fuel reactor is relatively oxidizing, and this should prevent any carbon deposition.

No tendencies of agglomeration were seen with the double and triple oxygen carrier mixtures. However, a few small agglomerates were formed during the operation with the single oxygen carrier. These were a few millimetres large and very soft. They were so soft that they broke apart during handling.

5.3 Evaluation of gas leakage between reactors

As explained in the experimental section, the leakage from the air reactor to the fuel reactor cannot be evaluated during operation with fuel. Instead, such evaluations are performed at conditions as similar to those during combustion as possible. Figure 11 presents data from leakage tests, which were performed on four different occasions. The duration of each test was approximately four minutes. Figure 11 is an attempt to express the air leakage to the fuel reactor as a function of the circulation. This is achieved by plotting the air leakage flow to the fuel reactor (equation 10) versus $\dot{V}_{AR,\,hot}$, which is simply the combined flows of air, nitrogen from the particle seals and CO_2 leakage adjusted for thermal expansion. Here, it is necessary to consider that the amount of solids in the air reactor has a significant impact on circulation. If it were possible to plot $\dot{V}_{O2\ to\ FR}$ against circulation in figure 11, the displayed tests with lower solids inventory, i.e. 235 g and 250 g, would end up further to the left in the figure since circulation would be lower relative to the periods with 280 g solids inventory.

It is clear that the air leakage is quite low. The figure also suggests that lower circulation leads to lower oxygen leakage. The measured leakage flow from the air reactor to the fuel reactor (0-0.02 L_n air/min, see figure 11) corresponds to 0-0.2% of the added air. This leakage flow could potentially oxidize a maximum of 0.2% of the added fuel. Thus, the experimental results should not be affected by the leakage from the air reactor to the fuel reactor.

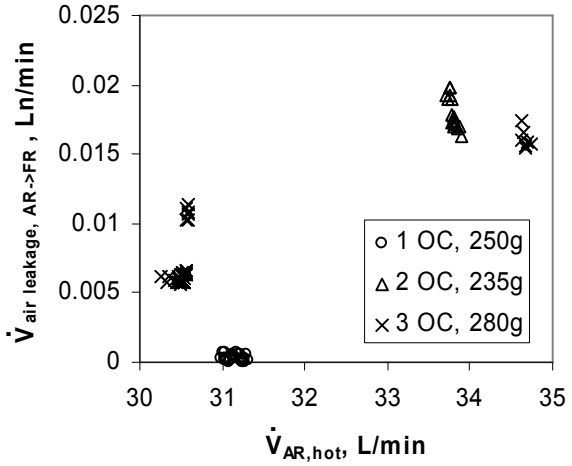

Figure 11. Evaluation of leakage from the air reactor to the fuel reactor. The leakage flow of air is shown versus the hot gas flow in the air reactor.

The gas leakage from the fuel reactor to the air reactor, calculated from equation (12), is approximately 3-6% of the reacted fuel. Figure 12 demonstrates a relationship between the size of

the gas leakage and circulation. The data originates from the combustion experiments presented above. Each cross corresponds to five minutes of fuel operation.

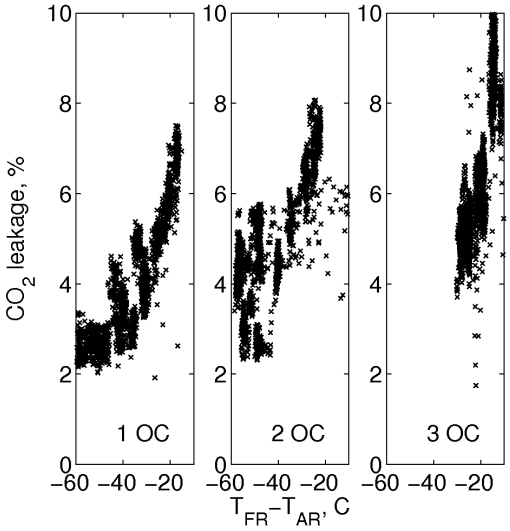

Figure 12. CO_2 leakage from fuel reactor to air reactor versus [$T_{fuel\ reactor}$ - $T_{air\ reactor}$], C.

5.4 Particle conversion

The conversion of the oxygen-carrier particles was evaluated on one occasion. This was done by terminating all fluidization in particle seals and air reactor and oxidizing the particles in the fuel reactor in air, as shown in figure 13. Analysis of the exhaust gas from the fuel reactor is delayed by a recirculation loop of the sampling gas. In order to determine the duration of this delay and find out exactly at what point air is introduced into the fuel reactor, the fuel reactor was first fluidized with nitrogen for approximately one minute, then CO_2 for another minute, and lastly air until the particles were fully oxidized.

The fuel conversion was excellent prior to fuel termination and evaluation of the particle conversion. The fraction of CH_4 was < 0.1% and the CO fraction was 0.75%, which is just above the equilibrium fraction at the temperature used in the fuel reactor, 850°C.

From the total solids inventory, the geometry of the reactor system and the height of the water column, the mass of solids in the fuel reactor was estimated to 60 g. Combining this estimation with the oxygen uptake during oxidation of particles (1.9 g), equation (7) yields $X_{fuel\ reactor} = 0.62$. Assuming that particles entering the fuel reactor are fully oxidized gives $\Delta X \approx 0.4$. Prior to the evaluation of ΔX, circulation was low, but not specifically known, which limits the usefulness of the result. No evaluation of the actual conversion of the particles from the air reactor was conducted. Figure 13 shows oxygen and carbon dioxide concentrations as a function of time. Far left in the figure, fuel termination is shown, followed by N_2 fluidization, CO_2 fluidization and finally air fluidization.

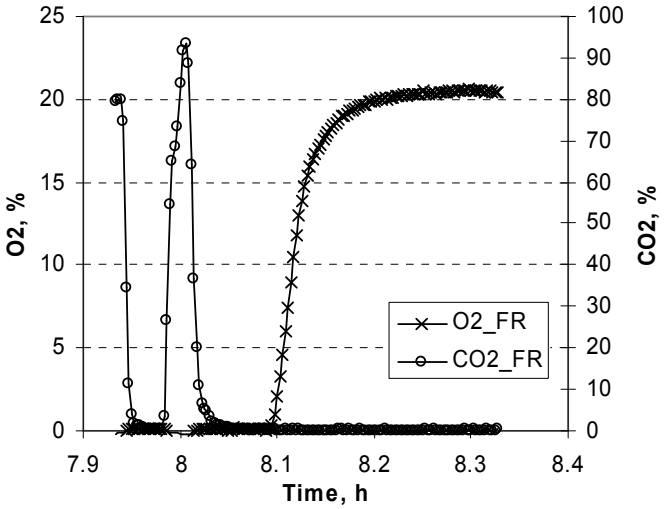

Figure 13. O_2 and CO_2 concentrations in the fuel reactor after fuel termination.

6. Discussion

The work in this paper has shown that Ni-based particles with commercial materials and spray-drying can be used in a continuous CLC reactor with methane as fuel. This is important, since a cornerstone for the CLC technology is developing oxygen carriers which are cost-effective. As was noted in the study, the use of a $NiO/NiAl_2O_4$ particle with small amounts of added MgO had positive effects on the methane conversion. This has been demonstrated both in a batch and continuous reactor. There have been several prior studies of CLC with the $NiO\text{-}Al_2O_3\text{-}MgO$ system. Villa et al. [10] compared red-ox properties of the oxygen-carrier systems Ni-Al-O and Ni-Mg-Al-O for use in chemical-looping combustion. The authors found that the Ni-Al-O samples consisted of merely two phases, cubic NiO and $NiAl_2O_4$ spinel, and that the Ni-Mg-Al-O system had similar composition, with Mg mainly, but not entirely, in the spinel phase. MgO, which has similar crystalline structure to NiO, was found to limit the growth of NiO-crystals, which was explained by the formation of a NiO-MgO solid solution, in which Ni^{2+} ions are stabilized against reduction. Johansson et al. [24] compared two Ni-based oxygen carriers in a 300-W chemical-looping combustor, one of which was supported on $MgAl_2O_4$ and the other on $NiAl_2O_4$. Results suggested that, in comparison to the $NiO/NiAl_2O_4$-particle, the particle supported on $MgAl_2O_4$ had better fuel-conversion capacity, but also produced higher fractions of CO (and H_2), a feature that was especially pronounced at $T_{\text{fuel reactor}} < 850°C$. A similar comparison ($NiO/NiAl_2O_4$ vs $NiO/MgAl_2O_4$) was conducted in batch experiments [25]. This study concluded that the particle supported on magnesium aluminate was more suitable for chemical-looping applications due to better methane conversion, better reforming properties and less likely to promote carbon deposition. Similar findings have been presented by Jerndal et al., who showed in a batch reactor that many different oxygen carriers based on $NiO/NiAl_2O_4$ with small additions of MgO in addition to $NiO/MgAl_2O_4$ have excellent methane cracking capability, in comparison to normal $NiO/NiAl_2O_4$ particles [26]. However, the oxygen transfer capability of these Mg-doped oxygen carriers was less compared to $NiO/NiAl_2O_4$ oxygen carriers, similar to the findings in this paper. This effect seems to be especially important at lower temperatures, < 900°C.

The use of MgO in the support material of Ni-based reforming catalysts has been reported to

suppress carbon deposition. Rostrup-Nielsen investigated coking on different Ni-catalysts during steam reforming of hydrocarbons [27], and found that MgO depressed carbon formation. He proposed that the presence of magnesium improved the steam adsorption on the catalyst, which, it was suggested, decreased carbon formation. Ruckenstein et al. [28] studied CO_2-reforming of methane over catalysts consisting of nickel/alkaline earth metal oxides, and suggested that MgO inhibits the Boudouard reaction over Ni. Koo et al. [29] investigated catalytic activity and coke formation in combined steam and carbon dioxide reforming of methane using MgO-promoted Ni/Al_2O_3-catalysts, and found that catalysts prepared with $20\%_{mass}$ MgO exhibited the highest catalytic performance and had high resistance to coke formation. Even though these findings are pertinent to reforming catalysts, they give an indication that it might be beneficial to use MgO in the inert of a Ni-based oxygen carrier which is to be used in applications of chemical-looping reforming, where coking is serious concern. Although the CLC process operates at quite different conditions in the fuel reactor in comparison to highly reducing reforming conditions, the adsorption of steam to the catalyst surface, suggested by Rostrup-Nielsen and others, is a phenomenon pertinent also to Ni-based, MgO-doped oxygen carriers, and the findings may imply enhanced steam reforming of hydrocarbons and would hence explain the improved methane-cracking capability of the MgO-containing carrier that has been referred to as N-VITOMg in this study. However, the inferior oxygen transfer capability of the Mg-doped Ni-based oxygen carriers, as suggested by Jerndal et al. and Johansson et al. could be a problem, since the bulk transfer of oxygen in the particle is of importance for CLC. Hence, the use of mixed oxides in the fashion presented here may be an interesting option.

7. Conclusions

Oxygen carriers prepared from commercially available raw materials by spray-drying were investigated in a batch reactor and a continuous 300-W reactor-system. An attempt to optimize the oxygen-carrier performance by mixing two different spray-dried Ni-particles was conducted. Here, a reference particle of $NiO/NiAl_2O_4$ was combined with a similar particle which contained small amounts of MgO. The former had good oxygen-transport capability while the latter had very good methane-conversion characteristics. The two spray-dried particles were evaluated in batch experiments, individually and mixed, and the combination turned out to perform optimally.

The findings from the batch tests were evaluated in a 300-W chemical-looping combustor at three temperatures, 750°C, 850°C and 950°C. In general, fuel conversion increased, as expected, with (a) decreased circulation, and (b) increased fuel reactor temperature. The operation with the reference particle was somewhat unstable, and the fuel conversion was unsatisfactory at 750°C, but good at the higher temperatures. With the mixture of the two spray-dried particles, operation was stable and, in comparison to the operation with only the reference particle, fuel conversion improved at all three temperatures, especially at 750°C. At low circulation, the fraction of unconverted methane was < 0.1% both at 850°C and 950°C. Furthermore, a third, impregnated, oxygen carrier was introduced into the mixture in order to improve the methane conversion even further. Excellent conversion of the fuel was obtained at relatively high circulation with this three-particle mixture.

The most important findings from the study are (a) the demonstration of the improvement of fuel conversion using a mix of particles with different properties, and (b) the demonstration of good results using particles manufactured by commercial methods and commercial raw materials, i.e. particles with attractive costs.

Abbreviations and denotations

AR	Air reactor
CLC	Chemical-looping combustion
CSIC	Consejo Superior de Investigaciones Científicas
FR	Fuel reactor
GRACE	Grangemouth Advanced CO2 Capture Project
LPS	Lower particle seal
Me/MeO	Metal/metal oxide
N-VITO	Spray-dried oxygen-carrier particles produced by VITO
N-VITOMg	Spray-dried oxygen-carrier particles produced by VITO
N-CSIC	Impregnated oxygen-carrier particles produced by CSIC
OC	Oxygen carrier
R_0	Oxygen ratio
SEM	Scanning electron microscopy
u_{mf}	Minimum fluidization velocity
UPS	Upper particle seal
u_t	Terminal velocity
VITO	Flemish institute for technological research
X	Particle conversion

Acknowledgements
This work was carried out within the EU-financed research project CLCGP (Chemical Looping Combustion CO2-Ready Gas Power), Contract Number 019800. The particles were supplied by VITO (Flemish institute for technological research) in Belgium and CSIC (Consejo Superior de Investigaciones Científicas) in Spain. The authors would like to acknowledge valuable technical contributions from Magnus Rydén.

References

[1] IPCC. 2005. *Special Report on Carbon dioxide Capture and Storage*.
[2] Ishida, M., Zheng, D., and Akehata, T. 1987. Evaluation of a chemical-looping-combustion power-generation system by graphic exergy analysis. *Energy* 12:147-154.
[3] Lyngfelt, A., Leckner, B., Mattisson, T. 2001. A fluidized-bed combustion process with inherent CO_2 separation - application of chemical-looping combustion. *Chemical Engineering Science* 56:3101-3313.
[4] Jerndal, E., Mattisson, T., and Lyngfelt, A. 2006. Thermal Analysis of Chemical-Looping Combustion. *Chemical Engineering Research and Design* 84:795-806.
[5] Leion, H., Lyngfelt, A., Johansson, M., Jerndal, E., and Mattisson, T. 2008. The use of ilmenite as an oxygen carrier in chemical-looping combustion. Accepted for publication in *Chemical Engineering Research and Design*.
[6] Johansson, M., Mattisson, T., Rydén, M. and Lyngfelt, A. Carbon Capture via Chemical-Looping Combustion and Reforming. *International Seminar on Carbon Sequestration and Climate Change*, Rio de Janeiro, Brazil, 24-27 October 2006.
[7] Cho, P., Mattisson, T. and Lyngfelt, A. 2004. Comparison of iron-, nickel-, copper- and manganese-based oxygen carriers for chemical-looping combustion. *Fuel* 83:1215-1225.
[8] Ishida, M., Yamamoto, M., Ohba, T. 2002. Experimental results of chemical-looping combustion with $NiO/NiAl_2O_4$ particle circulation at 1200 ºC. *Energy Conversion and Management* 43:1469-1478.
[9] de Diego, L. F., García-Labiano, F., Adánez, A., Gayán, P., Abad, A., Corbella, B. M., Palacios, J. M. 2004. Development of Cu-based oxygen carriers for chemical-looping combustion. *Fuel* 83:1749-1757.
[10] Villa, R., Cristiani, C., Groppi, G., Lietti, L., Forzatti, P., Cornaro, U., Rossini, S. 2003. Ni based mixed oxide materials for CH_4 oxidation under redox cycle conditions. *Journal of Molecular Catalysis A: Chemical*. Volumes 204-205:637-646.
[11] Linderholm, C., Abad, A., Mattisson, T. and Lyngfelt, A. 2008. 160 hours of chemical-looping combustion in a 10 kW reactor system with a NiO-based oxygen carrier. *International Journal of Greenhouse Gas Control* 2:520-530.
[12] Mattisson, T., Johansson, M., and Lyngfelt. A. 2006. The use of NiO as an oxygen carrier in chemical-looping combustion. *Fuel* 85:736-747.
[13] Lyngfelt, A., and Thunman, H. Construction and 100 h of operational experience of a 10-kW chemical looping combustor. Chapter 36 in *Carbon Dioxide Capture for Storage in Deep Geologic Formations - Results from the CO_2 Capture Project, Volume 1 – Capture and Separation of Carbon Dioxide From Combustion Sources.* Ed.: Thomas, D. Elsevier Science, London 2005, pp. 625-646.
[14] Johansson, E., Mattisson, T., Lyngfelt, A., Thunman, H. 2006. A 300 W laboratory reactor system for chemical-looping combustion with particle circulation. *Fuel* 85:1428–1438.
[15] Ryu, H. J., Bae, D. H., and Jin, G. T. 2003. Effect of temperature on reduction reactivity of oxygen carrier particles in a fixed bed chemical-looping combustor. *Kor J Chem Eng* 20:960–966.
[16] de Diego, L. F., García-Labiano, F., Gayán, P., Celaya, J., Palacios, J. M., Adanez, J. 2007. Operation of a 10 kW_{th} chemical-looping combustor during 200 h with a $CuO-Al_2O_3$ oxygen carrier. *Fuel* 86:1036-1045.

[17] Berguerand, N., Lyngfelt, A. 2008. Design and operation of a 10 kW_{th} chemical-looping combustor for solid fuels – Testing with South African coal. *Fuel* 87:2713-2726.
[18] Lyngfelt, A., Kronberger, B., Adanez, J., Morin, J.-X., and Hurst, P. 2005. The GRACE project. Development of oxygen carrier particles for chemical-looping combustion. Design and operation of a 10 kW chemical-looping combustor. *Greenhouse Gas Control Technologies* 7:115-123 (*7th International Conference on Greenhouse Gas Control Technologies*, Vancouver, Canada, 5th-9th September 2004).
[19] Rydén, M., Lyngfelt, A., and Mattisson, T. 2008. Chemical-looping combustion and chemical-looping reforming in a circulating fluidized-bed reactor using Ni-based oxygen carriers. Accepted for publication in *Energy & Fuels*.
[20] Johansson, M., Mattisson, T. and Lyngfelt, A. 2006. The use of $NiO/NiAl_2O_4$ particles in a 10 kW chemical-looping combustor. *Ind Eng Chem Res* 45:5911-5919.
[21] Dueso, C., de Diego, L. F., García-Labiano, F., Gayán, P, Abad, A., Adánez, J. 2008. Methane Combustion in a 500 W_{th} Chemical-Looping Combustion System Using an Impregnated Ni-based Oxygen Carrier. Submitted for publication.
[22] Kunii, D., Levenspiel, O. 1991. *Fluidization Engineering*. Reed Publishing Inc., Stoneham.
[23] Cho, P., Mattisson, T., Lyngfelt, A. 2005. Carbon formation on Nickel and Iron Oxide-Containing oxygen Carriers for chemical-looping combustion. *Ind Eng Chem Res* 44:668-676.
[24] Johansson, E., Mattisson, T., Lyngfelt, A., and Thunman, H. 2006. Combustion of Syngas and Natural Gas in a 300 W Chemical-Looping Combustor. *Chem Eng Res Des* 84**:**819-827.
[25] Johansson, M., Mattisson, T., Lyngfelt , A., Abad, A. 2008. Using continuous and pulse experiments to compare two promising nickel-based oxygen carriers for use in chemical-looping technologies. *Fuel* 87:988–1001.
[26] Jerndal, E., Mattisson, T., Thijs, I., Snijkers, F., Lyngfelt, A. 2008. NiO particles with Ca and Mg based additives produced by spray-drying as oxygen carriers for chemical-looping combustion. 9th International Conference on Greenhouse Gas Control Technologies, 16 - 20 November 2008. *Accepted for publication.*
[27] Rostrup-Nielsen, J. R. 1974. Coking on Nickel Catalysts for Steam Reforming of Hydrocarbons. *Journal of Catalysis* 33: 184-201.
[28] Ruckenstein, E., Hu, Y. H. 1995. Carbon dioxide reforming of methane over nickel/alkaline earth metal oxide catalysts. *Applied Catalysis A: General* 133:149-161.
[29] Kee Young Koo, Hyun-Seog Roh, Yu Taek Seo, Dong Joo Seo, Wang Lai Yoon, Seung Bin Park. 2008. Coke study on MgO-promoted Ni/Al2O3 catalyst in combined H2O and CO2 reforming of methane for gas to liquid (GTL) process. *Applied Catalysis A: General* 340:183–190.